Forward Genetic Analysis of Cellulose Biosynthesis Inhibitor Resistance
and
Wall Hydrolysis Sensitivity

by

Isaac Shim

A Thesis Submitted in Partial Fulfillment of the Requirements for the Degree of

Doctor of Philosophy

in

The Faculty of Science

University of Ontario Institute of Technology

September 2014

Abstract

The functional analysis of components involved in cellulose biosynthesis is central in understanding cell wall assembly and structure in plants. We conducted screens using the herbicides, isoxaben and flupoxam which inhibit cellulose biosynthesis in higher plants. Mutations resulting in a high degree of resistance to isoxaben (*ixr*) or flupoxam (*fxr)* were attributed to single amino acid substitutions in primary wall CESAs. Twelve novel resistance alleles were isolated and no cross-resistance was observed. Point mutations were mostly clustered around the C-terminal regions of CESA1 and CESA3, and CESA3 and CESA6 for *fxr* and *ixr* respectively. Resistance to isoxaben was also conferred by modification to the putative catalytic regions of CESA3. This resulted in cellulose deficient phenotypes characterized by reduced crystallinity and dwarfism. These results provide genetic evidence supporting CESA1-CESA3, and CESA3-CESA6 association with flupoxam and isoxaben respectively targeting and disrupting these interactions. The *ixr* and *fxr* mutants also exhibited enhanced saccharification under enzymatic degradation schemes which is consistent with the observed reduction in cellulose crystallinity.

A second forward genetic screen was performed using mild acid hydrolysis to isolate mutants with enhanced saccharification. This screen identified sixty-three *responsive to acid hydrolysis* (*rah*) lines. Unconventional strategies to increase sugar yields from plant biomass where highlighted. These included starch hyper-accumulators such as *starch excess 4* (*sex4*) loss-of-function mutants and the perturbation of polar auxin transport. Disruption of the serine/threonine kinase positive regulator of auxin efflux, PINOID (PID) was found to significantly enhance sugar release in *Arabidopsis* and similar effects were observed in the maize orthologue, BARREN INFLORESENCE 2 (BIF2). Furthermore, the application of N-1-naphthylphthalamic acid (NPA) in *Arabidopsis,* maize, *Miscanthus* and switchgrass phenocopied the enhanced wall saccharification effects of PID. This study attempted to elucidate some of the interactions of seemingly unrelated pathways in the context of wall biosynthesis and saccharification enhancement.

Acknowledgements

I would like to thank my supervisor, Dr. Dario Bonetta, for the wealth of learning opportunities and for offering me an enriching environment to grow as a scientist under his mentorship. I move on to future endeavours with an invaluable skill set. My committee members, Dr. Janice Strap, Dr. Ayush Kumar and Dr. Sonia Gazzarrini, have offered important insight and have challenged me intellectually over the course of my program. It has been a pleasure to work with all of my lab members, past and present, and to mentor several thesis students and volunteers over the years. They have enriched my graduate experience through our technical and philosophical discussions throughout my studies. I would like to thank Rob Law for his assistance during his time in the lab. Through the course of my graduate work, I have had the opportunity to collaborate with many people from whom I have learned a great deal. Through stimulating conversations and thoughtful approaches, they have broadened my scientific knowledge and enabled me to grow personally as well as a scientist. I am grateful for the wealth of support I received from my friends and family. They fostered inspiration, determination and courage enabling me to realize my potential. I would like to express deepest gratitude to my partner-in-life and better-half, Silvia Blank. Thank you for the persistent challenges, words of encouragement and showing me that we are indeed stronger together. Finally, I give a special thanks to my parents, Sung and Lynda Shim for providing me with unconditional love, support and guidance throughout my life journey.

Table of Contents

Publications Related to Thesis Work

Stamatiou, G., Vidaurre, D., Shim, I., Tang, X., Moeder, W., Bonetta, D., McCourt, P. (2013) "Forward Genetic Screening for the Improved Production of Fermentable Sugars from Plant Biomass". *PLOS ONE* 8(1) e55616. doi:10.137/journal. pone. 0055616

Strap, J., Latos, A., Shim, I., Bonetta, D. T. (2011) "Characterization of Pellicle Inhibition in *Gluconacetobacter xylinus* 53582 by a Small Molecule, Pellicin, Identified by a Chemical Genetics Screen. *PLOS ONE* 6(12): e28015. doi:10.1371/journal. pone. 0028015

Accreditation of Work

Chapter 2

Dr. Sean Cutler from the University of California Riverside provided the mutagenized seeds used in the isoxaben and flupoxam screen. Mr. Robert Law performed the initial flupoxam and isoxaben screen and contributed to producing the ^{14}C-glucose incorporation data. Gordon Hagen assisted with ^{1}H NMR data acquisition and analysis.

Chapter 3

Dr. George Stamatiou and Dr. Danielle Vidaurre from the University of Toronto generated the mutagenized population and performed the initial screen of the *responsive to acid hydrolysis* (*rah*) mutants under the supervision of Dr. Peter McCourt. They also provided the *Zea mays*, *Miscanthus* and *Panicum virgatum* tissue used in this study.

List of Tables and Figures

Tables:

Figures:

Supplemental

Table:

Figures**:**

Table:

Figures:

List of Abbreviations

AtCESA	cellulose synthase in *Arabidopsis thaliana*
ATP	adenosine triphosphate
bcsA	bacterial cellulose synthase A gene
BcsA	bacterial cellulose synthase A protein
bif	*barren infloresence* gene
CBI	cellulose biosynthesis inhibitor
c-di-GMP	cyclic diguanylic acid
cesA	*cellulose synthase* gene
CESA	cellulose synthase catalytic subunit
COB	cobra GPI-anchored protein
Col-0	*Columbia* wild-type ecotype
CSL	cellulose synthase-like protein
CSLD	cellulose synthase-like family D
CSR	class specific region
CTAB	cetyltrimethyl ammonium bromide
CTL/POM	chitinase-like protein
DAG	days after germination
DCM	dichloromethane
DMSO	dimethyl sulfoxide
DNA	deoxyribonucleic acid
EMS	ethylmethane sulfonate
ER	endoplasmic reticulum
er	*erecta* gene
F1	first generation
F2	second generation
FPU	filter paper units
fsx	flupoxam herbicide
fxr	flupoxam resistance gene
G-6-P	glucose-6-phosphate
GalA	galacturonic acid
GAX	glucuronoarabinoxylans
GBI	glycan biosynthesis inhibitor
GPI	glycophosphatidylinositol
GT	glycosyl transferase
GTP	guanosine triphosphate
GWD	glucan water dikinase
HG	homogalacturonan
HK	hexokinase protein

^{1}H NMR	proton nuclear magnetic resonance
HVR	hypervariable region
IAA	indole acetic acid
isx	isoxaben herbicide
isxH	reduced isoxaben
ixr	isoxaben resistanc gene
KOR	korrigan glucanase
LCMS	liquid chromatography-mass spectrometry
Ler	*Lansburg erecta* wild-type ecotype
MS	mass spectrometry
M2	second generation of a mutagenized population
NAD	nicotine adenine dinucleotide
NADH	nicotine adenine dinucleotide reduced
NPA	1-N-naphthylphthalamic acid
P-CR	plant conserved region
PCR	polymerase chain reaction
PID	Pinoid serine/threonine kinase
pid	*pinoid* gene
pin	PIN-formed polar auxin transporter gene
PIN	PIN-formed polar auxin transporter
PWD	Phosphoglucan water dikinase
pydA	2-(4-hydroxyphenyl)-5-pyrimidinol
RFLP	restriction fragment length polymorphism
rsw	radial swelling gene
SEX4	starch excess 4 phosphatase
sex4	*starch excess 4* gene
SSLP	simple sequence length polymorphism
SuSY	sucrose synthase protein
TC	terminal complex
THE	theseus kinase
THF	tetrahydrofuran
TLC	thin layer chromatography
TMD	transmembrane domain
rah	*responsive to acid hydrolysis*
RG	rhamnogalacturonan
RING	really interesting new gene protein
UDP	uridine diphosphate
XRD	x-ray diffraction
XyG	xyloglucan
ZFD	zinc-finger domain

Chapter 1: Introduction

1.1.1 Plant cell wall composition

An important property of plants physiology is the existence of cell walls. Cell walls connect cells into tissues and dictate the shape of plant organs. The primary cell wall is approximately 200 nm thick and completely coats the outside of the plasma membrane of every plant cell (Lodish *et al* 2000). They are instrumental in signaling plant cell growth and division by 'loosening' and accommodating expansion in key locations. It is a dynamic and indispensable compartment which is poorly understood despite its ubiquity and importance in plant morphology. Plant cell walls are of central importance to all life either directly or indirectly. They are the primary storage of the chemical energy from photosynthesis and account for the majority of the fixed carbon on the planet. Plant cell walls are also the basic raw starting materials for many industries such as lumber, paper and textile.

In plants, cell walls are required not only as a protective barrier from the environment, but also provide structural support, and resist internal turgor pressure. The porosity of this extracellular matrix allows water, ions and small soluble molecules such as peptides and hormones to diffuse across the cell wall and interact with receptors on the plant plasma membrane. Current models describe the plant cell wall as intertwined networks of cellulose, hemicellulose, pectin, structural glycoproteins such as extensins, and lignin (Somerville 2006). From a mechanical point of view the wall can be considered a composite material with rigid rods of cellulose microfibrils, which are embedded in an amorphous, gelatinous matrix, composed primarily of pectins that are stabilized by proteins and phenolics (Somerville 2006). Cellulose microfibrils are cross-

linked by hemicelluloses, which are highly branched polysaccharides with a backbone of about fifty β-(1-4)-linked xylose (Lodish *et al.* 2000). Each layer of cellulose microfibrils is parallel to one another while maintaining different orientations relative to adjacent layers. This plywood-like construction provides considerable lateral strength to the wall. It is the mechanical strength of the wall, coupled with the internal turgor pressure, which make plant tissues rigid. The cellulose microfibrils are complexed with hemicelluloses, which associate with the microfibril surface through hydrogen bonds and cross-link the microfibrils to one another and to other matrix components such as pectin. Importantly, the interlinked network of pectin and hemicellulose is required for cell-cell adhesion in plants (Carpita *et al.* 2000).

The term hemicellulose refers to polysaccharides extracted from cell walls under dilute alkali conditions and constitute up to a third of the mass of cell walls (Mohen *et al.* 2008). The more common hemicelluloses have β-(1-4)-linked backbones of glucose, xylose or mannose with equatorial configurations at C1 and C4 (Scheller & Ulvskov 2010). The two major types of polymers that constitute hemicellulose in the type-I primary cell walls of *Arabidopsis* are xyloglucan (XyG) and xylans. Xyloglucans make up 20-25% of dicot primary walls and are the most tightly associated to cellulose (Mohen *et al*. 2008). XyGs are found binding firmly to the exposed face of microfibrils and spanning the distance between them. XyGs are defined by a β-(1-4)-linked glucan backbone that is highly substituted with α-(1-6)-xylose side chains. They may also be β-(1-2)-linked to galactose, arabinose or fucose which in turn can be O-acetylated (Scheller & Ulvskov 2010). The collective resistance that plant materials pose to degradation from hydrolytic enzymes defines biomass recalcitrance and hemicelluloses are one of the

major contributors. Since they are the polymer which associates most closely with cellulose, they are likely involved in mediating deposition and determining wall strength (Somerville 2006). Their close associating acts to coat microfibrils effectively occluding cellulose and contributing to biomass recalcitrance.

Xylans are the most abundant noncellulosic polysaccharides in the primary and secondary walls of commelinid monocots and dicots respectively. Xylans possess a β-(1-4)-D-xylosyl backbone with occasional α-(1-2)-glucuronyl, α-(1-2)-4-O-methyl glucuronyl, arabinosyl and acetyl groups. Xylans are extracted by 4% KOH whereas xyloglucan extraction requires up to 24% KOH (Mohen *et al.* 2008). It is tempting to speculate that the increasing concentrations of base required for extraction reflects the extent of intermolecular hydrogen-bonding existing between the polymer and cellulose. Since hemicelluloses are in close association with cellulose, they may prevent self-aggregation of the microfibrils, tethering them to each other and other wall polymers (Scheller & Ulvskov 2010).

Analysis of the protein component of the wall reveals that the hydroxyproline-rich glycoprotein, extensin is a major component (Lamport 1971). This family of structural proteins is heavily and uniquely glycosylated with O-galactosyl serine and O-arabinosyl hydroxyproline (Lamport 1973). Extensins are self-assembling amphiphiles that generate scaffolding networks which are essential for wall development and plant viability (Cannon *et al.* 2008). These proteins intimately interact with pectins and together regulate wall functions.

Pectin refers to a mixture of heterogeneous, branched, and highly hydrated (non-crystalline) polysaccharides defined as material obtained from the cell wall upon

extraction with bivalent cation chelators (Carpita *et al.* 2000). They are likely the most structurally complex family of polysaccharides in nature and form a matrix that controls porosity, charge density and microfibril spacing within the cell walls. The gel-like property of the cell wall is derived in part from pectins. Like hyaluronan from animal cells, pectin contains multiple negatively charged saccharides that bind cations such as Ca^{2+} and become highly hydrated (Lodish *et al* 2000). Pure pectin tightly binds water and forms a semi-solid gel, a property exploited in the production of processed foods such as jams. Pectins are particularly abundant in the layer between the cell walls of adjacent cells called the middle lamella. Indeed, treatment of tissues with pectinase or other enzymes that degrade pectin frequently causes cells to lose their adhesion and separate from one another (Lodish *et al* 2000).

In addition to regulating cell-cell adhesion at the middle lamella, pectins are also involved in moderating wall pH and ion balance (Carpita *et al.* 2000). This is because they contain an α-(1-4)-linked galacturonic acid backbone (GalA). In fact, GalA accounts for 70% of cell wall pectin. There are three major types of this polysaccharide: homogalacturonan (HG), rhamnogalacturonan I (RG-I) and rhamnogalacturonan II (RG-II). HG is mostly a homopolymer of α-(1-4)-linked GalA residues accounting for approximately two thirds of pectin. HG can be methyl esterified at C-6 and O-acetylated at O-2 or O-3. RG-I accounts for 20-35% of pectin and consist of an alternating α-(1-4)-GalA and α-(1-2)-rhamnose polymer which is highly substituted with a variety of side chains at multiple sites (Mohen *et al.* 2008). RG-II is the most diverse and complex group of pectin which accounts for approximately 10% of pectin and contains 12 different types of sugars in over 20 different linkages (Mohen *et al.* 2008*)*. Due to its

structural complexity and heterogeneous composition, pectins are very amorphous and highly hydrated. As a consequence they are easily hydrolyzed and removed by mild aqueous washes. Pectins are an indispensable component and should be included in any investigation of cell walls. However, unlike cellulose and hemicellulose, pectins do not contribute significantly to biomass recalcitrance.

The distribution of the lignin, hemicellulose and pectin components differs between the two basic cell wall-types, primary and secondary. The primary wall is the first to be synthesized and is the terminal wall in many soft tissues of plants. Secondary walls, on the other hand, form between the primary wall and the plasma membrane at differentiation and provide most of the structural support attributed to cell walls. They contain less pectin, more cellulose, xylan and lignin than primary walls (Mohen *et al.* 2008). Primary cell walls are further divided into two types. Cells of dicotyledonous and non-commelinoid monocotyledonous plants are encapsulated by type-I primary cell walls. *Arabidopsis* and the vast majority of angiosperms produce type-I walls, which are characterized by cellulose microfibrils that are cross-linked by xyloglucans (Yokoyama & Nishitani 2004). Both polymers are present in approximately equal amounts and this cellulose-xyloglucan scaffold is embedded in a pectin polysaccharide matrix (Carpita *et al.* 2000). In contrast, type-II walls are generally pectin poor and the cellulose microfibrils are interlaced with glucuronoarabinoxylans (GAXs) (Carpita *et al.* 2000). Many current agriculturally significant crops and potential future bioenergy crops fall in the commelinoids clade of monocots and consequently have type-II primary walls. Some examples include: *Saccharum* (sugarcane), *Maize* (corn), *Triticum* (wheat), *Hordeum* (barely), *Avena* (oats), *Oryza* (rice), *Miscanthus* and *Panicum* (switchgrass). Given the

differences in the two types of walls, effects produced in *Arabidopsis* may not necessarily be directly transferable to commelinoids. Therefore, conclusions made about cell wall structure in *Arabidopsis* must be empirically verified with a member of the commelinoid family to ensure transferability to crops in the field such as maize.

Another important component of the cell wall matrix, especially in woody tissues, is lignin. Lignin is the most abundant non-polysaccharide wall polymer accounting for up to 30% of the composition of plant cell walls and contributes greatly to biomass recalcitrance. It is very abundant in wood and accumulates in the walls of the xylem. Lignin is a polyphenolic compound which forms a matrix surrounding hemicelluloses and cellulose microfibrils forming lignocellulose. Lignin provides strength against compression forces on the wall. It is composed of the phenylpropanoid monomeric units: *p*-coumaryl, coniferyl and sinapyl alcohols called monolignols which are biosynthesized from phenylalanine through the phenylpropanoid pathway (Carpita *et al.* 2000*)*. Lignin is relatively hydrophobic and is a major contributor to wall integrity through the crossing-linking of cell wall polysaccharides with covalent bonds. By having multiple monolignol monomeric units with each capable of interlinking through a variety of different bonds, lignin is a highly branched heterogeneous material with a complex three-dimensional structure (Schoemaker & Piontek 1996). The covalent nature of the bonds within lignin combined with the covalent cross-linking with other wall polymers, makes lignin essential for wall strength and integrity. This robust property consequently also fosters wall resistance to chemical and enzymatic degradation. This likely serves to provide plant cell walls with protection against pathogen invasion and herbivory by increasing the energy required to access and process the constituent sugars.

Lignin is required to maintain vascular plant morphology and lignin deficient mutants show gross phenotypic effects such as dwarfism and reduced viability precluding the option of simply removing it from the wall (Li *et al.* 2008). A deeper understanding of the lignin biosynthetic pathway is required to reduce its effects of recalcitrance on lignocellulosic biomass. Predominant incorporation of *p*-coumaryl, coniferyl and sinapyl alcohols forms *p*-hydroxyphenyl (H), guaiacyl (G) and syringyl (S) types of lignin respectively. The proportion of each type varies greatly between the walls of different terrestrial plant species. Although lowering the total amount of lignin results in decreased viability, it has been shown that raising the S/G ratio of lignin results in less Kraft pulping time in poplar (Carroll & Somerville 2009).

From an industrial perspective, the cellulose microfibrils which are in strong association with hemicellulose and lignin form what is commonly referred to as lignocellulose. Lignocellulosic biomass is one of the most abundant organic materials on the planet and is a substantial carbon sink. Examples include: all naturally occurring terrestrial vegetation such as trees, grasses and shrubs; waste biomass produced as low value byproducts from industries such as agriculture, paper and lumber; and finally, high yielding energy crops such as *Miscanthus* and switch grass engineered for rapid growth and reduced recalcitrance (Carroll & Somerville 2009). Lignocellulose is extensively cross-linked by covalent and hydrogen bonds and is a very robust material which resists hydrolytic degradation. Hydrolysis of lignocellulose releases its constituent monosaccharides, which can be subsequently fed to a variety of microorganisms to produce a diverse array of products. Most notably, biodegradable bio-polymers and cellulosic biofuels have the potential to greatly displace petroleum-based energy and

plastic demand. Cellulosic biofuels are biologically derived fuels produced with carbohydrates from lignocellulosic biomass as the sole carbon source for fermentation. For this reason and because of its abundance and low cost, lignocellulosic biomass has great potential as an energy feedstock. Plant biomass is therefore considered a renewable carbon-neutral resource and cellulosic biofuels offers a practical alternative to fossil fuels. Understanding the underlying mechanisms involved in cellulose biosynthesis and the genetic factors that promote wall hydrolysis sensitivity are necessary to facilitate the advent of cost-competitive cellulosic biofuels. The genetic and biochemical investigation of select mutants in the model organism, *Arabidopsis* provides the potential to improve our understanding of one of nature's fundamental processes.

In addition to understanding cellulose synthesis, one of the research goals here was to understand the nature of the association between various wall matrix polymers and their contribution to cell wall structure. Resistance to the digestive enzymes of pathogens and herbivores was developed in terrestrial plants likely as a result of strong selective pressures. This resistance has unfortunately translated to lignocellulose displaying exceptional recalcitrance to current hydrolytic strategies. The structure and organization of the cell wall pose significant barriers to the action of hydrolytic enzymes. Buried within the cell wall are the core cellulose microfibrils which are highly crystalline and chemically inert. The microfibrils are sequestered by sheaves of hemicellulose which are in turn covalently bonded to lignins (Somerville 2006). This matrix of heteropolymers in which cellulose microfibrils are embedded presents both physical and chemical barriers to degrading enzymes and significantly hinders hydrolysis.

1.1.2 Starch metabolism

Although starch is not a plant cell wall component, it is an effective and unconventional means to enhance biomass saccharification and increase yields. Many of the hydrolytic sensitive hits in the forward genetic screen of this study were in fact starch metabolism mutants warranting a review of starch structure and metabolism. The following brief introduction overviews the relevant structural and biosynthetic information required for this particular study.

Starch is an insoluble semi-crystalline polysaccharide and is the major energy carbohydrate storage in plants. Starch is stored as granules in plants and is comprised of two related polymers: amylose and amylopectin. Amylose is a linear polymer of α-1-4-D-glucose which often branches with addition of glucose side chains bonded via α-(1-6)-glycosidic linkages forming amylopectin. These chains aggregate and cluster forming insoluble semi-crystalline granules and organize into lamellae (Kotting *et al.* 2009). Pulse-chase experiments using $^{14}CO_2$ show that starch is synthesized during photosynthesis and is not simultaneously consumed resulting in the lack of turnover resulting in accumulation in *Arabidopsis* leaf tissue (Zeeman *et al.* 2002). The starch is hydrolyzed into maltose and glucose in order to sustain cell metabolism when energy from photosynthesis is unavailable. Starch granule metabolism requires a phase transition from a crystallized maltodextrin polymer into a soluble form. It has been shown by ^{33}P labeling experiments that this phase transition requires the phosphorylation of C-6 and C-3 of the amylopectin by glucan water dikinase (GWD) and phosphoglucan water dikinase (PWD) respectively in *Arabidopsis* (Kotting *et al.* 2009). Phosphorylation allows for solubilization of the glucan. The solubilized phosphoglucans must then be

dephosphorylated by the phosphoglucan phosphatase, Starch EXcess 4 (SEX4) in order to be further hydrolyzed by β-amylases (Hejazi *et al.* 2010). The lack of dephosphorylation results in accumulation of phosphoglucans and the inability to metabolize starch in SEX4 deficient mutants (Hejazi *et al.* 2010). These mutants accumulate up to three times more starch than wild-type in larger layered granules in *Arabidopsis* leaf tissue.

1.2.1 Cellulose biosynthesis

The cell wall is secreted by each plant cell and collectively forms a dynamic extensively inter-linked network with incredible strength and flexibility. These properties of the wall are mainly attributed to the molecular properties of cellulose, the main constituent of the wall. Currently, there is only a rudimentary understanding of the cellulose biosynthetic process and even less is known about the molecular factors involved in its regulation. A deeper understanding of cellulose biosynthesis has the potential to facilitate the advent of genetically engineered cellulosic biofuel energy crops and enhance herbicide resistance systems in existing commercial crops. Finally, cellulose biosynthesis could be manipulated and modified to manufacture novel cellulose bio-plastics with tunable properties.

Cellulose biosynthesis occurs on the exoplasmic face of the plasma membrane and produces insoluble cable-like structures known as microfibrils. In higher plants, these are thought to be comprised of 36 glucan chains held in a crystalline structure by hydrogen bonds and Van der Waals forces (Somerville 2006). All natural cellulose in plants consists of parallel glucan chains providing evidence for their simultaneous

production during microfibril synthesis. Cellulose microfibrils are assembled at the plasma membrane by cellulose synthase complexes. Cellulose synthase can be visualized microscopically by freeze-fracture as a membrane localized complex found at one end of cellulose microfibrils (Mueller & Brown 1980). It appears as six globular protein complexes arranged in a hexagonally symmetric manner with a diameter between 25 and 30 nm called rosettes or terminal complexes (TC) (Delmer 1999). Based on measurements from electron micrographs compared with calculated dimensions, it has been proposed that each of the six subunits of a rosette synthesizes six β-1, 4-glucan chains which subsequently co-crystallize to form a 36-chain cellulose microfibril (Somerville 2006). Cellulose synthase A (CESA) is a uridine diphosphate-α-D-sugar (UDP-sugar) dependent β-glycosyltransferase (Chamock *et al.* 2001). Like chitin and hyaluronan synthases, it belongs to the processive glycosyl transferase (GT) II family. This particular class of enzyme is characterized by the ability of its members to 'invert' the stereochemistry of the anomeric (C-1) of the donor UDP-sugar. In the case of cellulose synthase, the α-linked UDP-glucose is used to generate a β-linked product, namely cellulose (Figure 1.2.1). Due to the poor nucleophilicity of sugar hydroxyl groups, such inversions are thought to require the deprotonation of the acceptor by a base to facilitate nucleophilic attack at the anomeric carbon of the donor sugar (Chamock *et al.* 2001). The accepted general features of cellulose synthases includes a catalytic aspartate D acting as a base, a DxD motif required to complex metal ions to bind UDP-glucose and an additional D and a QxxRW motif in the glucan binding domain are features common in all CESAs (Saxana *et al.* 2001). Finally, it is well accepted that elongation occurs at

the non-reducing end of the chain which is supported by silver labeling experiments (Koyama *et al.* 1997) and x-ray crystal data (Jing & DeAngelis 2000).

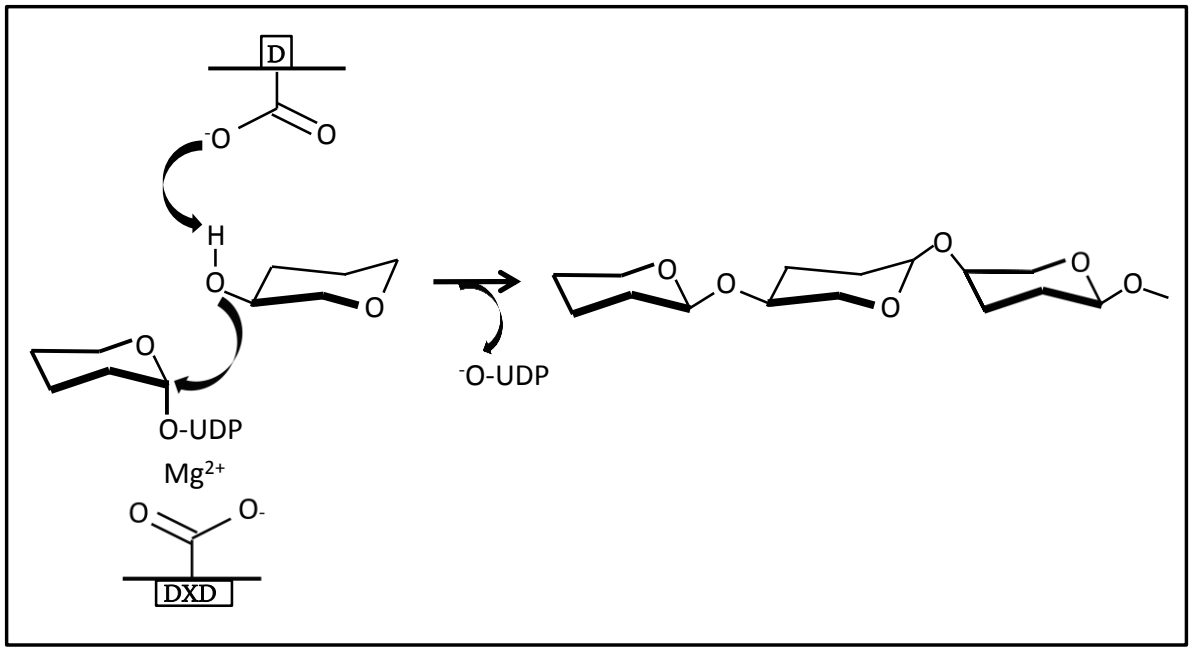

Figure 1.2.1: The putative mechanism for glycan synthesis in type-II glycosyl transferases. Chain elongation occurs at the non-reducing C4 end of glucose and is catalyzed by conserved aspartate residues represented by the boxed D and DXD. The stereochemistry of the anomeric carbon of the incoming glucose monomer is inverted during cellulose synthesis. The negatively charged phosphates of UDP are stabilized by DXD aspartate complexed Mg^{2+} ions. Catalytic aspartates enhance the nucleophilicity of the attacking hydroxyl and stabilize the incoming monomer (Adapted from Charnock *et al.* 2001).

1.2.2 Cellulose biosynthesis in *Gluconacetobacter xylinus*

The investigation of cellulose biosynthesis was pioneered in the Gram-negative bacterium, *Gluconacetobacter xylinus*. Although other genera of bacteria also produce cellulose, *G. xylinus* produces significantly larger quantities of the polymer. The cellulose is secreted and exists as a relatively pure, crystalline extracellular pellicle that is not incorporated as a composite in the cell wall like it is in plants. Given these characteristics, *G. xylinus* quickly became the model organism for the investigation of cellulose biosynthesis. Early spectroscopic experiments showed that UDP-glucose could serve as a substrate for some glycosyl transferases (Leloir 1971). The next breakthrough came more than a decade later when cellulose was synthesized *in vitro* for the first time at levels comparable to rates observed *in vivo* (Aloni *et al.* 1982). The synthesis required the presence of cyclic diguanylic acid (c-di-GMP) produced by diguanylate cyclase from guanosine triphosphate (GTP). The discovery of this activator of synthesis in *G. xylinus* enabled the purification and ultimately identification of an eighty-three kilo Dalton (kD) protein bound to cellulose (Lin & Brown 1989). This purified protein was later shown by the same group to also bind UDP-glucose solidifying its place as the putative catalytic subunit for cellulose biosynthesis (Lin *et al*. 1990). Soon after, an operon containing four genes in *G. xylinus* was isolated through genetic complementation in strains lacking cellulose synthase activity (Wong *et al.* 1990). The genes were named *bacterial cellulose synthase A, B, C* and *D* (*bcsA, B, C, D*). Eventually, the *G. xylinus bcsA* was found to harbor the catalytic subunit for cellulose synthase activity. Site-directed mutagenesis studies later revealed that substitutions of key conserved residues resulted in the drastic reduction or loss of cellulose synthase activity (Saxana *et al.* 1995). In the globular

region of all cellulose synthase catalytic subunits (CESA) exists putative catalytic aspartates and a glutamine-arginine-tryptophan (QxxRW) motif which are strictly conserved in all cellulose synthases (Saxana *et al.* 1995 and Saxana & Brown 1997).

Solved crystal structures for the non-processive spore-coat protein, SpsA from *Bacillus subtilis* has helped to suggest the conformation of the catalytic region of cellulose synthase subunits (Chamock & Davies 1999). Structural and functional data suggests that the nucleotide-binding domain (A domain) contains the "D, DxD" conserved D residues and the acceptor-binding (B domain) domain possesses a fourth invariant D in SpsA (Chamock & Davies 1999). Although SpsA shows strong sequence similarity to the catalytic domain of CESAs there are many differences which limit its use as a model. There is low similarity in the C-terminus region and the characteristic QxxRW sequence found only in type-II processive glycosyl transferases (GTs) is absent in SpsA.

Structural information on cellulose synthase from *bcsA* has been generated *ab initio* using genetic algorithms (Saxena *et al.* 2001). Protein structures were predicted by selecting for the "fittest" structures using basic protein building principles. The genetic algorithm predicts the QxxRW motif to be close to the central cavity containing the conserved aspartate residues believed to be the catalytic pocket (Saxana *et al*. 2001). The positioning and orientation of this motif along with mutagenesis studies have implicated its involvement in glucan binding. It has been predicted that the active site cavity can accommodate two UDP-glucose molecules and that polymerization occurs *via* the formation of a conformationally unstable cellobiose (Saxana *et al*. 2001). This model requires the existence of two catalytic centers per subunit and a two-glucose translocation

mechanism. Although evidence for two centered models exists for hyaluronan synthase in *Pasteurella multocida* (Jing & DeAngelis 2000), duplicated catalytic sites have not been observed in plant CESA proteins. Recently, a BcsA-BcsB complex was crystallized in *Rhodobacter sphaeroides* (Morgan *et al.* 2012). This group predicted a model of cellulose synthesis which occurrs through a single catalytic center composed of three aspartates. They argue that the nascent glucan chains translocated the membranes one glucose monomer at a time through a channel lined with conserved residues. In this model, the QxxRW motif is responsible for coordinating the incoming UDP-glucose and the 180^{o} rotation about the acetal of successive monomers is directed by steric constraints within the catalytic pocket.

Although much has been learned from studying cellulose synthesis in bacteria, translating this knowledge to the same process in plants has its limits. Even though working with *G. xylinus* to study cellulose biosynthesis is advantageous in many ways, there are many inherent differences in the process and function when compared to plants. The most important difference between cellulose synthesis in bacteria and plants is in the arrangement of the CESA subunits in the multimeric complex. Functional plant cellulose synthase complexes called 'rosettes' display six-fold symmetry. In contrast, the Bcs of bacteria are arranged into linear arrays resulting in cellulose with a different structure and function than the cellulose of plants. It seems that the inter-CESA interactions are not only essential for proper function but are also dynamic to accommodate the various tissue types and developmental stages found in plants (Carroll *et al.* 2012). The composition of rosettes and stoichiometric ratios contribute an additional layer of complexity unique to plant CESAs which is impossible to investigate in *G. xylinus*.

1.2.3 Cellulose biosynthesis in *Arabidopsis thaliana* and higher plants

As previously mentioned, unlike bacterial cellulose synthases (*bcs*), CESAs in plants are arranged into highly ordered multi-subunit structures with six-fold rotational symmetry called rosettes. Figure 1.2.3A shows the hypothetical model of the rosette structure composed of 36-CESA subunits. This model predicts that at least three types of CESA polypeptides are required for spontaneous rosette assembly, α_1, α_2 and β. Two different types of α isoforms can be distinguished, one which interacts with two isoforms α_2 and α_1 which interacts with only the β subunits.

*Arabidopsis cesA*s were initially identified based on sequence identity to *bcsA* genes from *G. xylinus.* In *Arabidopsis*, the *cesA* genes encode predicted integral membrane proteins ranging from 985-1088 amino acids in length each with eight putative transmembrane domains (TMD) (Delmer 1999). The TMDs are distributed as one cluster of two and another of six TM domains marking the boundaries between three major hydrophilic cytoplasmic domains (Figure 1.2.3B). The cytosolic N-terminal domain is 180-280 amino acids in length and includes a highly variable region (HVR) of unknown function. Additionally, they contain a cysteine-rich (CxxC) domain similar to the REALLY INTERESTING NEW GENE (RING)-type zinc-finger motif implicated in inter-CESA interactions (Kurek *et al.* 2002). The large, central, putative catalytic domain lies between the two TMD clusters and contains the D, DxD, QxxRW amino acid signature characteristic of many glycosyltransferases such as chitin, hyaluronan as well as glucosylceramide synthases (Holland *et al.* 2000*)*. Site-directed mutagenesis experiments involving the substitution of the D and QxxRW residues in chitin synthase II and cellulose synthase in *G. xylinus* showed that these residues are required for activity

(Nagahashi *et al.* 1995 and Saxena & Brown 1997). Site-directed mutagenesis also reveals that substitution of these conserved residues results in the loss of substrate binding in the cellulose synthases of *G. xylinus* and *Gossypium hirsutum* (cotton) and in the chitin synthase II of *Saccharomyces cerevisiae* (Saxena *et al.* 2001). Although the arginine to lysine substitution can be tolerated within the QRRRW domain of chitin synthase II, it results in reduced activity (Saxena & Brown 1997).

The globular region of CESAs in plants contains large insertions in the soluble domains not found in *G. xylinus* (Saxana *et al.* 2001). The insertions in the soluble loop have been identified as the plant-conserved region (P-CR) and class-specific region (CSR) (Figure 1.2.3B). As a result, the catalytic globular region in plant CESAs are considerably larger; around 530 amino acids in length compared to 285 amino acids in *G. xylinus*. The functional significance of these inserted regions is not currently known. However, it has recently been speculated that the P-CR/CSR forms lobes in the globular domain and participates in inter-CESA interactions. This is based on *in silico* models generated by aligning a CESA catalytic domain from *G. hirsutum* (cotton) with the CESA crystallographic data of *Rhodobacter sphaeroides* and the SpsA crystal data from *Bacillus subtilis* (Sethaphong *et al.* 2013). Limitations in modeling plant cellulose synthases without the availability of their crystal structures become more evident upon attempting to reveal protein interactions. Without knowing CESA conformations or the relative spatial orientation of potentially interacting groups, it is difficult to discern associations. Fortunately, as will be discussed later, the absence of this data does not preclude investigations of intermolecular CESA interactions by indirect means. Genetic complementation studies of cellulose deficient mutant lines along with the application of

chemical genetics allows for the exploration of CESA protein associations in *Arabidopsis*.

It has become apparent from genetic and biochemical studies in that the ten *cesA* genes in *Arabidopsis* (64% average amino acid sequence identity) have diverged enough for subfunctionalization (Taylor *et al.* 2003). For example, CESAs 1, 2, 3, 5, 6 and 9 show evidence to have roles in primary wall synthesis whereas CESAs 4, 7 and 8 synthesize secondary wall cellulose (Taylor *et al.* 2003 and Wang *et al.* 2008). Indirect evidence suggests that CESA1, 3 and 6 are involved in primary wall synthesis in *Arabidopsis*. For example, GFP-fused CESA3 and CESA6 are co-expressed and migrate together along the cell surface in the hypocotyls of etiolated seedlings (Desprez *et al.* 2007). In addition, CESA3 and CESA6 have been shown to co-immunoprecipitate using either anti-CESA3 or anti-CESA6 antibodies interchangeably under non-denaturing conditions (Wang *et al.* 2008). Membrane yeast two-hybrid (My2H) studies were conducted using constructs containing primary and secondary wall CESAs showing that primary and secondary CESAs interact and exhibit some cross-functionality (Carroll *et al.* 2012 and Timmers *et al.* 2009).

The cellulose deficiency phenotypes of *cesA1, 3* and *6* mutants suggest that they are required for primary wall synthesis and the varying severity of the phenotypes imply unequal contribution of each CESA to the overall catalytic activity of the complex (Persson *et al.* 2007). CESAs 2, 5 and 9 show high sequence similarity to CESA6 and are collectively known as CESA6-like subunits. While these CESAs can substitute each other in a complex, they are only partially functionally redundant. Differences in expression patterns amongst the CESA6-like proteins suggest that the subunit

composition of primary wall rosettes may be tissue type and developmental stage specific (Persson *et al.* 2007). Furthermore, null mutants of *cesA1* and *3* are lethal while null mutants of *cesA6*-like exhibit only mild growth defects (Persson *et al.* 2007). Although null mutants of *cesA2, 5, 6* or *9* show only mild growth-defective phenotypes, *cesA2, 6* and *9* triple mutants are gametophytically lethal (Persson *et al.* 2007). These results support the hypothesis that three unique components, CESA1, 3 and CESA6-like proteins, are required in primary cell wall cellulose synthase complexes.

Mutant analysis has also highlighted differences in the functional characteristics of CESA protein domains. Complementation of *radial swelling* mutants, *rsw*1/*cesA1* and *rsw*5/*cesA3* with chimeric proteins show that CESA C-terminal domains are specifically recognized by adjacent subunits in the cellulose synthase complex and are not interchangeable (Wang *et al*. 2006). The *rsw1-1* and *rsw5-1* mutations cause a temperature dependent cellulose deficiency phenotype resulting from an A(549)V change in the catalytic region of CESA1 or a P(1056)S amino acid substitution in the C-terminus of CESA3 respectively (Aroli *et al.* 1998). These mutants show radial root swelling phenotypes at the restrictive temperature (30^{o}C) but not at the permissive temperature (18 ^{o}C–20 ^{o}C). Chimeric constructs were made by swapping the N-terminus coding region up to the beginning of TMD1 of CESA1 and CESA3 (Wang *et al*. 2006). In this manner two chimeric proteins were created with the N-terminus of one CESA and the remainder of the protein from the beginning of TMD2 to the C-terminus of the other. The results from these experiments indicate that formation of functional CESA complexes requires placement of specific CESA subunits in a particular arrangement. It is the catalytic and/or C-terminal rather than the N-terminal domain which is recognized by adjacent

CESAs and permits access to their respective sites (Wang *et al*. 2006). The mutant *rsw*5 is particularly interesting since it implicates the C-terminal soluble region of CESA3 of being involved in inter-CESA associations (Wang *et al*. 2006). The C-terminal region of CESA proteins is a short cytoplasmic segment of around twenty hydrophilic amino acids. There is not much sequence similarity in this region of SpsA and plant CESAs, thus details about its 3-D structure remains unresolved.

Recently, a computationally predicted 3-D structural model of the 506 amino acids of cotton CESA within the catalytic cytosolic loop between TMD2 and TMD3 has become available (Sethaphong *et al*. 2013). This model predicts that the plant-conserved region (P-CR/CSR) folds into distinct subdomains on the periphery of the catalytic region. The computational results suggest that the P-CR/CSR form motifs which extend away from the catalytic center. These regions are speculated to be involved in inter-CESA interactions to form the multimeric cellulose–synthesis complexes (rosettes) that are characteristic of plants (Sethaphong *et al*. 2013).

It has been suggested that the CESA proteins undergo phosphorylation and may be regulated at the protein level in such a manner (Chen *et al*. 2010, Taylor 2007 and Somerville 2006). Through LCMS/MS analysis of plasma membrane fractions, several phosphorylation sites were identified in the CESAs clustered at the N-terminus (Nuhse *et al*. 2004). Targeted proteolysis of the secondary wall subunits *via* the proteasome was shown to be linked to phosphorylation (Taylor 2007). More recently, serines known to be phosphorylated were mutated to disrupt phosphorylation. Modulation of CESA1 sites resulted in cellulose deficiency phenotypes (Chen *et al*. 2010). In addition, over-expression of purple acid phosphatase was shown to activate membrane bound

cellulose/callose synthases in tobacco cell culture further suggesting CESA activity being modulated by phosphorylation (Kaida *et al*. 2009). Moreover, over-expression of the plasma-membrane-bound receptor-like kinase, THESEUS1 (THE1) decreased the growth inhibition and enhanced ectopic lignification phenotypes in the etiolated seedlings of *procuste1* (*cesA6*) (Hematy *et al*. 2007). The authors suggest that THE1 mediates the response of elongating cells to the perturbation of cellulose synthesis and may act as a cell-wall-integrity sensor. As intriguing as this evidence may be, direct evidence for the interaction of any particular purple acid phosphatase or kinase with CESAs remains elusive.

Mutants of a number of non-*cesA* genes have been observed to display cellulose deficiency phenotypes. For instance, the *korrigan* (*kor*) gene encodes a membrane β-1,4 glucanase which when knocked-out exhibits reduced cellulose accumulation and altered pectin composition (Nicol *et al*. 1998). It is plausible that KOR may have a role in removing non-crystalline glucan chains from the growing microfibril contributing to processivity (Somerville 2006). Another protein implicated in cellulose biosynthesis is COBRA (COB), a glycophosphatidylinositol (GPI) anchored protein found in the cell wall. Mutations in the COB gene have been shown to result in extremely dwarfed and cellulose deficient plants (Roudier *et al*. 2005). Also, *chitinase-like-1* (*ctl1 /pom1*) mutants display reduced root cell expansion and decreased cellulose content (Hauser *et al*. 1995). Recently, POM1 has been implicated in cooperatively affecting glucan chain assembly and mediating CESA-microtubule interaction (Sánchez-Rodríguez *et al.* 2012). Although it is quite conclusive that the proteins mentioned contribute to cellulose synthesis to some extent, the contribution of other proteins is somewhat more

contentious. For instance, there is conflicting evidence whether SUCROSE SYNTHASE (SuSY) is associated with the cellulose synthases. It has been proposed that SuSY is a major component of the catalytic unit of the cellulose synthase complex (Fujii *et al*. 2010). However, a quadruple mutant of four sucrose synthase genes, in which sucrose synthase activity is severely diminished, shows no difference in cellulose content in stems when compared with wild-type in *Arabidopsis* (Barratt *et al*. 2009). The genetic evidence indicates that SuSY it is a non-essential component of cellulose biosynthesis in *Arabidopsis* in contradiction to the biochemical evidence.

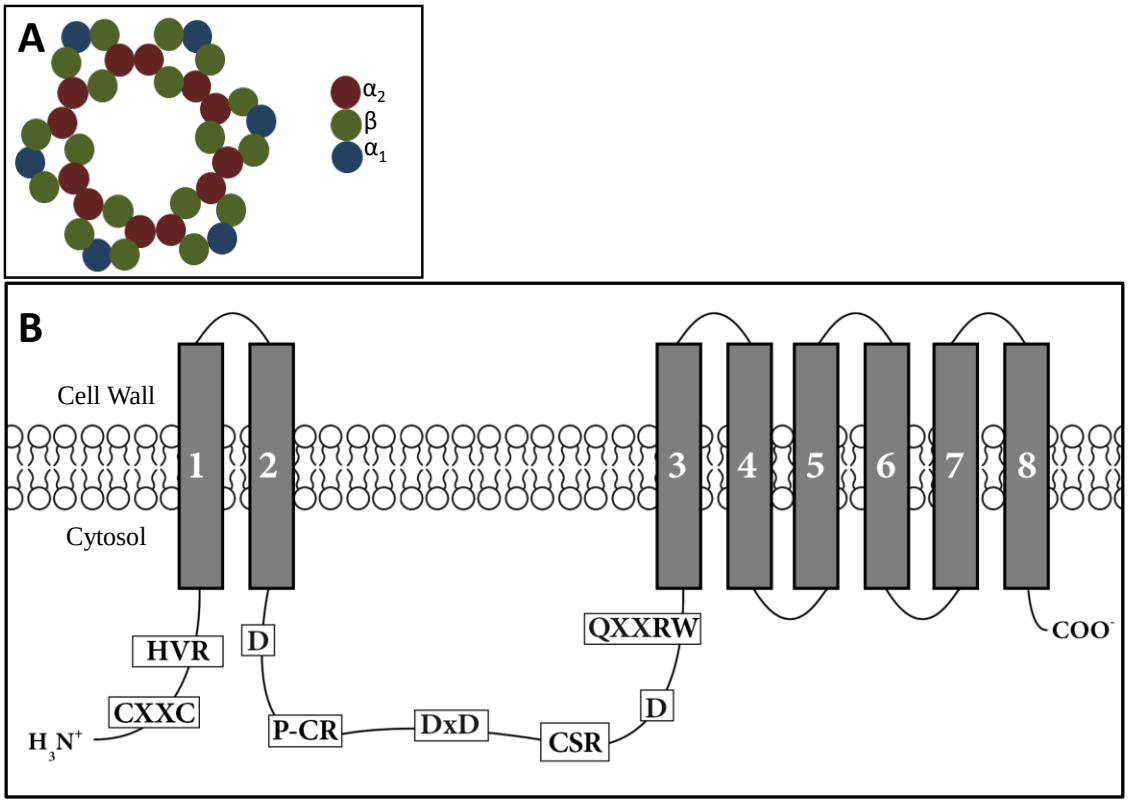

Figure 1.2.3: General features of CESAs.

A) Illustration of the hypothetical rosette model for plant CESAs. Rosettes are composed of thirty-six CESA subunits of at least three different types based on the inter-CESA interactions required (Adapted from Doblin *et al*. 2002).

B) Cartoon illustration of an individual CESA subunit based on amino acid sequence analysis. CESA subunits contain eight transmembrane domains (TMD) in two clusters and a large cytosolic domain between them containing the catalytic aspartates (D, DxD,D) and the QxxRW domain. The plant-conserved region (P-CR) and class specific region (CSR) also lie in this region between TMD 2 and TMD 3. The cytosolic domain N-terminal to TMD 1 contains both a conserved CxxC domain and a hyper variable region (HVR) (Adapted from Scheible *et al*. 2001).

1.2.4 Summary

Cellulose is made by type-II glycosyl-transferases in plants called CESAs. They have characteristic features which include: Catalytic aspartates, QxxRW and P-CR regions in the large soluble domain along with 8 TMDs. They organize into symmetric complexes of approximately 36 CESAs called rosettes. Although the exact stoichiometric ratio is not known, functional rosettes consist of at least 3 different types of CESA subunits: CESA4, CESA7 and CESA8 for secondary wall synthesis and CESA1, CESA3 and a CESA6-like for primary wall synthesis. Both genetic and biochemical evidence supports the assertion that primary CESAs interact, and that this interaction is essential for rosette assembly and ultimately cellulose production. Many non-CESA proteins have been implicated in playing a role in cellulose biosynthesis but evidence of direct association with the complex remains elusive. It is likely that microfibrils have to undergo modification by non-CESAs in order to effectively perform their function but the extent these proteins are involved is not currently known.

1.3.1 Cellulose biosynthesis inhibitors (CBIs)

Cellulose biosynthesis inhibitors (CBIs) are applied in order to probe the underlying molecular processes of cellulose synthesis. CBI's are a chemically diverse group of small molecules that have been shown to specifically reduce cellulose production (Heim *et al.*1989 and Strap *et al.* 2011). The CBIs this study will be discussing in extensive detail are isoxaben and flupoxam. Although it is known that these molecules disrupt the cellulose biosynthetic pathway through indirect methods, the exact mode of action remains elusive. Despite this, CBIs are applied to induce loss of function chemically on

to a mutagenized population and the genes responsible for genetic rescue are examined. Due to the specificity of the CBIs, genes uncovered through this forward genetic approach will likely be involved in the process of cellulose biosynthesis.

Isoxaben (N-3[1-ethyl-1-methylpropyl]-5-isoxazolyl-2,6-dimethoxybenzamide) is an extremely potent pre-emergent herbicide with an IC50 of 4.5 nM in *Arabidopsis* (Heim *et al.* 1989). It is a small and hydrophobic molecule with a molecular weight of 332.4 g/mol and a very hydrophobic $\log K_{ow}$ of 3.90 at pH 7. The structure of isoxaben is given in Figure 1.3.1A. Sensitive plants growing in the presence of isoxaben fail to incorporate ^{14}C-glucose into cellulose in *Arabidopsis* (Heim *et al.* 1989). Exposed non-resistant plants lose cell anisotropy due to a loss of cell wall integrity. The lack of cellulose diminishes the mechanical strength of the wall and is unable to withstand the turgor pressures causing the cells to grow isotropically. Mutations that confer high degrees of ISOXABEN RESISTANCE (IXR) are of interest since they indirectly reveal information about the mechanics of cellulose biosynthesis and CESA proteins. Single amino acid substitutions in the C-terminal region of CESA3 and CESA6 have previously been implicated in isoxaben resistance in *Arabidopsis* (Scheible *et al.* 2001 and Desprez *et al.* 2002). It is speculated that isoxaben specifically binds and prevents CESA3-CESA6 association in primary wall rosette assembly. This notion is supported by the semidominant, allele specific nature of the resistance phenotype.

Flupoxam 1-[4-chloro-3-(2,2,3,3,3-pentafluoropropoxymethyl)phenyl]-5-phenyl-1*H*-1,2,4-triazole-3-carboxamide is a tricyclic aromatic triazole herbicide (Figure 1.3.1B). The effects of flupoxam are similar to that of isoxaben with a similar IC50. In cultured cotton fibers, isoxaben and flupoxam produce spherical cell protrusions, detachments of

the plasma membrane from the cell wall, increased pectin accumulation, wall thinning and reduced cell division along with incipient vacuole formation (Vaughn and Turley 2001). Sensitive plants exposed to flupoxam will result in reduced cellulose incorporation, decreased root and hypocotyl elongation and a loss of anisotropy of the cells. Much less research has been conducted on this herbicide and there are currently no resistant alleles available in literature.

Pellicin ([2E]-3-phenyl-1-[2,3,4,5-tetrahydro-1,6-benzodioxocin-8-yl]prop-2-en-1-one) is named for its ability to abolish pellicle production in *G. xylinus*. The structure of Pellicin is given in Figure 1.3.1C. It was identified in a chemical genetics screen of 10,000 small molecules (Strap *et al.* 2011). Although the mechanism of action remain elusive, it is deemed a CBI because of it specific effects. Indeed, Pellicin treated pellicles exhibited much lower crystallinity and a decrease in the production of type-I cellulose (Strap *et al.* 2011). This observation illustrates the difference in the process in the two organisms. Pellicin was found only in the extra-cellular fraction of treated bacterial cells determined by high performance liquid chromatography (HPLC), suggesting that the molecule acts by inhibiting crystallization outside the cell. Interestingly, Pellicin appears to have no direct effect on cellulose biosynthesis in *Arabidopsis.*

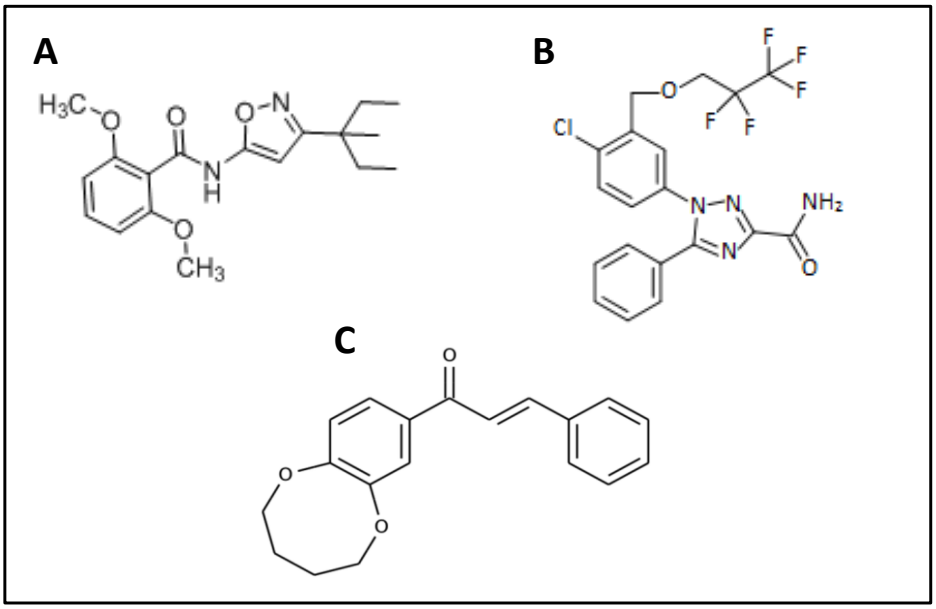

Figure 1.3.1: Chemical structures of the cellulose biosynthesis inhibitors (CBIs) discussed in this study.

A) The chemical structure of isoxaben (isx).

B) The chemical structure of flupoxam (fsx).

C) The chemical structure of Pellicin.

1.3.2 Isoxaben resistance (IXR)

Isoxaben inhibits the incorporation of glucose into cellulose microfibrils with an I_{50} of 4.5 nM in *Arabidopsis* and is a specific inhibitor of cellulose biosynthesis (Heim *et al.* 1989). Mutations in the C-termini of CESA3 and CESA6 proteins, designated *ixr1* and *ixr2* respectively, confer resistance to high concentrations of isoxaben (Scheible *et al.* 2001 and Desprez *et al.* 2002). Homozygous *Arabidopsis* mutants with the *ixr1-1* G(998)D and *ixr1*-2 T(942)I alleles are 300 and 90 times more resistant to isoxaben than wild-type (Scheible *et al.* 2001). The G998D substitution of *ixr1-1* results in the insertion of a charged residue in the N-terminus end of TMD8 and the T(942)I substitution of *ixr*1-2 occurs in the extra-cellular loop between TMD7 and TMD8 of CESA3 (Scheible *et al.* 2001). Finally, the *ixr2* mutation results in a R(1064)W amino acid substitution in the soluble C-terminus domain of CESA6 (Desprez *et al.* 2002). These single amino acid substitutions appear to affect the herbicide target since no alteration in uptake or detoxification of the herbicide is observed in the *ixr* mutants (Scheible *et al.* 2001). Allele specific CBI resistance in *ixr1* and *ixr2* suggests that CESA3 and CESA6 interact in a manner which is disrupted by isoxaben in wild-type. The semi-dominant characteristic of isoxaben resistance supports the previously proposed model of the functional rosette being composed of three distinct types of interacting CESA subunits. In the heterozygous state, the mutant subunits are present along with wild-type CESAs forming rosettes with varying composition; accounting for intermediate resistance to isoxaben (Scheible *et al.* 2001). The observation of isoxaben inhibiting primary wall synthesis and resistance arising only from modifications of primary wall CESA subunits further validates this model. Since the *ixr* mutants have no distinguishing phenotype in

the absence of the herbicide, the isoxaben binding site(s) must be separate or only partially overlap with the inter-CESA binding sites. This would account for the observed herbicide resistance in the absence of any cellulose deficiency phenotypes. With the exception of the catalytic region, structural modeling data remains elusive for all CESA components. Therefore, this CESA interaction model mediated by the C-termini association which is disrupted by isoxaben binding is still speculative and direct evidence for the physical interaction of this nature is not currently available.

Substitutions conferring resistance to isoxaben are not restricted to the C-terminal regions. Indeed, *ixr1-6* S(377)F introduces a bulky side chain next to the most N-terminal catalytic aspartate, resulting in decreased cellulose content, crystallinity, plant height and most interestingly confers resistance to isoxaben (Latsavongsakda *et al*. 2013). Also, the absence of resistance alleles in any other genes apart from *cesA3* and *cesA6* supports the model of the herbicide acting by disrupting the required interaction of these two CESAs and preventing cellulose biosynthesis. Further characterization will shed more light on isoxaben's mode of action and will be discussed in greater detail in the results and discussion sections of the following chapter.

1.3.3 Summary

Isoxaben and flupoxam are pre-emergence herbicides and are known CBIs in plants. They specifically inhibit the incorporation of glucose into cellulose by an unknown mechanism. Point mutations conferring resistance to high concentrations of isoxaben have clustered to a 100 amino acid region adjacent to the C-termini of CESA3 and CESA6 (Scheible *et al.* 2001 and Desprez *et al.* 2002). Only three alleles of *isoxaben*

resistance (*ixr)* have been described and there are no entries regarding flupoxam resistance available in published literature. The reported *ixr* alleles all produce proteins carrying a single amino acid substitution in regions near the C-termini of CESA3 and CESA6. In light of the compelling evidence for requisite CESA3-CESA6 interaction in primary wall synthesis along with the allele specific nature of isoxaben resistance, it is reasonable to speculate that the herbicide acts by disrupting this particular association.

1.4.1 Influence of polar auxin transport on plant cell wall integrity

Auxins are a group of ubiquitous and essential small molecule phytohormones. Auxins are multifunctional plant hormones which influence virtually every facet of plant growth and development. The most common and archetypical auxin is indole-3-acetic acid (IAA) and is generally synonymous with the word 'auxin' (Figure 1.4.1A). Considering the ubiquitous nature of the auxin hormones in plant physiology, it comes as no surprise that they have been observed to be intimately involved in cell wall modification during cell growth. Auxins have been implicated in playing an essential role in wall-expansion by 'Acid Growth'. The Acid Growth Theory states that when susceptible cells are exposed to auxin, they increase excretion of protons into the extracellular space of the wall resulting in a decrease in apoplastic pH (Rayle and Cleland 1992). The lowered wall pH then activates 'wall-loosening'proteins. By loosening the wall in the presence of an increased turgor force, individual plant cells can expand rapidly. The plant cell wall has high tensile strength and polysaccharide chains must be loosened to accommodate growth or irreversible expansion. The outward turgor force required for cell growth in higher plants is achieved through increasing the volume of the cytosol and vacuole. The

direction of cell expansion is determined by localized loosening of the primary cell wall induced by auxin mediated expansins (Cosgrove 2000).

The first expansins were isolated from extracts from the growing hypocotyls of dark-grown cucumber seedlings (McQueen-Mason *et al.* 1992). These small wall-loosening proteins could only be isolated in the active form in the walls of rapidly growing cells and each alone possessed the ability to induce cell wall extension in heat-inactivated cell walls (McQueen-Mason *et al.* 1992). These 29-30 kD proteins, now known as α-expansins, mechanically weaken pure cellulose paper in extension and stress relaxation assays without any detectable cellulase activity (McQueen-Mason & Cosgrove 1994). Furthermore, the expansin-triggered loosening of the wall is reversed when the pH is neutralized showing that expansin does not break covalent bonds in cellulose.

The currently held model is that expansion of the wall surface area involves slippage or movement of cellulose microfibrils through the expansin mediated disruption of non-covalent interactions. By loosening the linkages between cellulose microfibrils, expansins allow the wall to yield to the tensile stresses created in the wall through turgor pressure enabling polymer advance (Cosgrove 2000). The molecular mechanistic details by which expansin loosens the cellulosic network remains to be elucidated. X-ray crystallography data of a β-expansin found predominantly in grasses has fostered the hypothesis that the wall-loosening action of the protein on the wall is through the disruption of the hydrogen bonding of hemicellulose on the surface of cellulose microfibrils (Yennawar *et al.* 2006). Hemicelluloses extensively cross-link cellulose microfibrils together, forming a strong load-bearing network. Expansin is thought to

transiently disrupt the cellulose-hemicellulose association allowing slippage and movement of cell wall polymers accommodating growth (Yennawar *et al.* 2006).

Given the central role of auxin in cell growth in plants, it is not surprising to find the hormone involved in cell wall expansion and cellulose biosynthesis. Auxin indirectly promotes the activity of expansins which loosen the cell wall. Auxin flow is achieved by the localization of PIN-FORMED auxin-transport proteins (PIN). It has also been shown that polar PIN localization is disrupted when the cellulose microfibrils of the wall are degraded and wall integrity compromised (Feraru *et al*. 2011). PIN localization is required to direct the auxin flow and ultimately dictates extension-mediated wall loosening. It is becoming apparent that auxin affects cellulose deposition or even synthesis but the mechanistic details remain obscure. Interestingly, the isoxaben resistant allele, *ixr1-1* was found to have increased tolerance to 1-N-naphthylphthalamic acid (NPA), a polar auxin transport inhibitor (Tegg *et al.* 2013). Isoxaben was also observed to induce hyperalignment of both PIN1 and microtubules to predicted stress directions (Heisler *et al.* 2010). Additionally, a weak allele of *cesA3* carrying the amino acid substitution P(578)L was found to cause PIN localization defects and resistance to isoxaben (Feraru *et al*. 2011). These findings suggest that there is a direct link between auxin transport and cellulose biosynthesis, but future work is needed to elucidate the mechanistic details.

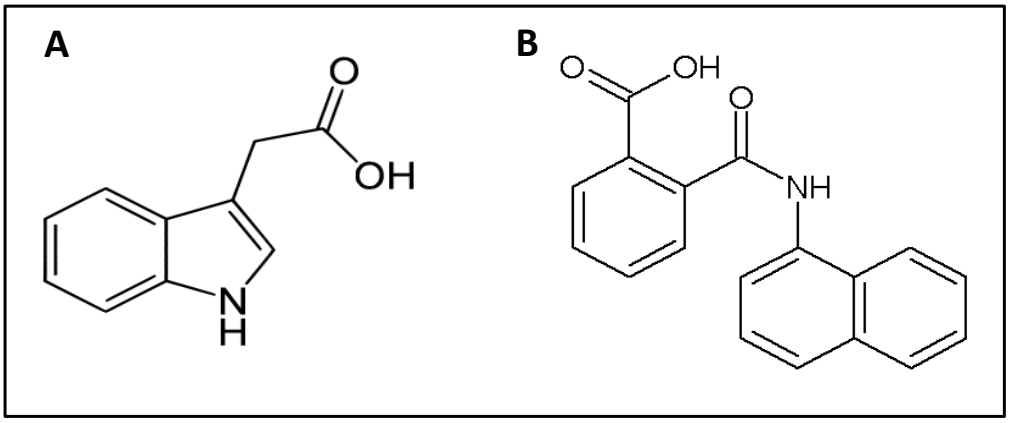

Figure 1.4.1: Chemical structures of a natural auxin and synthetic auxin transport inhibitor.

A) The chemical structure of indole-3-acetic acid (IAA).

B) The chemical structure of napthylphthalamic acid (NPA).

1.5 Rationale

Cellulose is one of the most abundant organic compound on the plant and is an underutilized feedstock for biofuel and many other potential applications. The development of cellulosic technology is currently limited by biomass recalcitrance resulting in prohibitively high costs to access and degrade the bio-polymer. The challenge lies in enhancing accessibility and decreasing crystallinity of the cellulose without compromising the organism's viability. Forward genetic screens directed at enhancing cellulose accessibility and perturbing the cellulose biosynthetic pathway were conducted in this study to gain insights into the complex and dynamic processes involved in plant cell wall development. Forward genetic screens have no mechanistic bias and can potentially uncover novel processes that improve saccharification and shed light towards elucidating the cellulose biosynthetic pathway. Cellulose biosynthesis inhibitors (CBI) are small molecules which specifically obstruct this process by various and mostly unelucidated mechanisms. Investigation of mutants with heritable resistance to isoxaben and flupoxam were conducted in this study and will shed light on the molecular details of the mode-of-action of these herbicides and provide insights and information about cellulose biosynthesis in general. Further study of mutants with improved wall degradation profiles and CBI resistance will help inform novel approaches in the development of energy crops and enhanced herbicide and resistance systems for existing crops. This study will describe genetic and chemical enhancement of biomass saccharification utilizing cellulase, xylanase, peroxidase and amylase to target cellulose, hemicellulose, lignin and starch respectively.

Chapter 2: Forward Genetic Analysis of Cellulose Biosynthesis Inhibitor Resistance in *Arabidopsis thaliana*

2.1 Introduction

In order to clarify the current understanding of isoxaben and flupoxam and to gain a deeper understanding about cellulose biosynthesis, a forward genetic screen for resistance was conducted. A screen of one million mutagenized M2 seeds generated twelve novel resistance mutant lines carrying mutations exclusively in primary wall CESAs. Analysis of radiolabeled glucose incorporation rates into cellulose revealed that CBI resistance conferring perturbations of the primary wall subunits need not result in negative effects to the catalytic activity of the CESAs. Furthermore, almost all of the CBI resistant mutants showed decreases in crystalline cellulose which translated to enhanced hydrolytic sensitivity against enzymatic digestion schemes. A subset of double mutants, homozygous for isoxaben and flupoxam resistance alleles exhibited genetic complementation providing additional evidence for primary CESA interaction.

The mode of action of isoxaben is also investigated from the perspective of the herbicide. Evidence is presented suggesting that the parent compound need not be the only biologically active structure. Indeed, isoxaben contains a labile bond that when broken is able to recyclize into a structure resembling flupoxam. Chemically reduced-isoxaben (isxH) is a distinct compound and behaves indistinguishably from its parent. Chemical analogues of isxH were tested on *Arabidopsis* yielding interesting results. These analogues elicit interesting glycan biosynthesis inhibitory and auxin-like effects. These structures and approaches will give the examination of CESA-CBI interactions new tools and additional perspectives in the future.

2.2 Results

2.2.1 Ethyl methane sulfonate (EMS) mutagenesis generated *isoxaben resistance* (*ixr*) and *flupoxam resistance* (*fxr*) alleles

Novel mutations that confer resistance to isoxaben or flupoxam were generated in the *Landsberg erecta* (*Ler*) eco-type of *Arabidopsis* by ethylmethyl sulfonate (EMS) mutagenesis. Twelve mutant lines were found to be resistant to 20 nM of either herbicide in a semi-dominant fashion although none were cross-resistant. Six lines were resistant to isoxaben and six to flupoxam. Over one million M2 seeds were sown and the M3 generation was retested on the herbicides. All twelve of the mutant lines were found to harbour a single nucleotide polymorphism (SNP) in a primary wall *cesA* resulting in an amino acid substitution (Table 2.2.1). These SNPs were found by sequencing the genes for CESA1, 3 and 6. Representative chromatograms from each of the primary wall *cesA*s are shown in Figure 2.2.1B and indicate that the lines are indeed homozygous for their respective alleles.

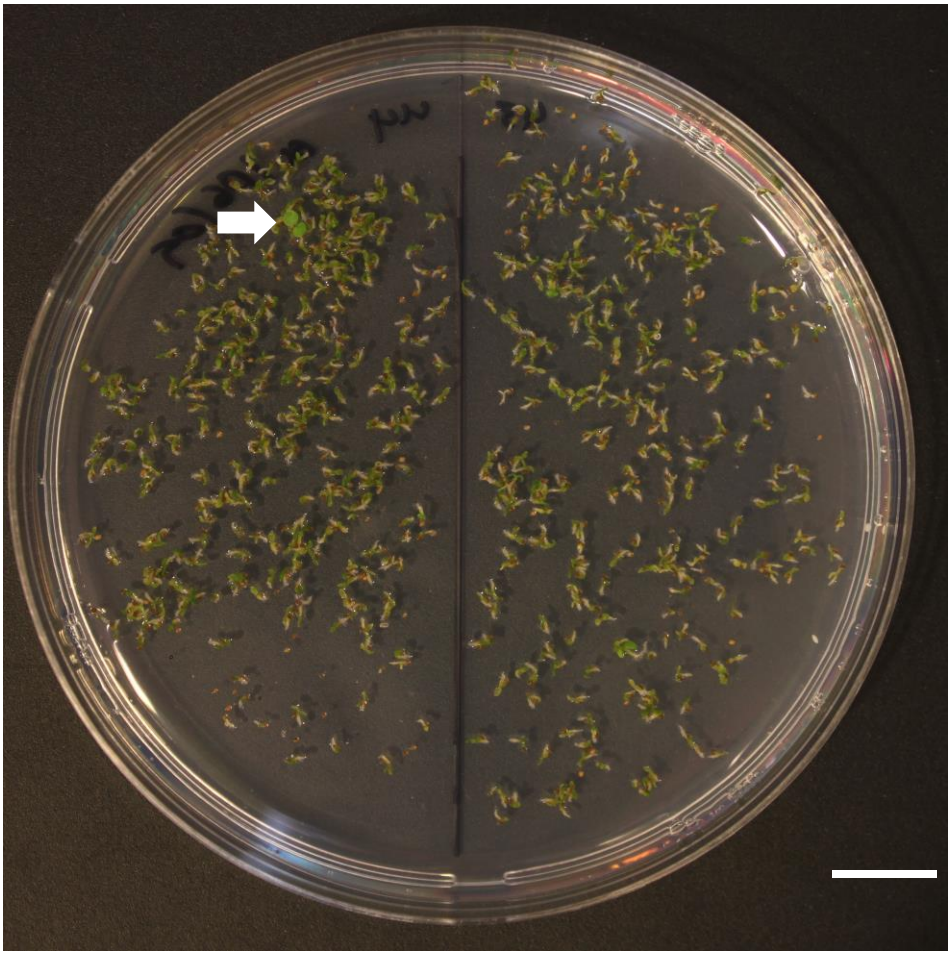

Figure 2.2.1A: An example of a plate used in the selection for CBI resistant mutants. The top left quadrant of the agar plate image shows a mutant line displaying the resistant phenotype being selected for in this screen (arrow). This screening method was incredibly high throughput and the resistance phenotype was easily identified (bar = 1 cm).

Table 2.2.1: List of isoxaben and flupoxam resistant alleles. Some mutants on this list: *ixr1-1, ixr1-2* and *ixr2-1* have been described previously (Scheible *et al.* 2001 and Desprez *et al.* 2002) and others: *ixr1-1B* and *fxr1-1* are unpublished and were generated (Bonetta unpublished).

Eco-type	**Allele**	**Codon Change**	**Substitution**	**Protein**
Col	*ixr1-1*	GGT → GAT	G(988)D	CESA3
Ler	*ixr1-1B*	GGT → GAT	G(998)D	CESA3
Col	*ixr1-2*	ACC → ATC	T(942)I	CESA3
Ler	*ixr1-3*	GGT → AGT	G(998)S	CESA3
Ler	*ixr1-4*	AGG → AAG	R(806)K	CESA3
Ler	*ixr1-5*	CTT → TTT	L(797)F	CESA3
Ler	*ixr1-6*	TCT → TTT	S(377)F	CESA3
Ler	*ixr1-7*	CGT → CAT	R(279)H	CESA3
Col	*ixr2-1*	CGG → TGG	R(1064)W	CESA6
Ler	*ixr2-2*	TCT → TTT	S(1002)F	CESA6
Col	*fxr1-1*	TCG → TTG	S(1040)L	CESA3
Ler	*fxr1-2*	TCT → TTT	S(1037)F	CESA3
Ler	*fxr1-3*	TCT → TTT	S(983)F	CESA3
Ler	*fxr2-1*	GGG → AGG	G(1013)R	CESA1
Ler	*fxr2-2*	CCG → CTG	P(1010)L	CESA1
Ler	*fxr2-3*	GGT → GAT	G(1009)D	CESA1
Ler	*fxr2-4*	TCG → TTG	S(307)L	CESA1

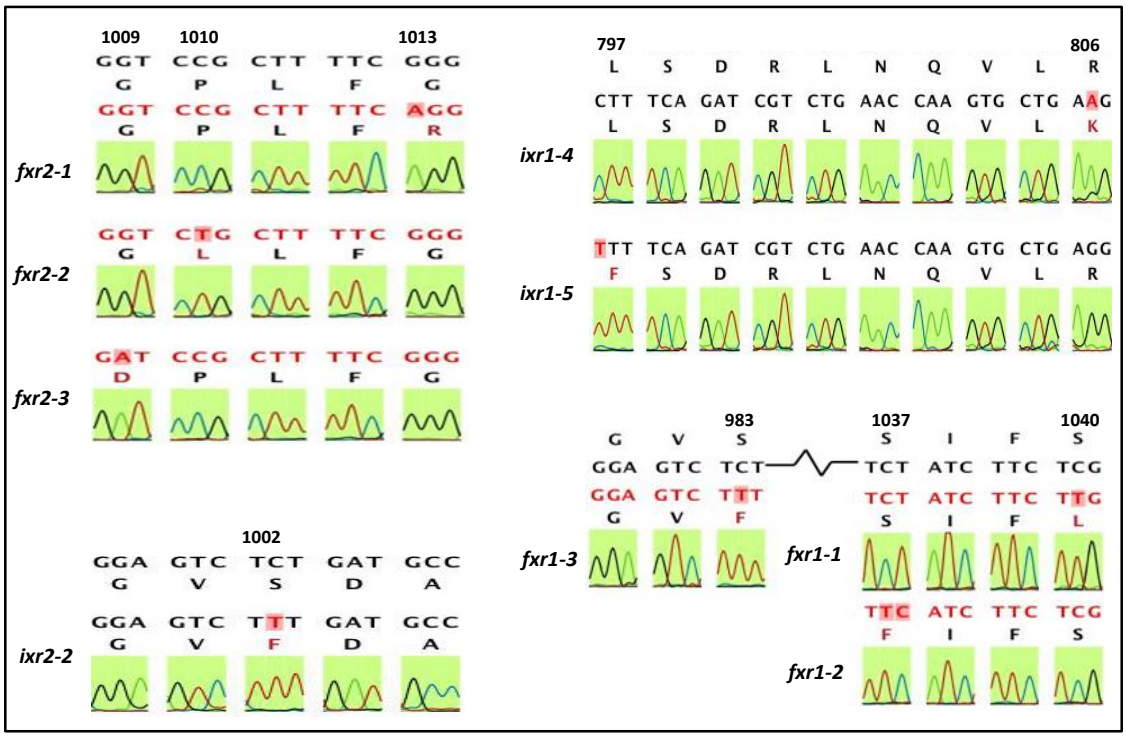

Figure 2.2.1B: Chromatograms from Sanger sequencing of select mutants. DNA was amplified and sequenced using BigDye® termination. Chromatograms have been aligned to show the proximity of some of the substitutions to each other. The nucleotides changed are highlighted in red. Above the chromatograms are the corresponding amino acid and nucleotide sequences for the *Ler* wild-type along with the amino acid position for substitutions.

2.2.2 Alleles of *cesA1* and *cesA3* confer flupoxam resistance (*fxr*)

Compared to isoxaben, much less is known about flupoxam and its mode of action. For instance, there are currently no published alleles for *flupoxam resistance* (*fxr*). This study produced six *fxr* alleles found in only two genes. The primers used to amplify the regions containing the SNP are shown in Table 2.3.2. The alleles on *cesA3* and *cesA1* were designated *fxr1* and *fxr2* respectively. Flupoxam and isoxaben both produce the same effects on sensitive plants with similar IC50 values. Interestingly, *fxr1-2* displays reduced fertility and reduced plant height. With flupoxam resembling isoxaben in its effects on plants, it is natural to suggest that they have similar mechanisms of action. Evidence from this study suggests that flupoxam inhibits cellulose synthesis by disrupting the CESA1-CESA3 interaction. The primary wall deficiency phenotypes of mutants such as *fxr1-2* further suggest that the inter-CESA binding site overlaps with the herbicide binding site(s). Considering that no cross-resistant line has been isolated, that is a line containing one allele which confers resistance to both herbicides; it is tempting to propose that both herbicides target two separate sites on the same complex. Isoxaben and flupoxam both disrupt the primary wall complexes with the former targeting the CESA3-CESA6 and the later the CESA3-CESA1 interactions.

2.2.3 Clustering of IXR and FXR provides support for primary wall CESA interaction

The allelic series that we have isolated points to a number of interesting aspects of CESA complex assembly. Isoxaben resistance is localized to CESA3 and CESA6, whereas flupoxam resistance is only found on CESA3 and CESA1. A local alignment of the primary wall CESAs is shown in Figure 2.2.3A. This alignment reveals that *fxr1-3* and *ixr2-2* both substitute the same serine for phenylalanine in CESA3 and CESA6 respectively. *fxr2-1* results in G(1013)R amino acid substitution on CESA1 which corresponds to G(99)8 in CESA3. *ixr1-1* and *ixr1-3* produce CESA3 is G(998)D and G(998)S substitutions respectively. The same glycine being substituted three times independently suggests that it is a key residue for resistance to both herbicides. Since no single allele confers resistance to both herbicides, the two herbicides likely bind to distinct sites, but this does not preclude both binding to the same complex. Indeed, the clustering of *fxr2* mutations on the C-terminus of CESA1 and of *ixr1* and *fxr1* to the C-terminus of CESA3 appears to define a highly conserved region where the action of the herbicides takes place.

Approximately half of the mutants resistant to the CBIs results from the substitution of a serine residue to phenylalanine or leucine in a primary wall CESA. Both Figure 2.2.3B and Figure 2.2.3C show cartoon depictions of a generic CESA with the relative positions of the CBI resistance alleles of this study. All alleles of *ixr* and *fxr* reside in genes encoding primary wall CESAs. Furthermore, an allele of CESA1 confering resistance to isoxaben has not been observed. Similarily *cesA6* never harbours flupoxam resistance alleles. However, *cesA3* possess both *ixr* and *fxr* alleles. Based on this evidence as well as with evidence existing in literature (Delmer 1999, Scheible *et al.*

2001 and Desprez *et al.* 2002), a model for primary CESA rosette assembly is proposed (Figure 2.2.3D). This model predicts a stoichiometric ratio of CESA1: CESA3: CESA6 of 2:3:1 with CESA1 only interacting with CESA3 and CESA3 interacts with both CESA1 and CESA6. Although this model fits available evidence, it is highly speculative and further direct evidence for this stoichiometric ratio of CESA is necessary. Isoxaben and flupoxam most likely bind at the junctions of CESA3-CESA6 and CESA1-CESA3 respectively eliciting subunit dissociation.

Many substitutions can independently confer resistance to isoxaben or flupoxam. This suggests that either there are multiple binding sites for these CBIs, the sites of substitution define a single binding site, or each of the substitutions allosterically alter the site of action. The possibility of multiple binding sites is unlikely since only one substitution is necessary for resistance. Consequently, the multiple binding site theory requires isoxaben and flupoxam to elicit effects only when all binding sites are occupied. It is likely that the mode of resistance is a combination of the latter two of the three possibilities.

The mutants with substitutions in membrane spanning regions were the most resistant to their corresponding herbicides. Coupled with the high hydrophobicity of isoxaben and flupoxam, suggests that the binding site of these CBIs lie within the membrane. Resistant alleles with substitutions outside the binding site would act allosterically by indirectly altering the site of action to disfavor CBI binding. These allosteric modifications may result in slight global changes resulting in decreased binding affinity at the site of CBI action. These alleles exhibit relatively lower resistance compared to alleles with modifications directly in the site of action.

Figure 2.2.3A: Local alignment of the primary wall CESAs. The amino acid substitutions resulting in CBI resistance are in bold red. All of the substituted residues are conserved amongst the three CESAs except *fxr1-1*. There is a 15 amino acid stretch which contains 6 substitutions.

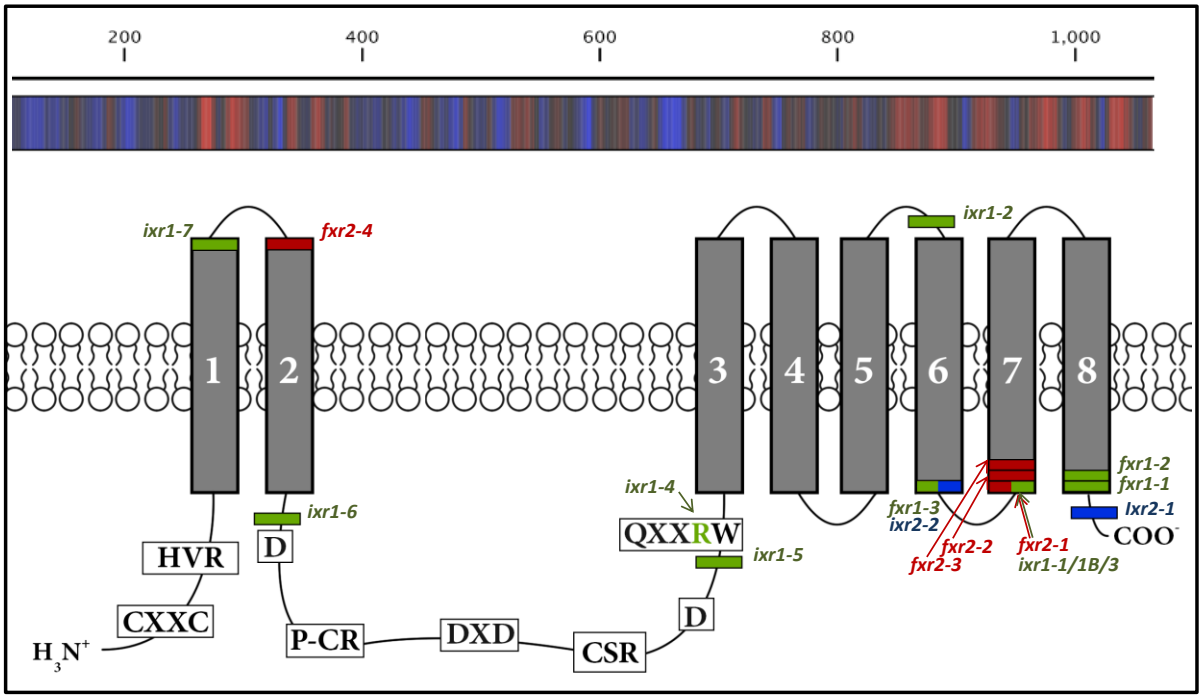

Figure 2.2.3B: Schematic of a generalized CESA protein. On the top of the figure is a Kyte-Doolittle hydrophobicity plot generated using the amino acid sequence of CESA3 with red indicating hydrophobic regions and blue representing regions of hydophilicity. The amino acid positions are displayed above. The plot is aligned with the generic CESA cartoon from Figure 1.2.3B with the CBI resistance alleles superimposed illustrating their relative positions. The red, green and blue boxes represent alleles in CESA1, CESA3 and CESA6 respectively. Boxes of two colors indicate substitutions at the same residue on different CESAs.

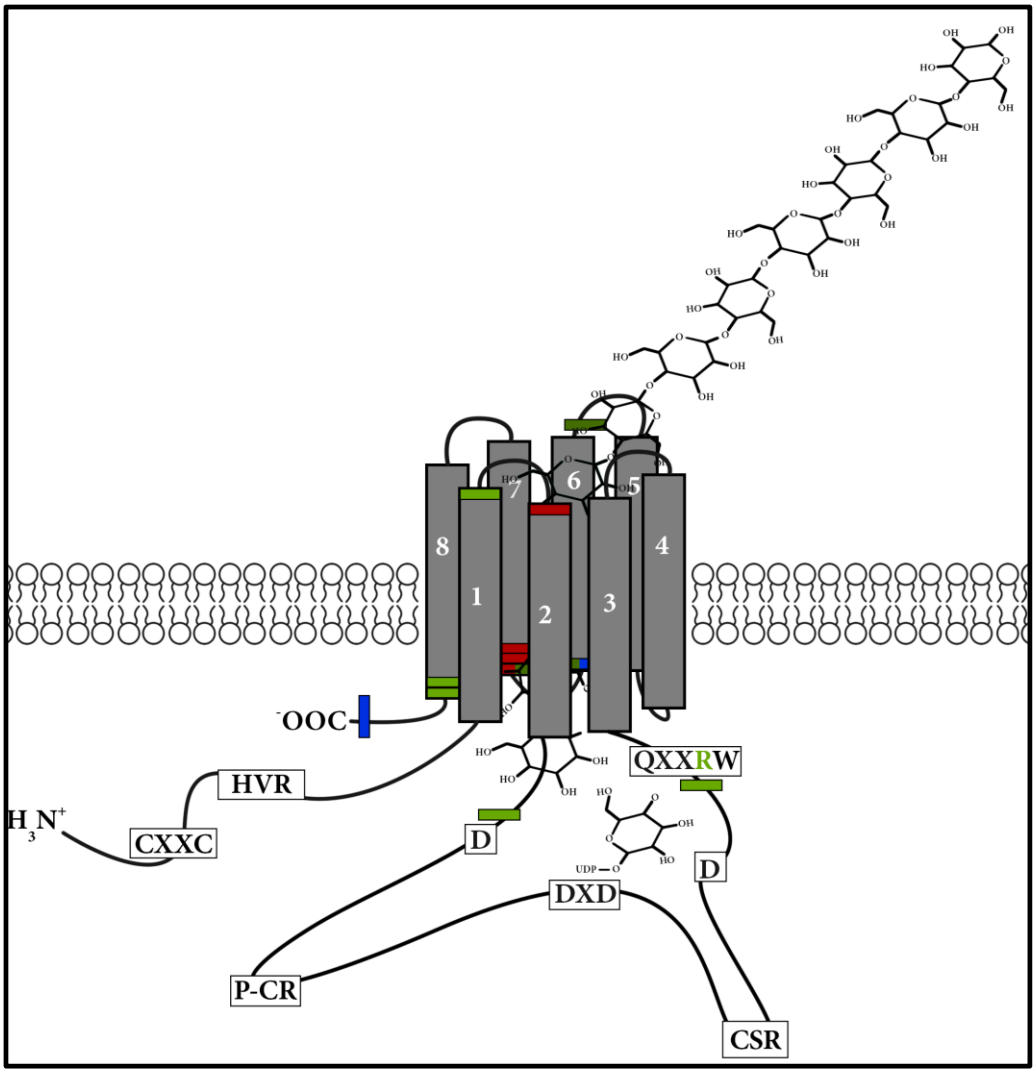

Figure 2.2.3C: An illustration of a possible three-dimensional conformation of a CESA. This depiction shows the alleles of *ixr* and *fxr* alleles superimposed. The figure shows a glycan chain being excreted from a pore-like subunit. The TMDs are numbered and the red boxes denote CESA1 alleles, the green and blue and boxes represent CESA3 and CESA6 alleles respectively. The CXXC, HVR, P-CR, CSR, QXXRW and catalytic aspartates (D, DXD, D) are represented by textboxes in their relative positions along the CESA subunit in the cytosol (Adapted from Delmer 1999 and Richmond 2000).

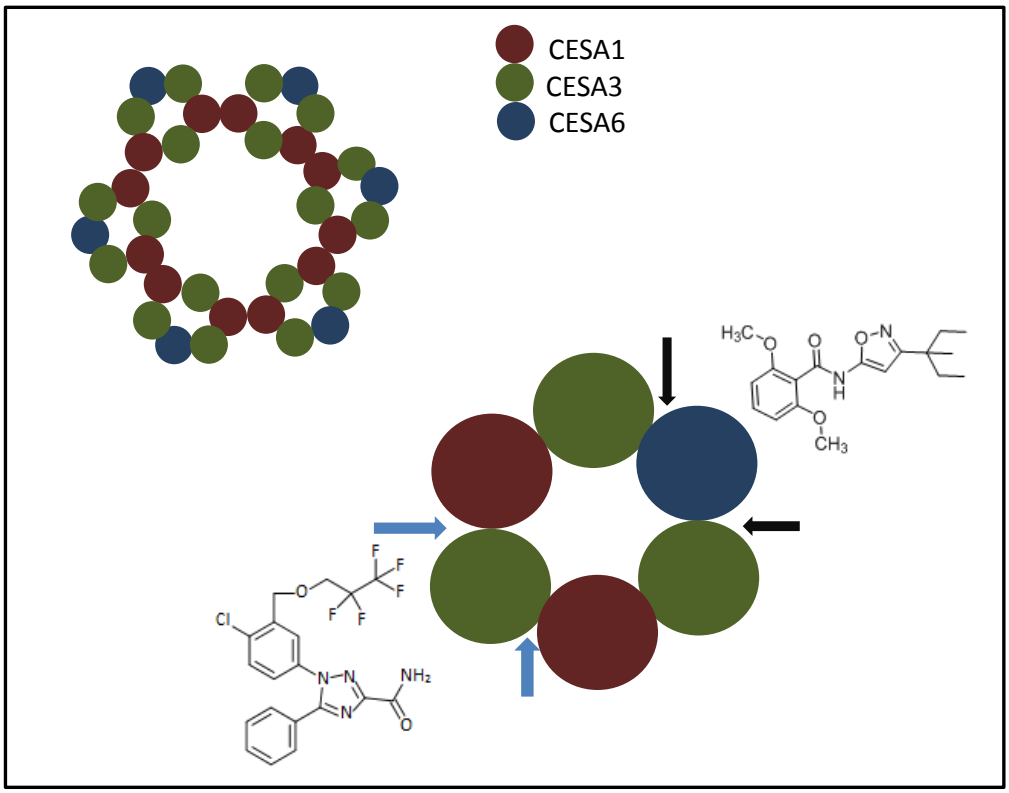

Figure 2.2.3D: The proposed model of the primary wall rosettes. The complex consists of two CESA1 subunits and three CESA3 subunits for every one CESA6. In this model isoxaben and flupoxam disrupts CESA3-CESA6 and CESA1-CESA3 interactions respectively. Although the above figure depicts interactions between the hexamers occurring through CESA1, this model does not exclude it occurring through CESA3.

2.2.4 *ixr* and *fxr* mutants show varying degrees of herbicide resistance

In order to confirm the level of CBI resistance conferred by the *ixr* and *fxr* mutations, each mutant's sensitivity to their respective CBI was quantified by measuring root lengths in increasing concentrations of the herbicide. This information can help to distinguish primary binding sites versus weak associations with the destabilizing CBI. The degree of resistance to the herbicides was quantified by measuring the root lengths of light grown seedlings 5 days after germination (DAG). The *ixr* alleles show a wider range of resistance when compared to flupoxam resistance. The general trend for isoxaben resistance is that substitution in the TMDs confers the most resistance followed by those in cytosolic regions. The *cesA6* alleles conferred the least resistance (Figure 2.2.4A). The resistance curves for the *fxr* alleles are much less dispersed. The CESA1 alleles are the most resistant followed by those in CESA3 (Figure 2.2.4B). CBI resistance brought about by amino acid substitutions within TMDs appear to result in the highest level of resistance for flupoxam as well. CBIs may accumulate in the plasma membrane and disrupt inter-CESA interaction within the hydrophobicity of this space.

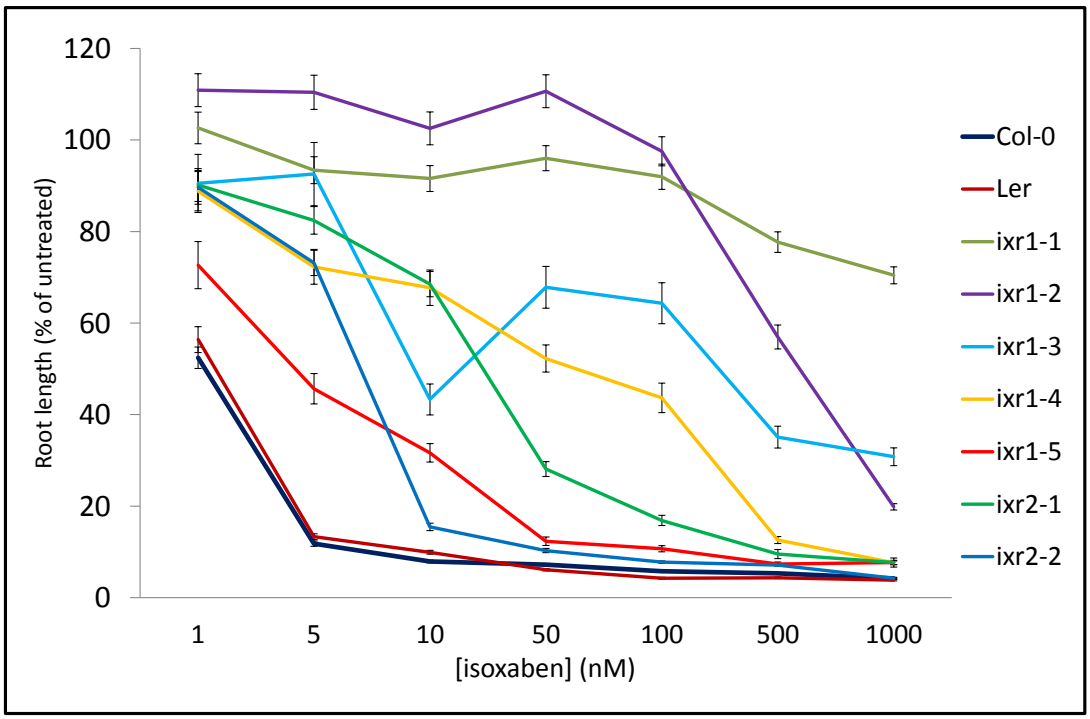

Figure 2.2.4A: Resistance profiles of *ixr* mutants to isoxaben. The root lengths of 5 DAG seedlings plotted against increasing concentrations of isoxaben are shown. The vertical axis is expressed as a percentage of the root lengths on media containing no herbicide (untreated). Values are averages +/- standard deviation (n = 20).

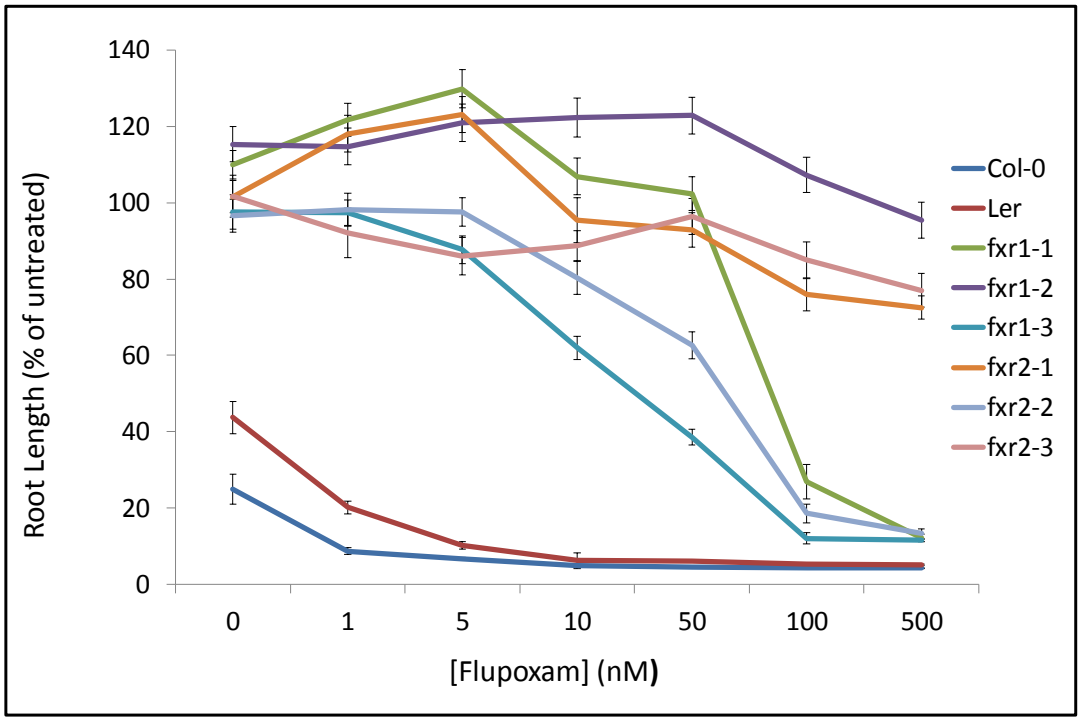

Figure 2.2.4B: Resistance profiles of *fxr* mutants on flupoxam. The root lengths of 5 DAG seedlings plotted against increasing concentrations of flupoxam are shown. The vertical axis is expressed as the percent of untreated root lengths and complete insensitivity would be 100%. Values are averages +/- standard deviation (n = 20).

2.2.5 Cellulose deficient morphological phenotypes are displayed by some *ixr* and *fxr* mutants

The mutants were examined for obvious perturbations in cellulose biosynthesis by looking for morphological irregularities. The severity of the cellulose deficiencies caused by the SNPs will provide insight into the importance of their roles in the overall process. Point mutations which confer high resistance but show little cellulose defects indicate that those sites are in regions required for herbicide action but are not important in the catalytic activity. Whereas SNPs that show low resistance and significant cellulose deficiency phenotypes are indicative of being in regions important for activity but likely induce resistance indirectly. These SNPs are probably not in the binding site of the herbicide but alter it allosterically. For this investigation, morphological phenotypes such as: loss of cell anisotropy, stunted growth and shortened hypocotyls are examined. Figure 2.2.5A and Figure 2.2.5B show light-microscope images of *Arabidopsis thaliana* screened on isoxaben and flupoxam respectively illustrating cellulose deficiencies in the sensitive seedling.

The most resistant mutants seem to lack wall deficiency phenotypes and had plant heights 75-90% of wild-type. The mutants that were moderately resistant displayed additional cellulose deficiency phenotypes. The mutants: *ixr1-3, ixr1-4* ixr*1-6* and *fxr1-2* displayed the most severe growth defects and were shorter in stature and smaller in overall size (Figure 2.2.5C and D). *fxr1-2* displayed a 'bumpy' and short silique phenotype in addition to having a short stature (Figure 2.2.4E and F). *ixr1-5* displays a strong and incompletely penetrant blistering phenotype when no herbicide is present yet maintains moderate resistance to the chemical (Figure 2.2.5G). If isoxaben and flupoxam targets were at the active site of the CESAs then a strong correlation between resistance

and cellulose deficiency would be observed. The ability of mutants to be highly resistant to CBIs without any cellulose deficiencies indicates that isoxaben and flupoxam must act by disrupting cellulose biosynthesis at sites other than the catalytic center. The observation of mutants with high resistance and virtually no morphological consequences suggest that these herbicides act on CESAs allosterically or by other indirect means.

Figure 2.2.5A: Isoxaben sensitivity in wild-type compared to the resistant phenotype. The blistering phenotype (white arrows) is apparent in *Ler* as the cellulose deficient walls are incapable of effectively resisting the internal turgor pressures. Resistant lines such as *ixr1-3* (right) display no blistering in the presence of isoxaben and can tolerate high concentrations of the herbicide. The seedlings are 5 DAG and on 5 nM of isoxaben (bar = 1 mm).

Figure 2.2.5B: The flupoxam sensitivity phenotype. Wild-type in the presence (left) of flupoxam is juxtaposed with the same ecotype growth in the absence of the CBI (right). Five DAG seedlings of *Ler* display obvious blistering (white arrows) on 5 nM of flupoxam which is absent in the control (bar = 1mm).

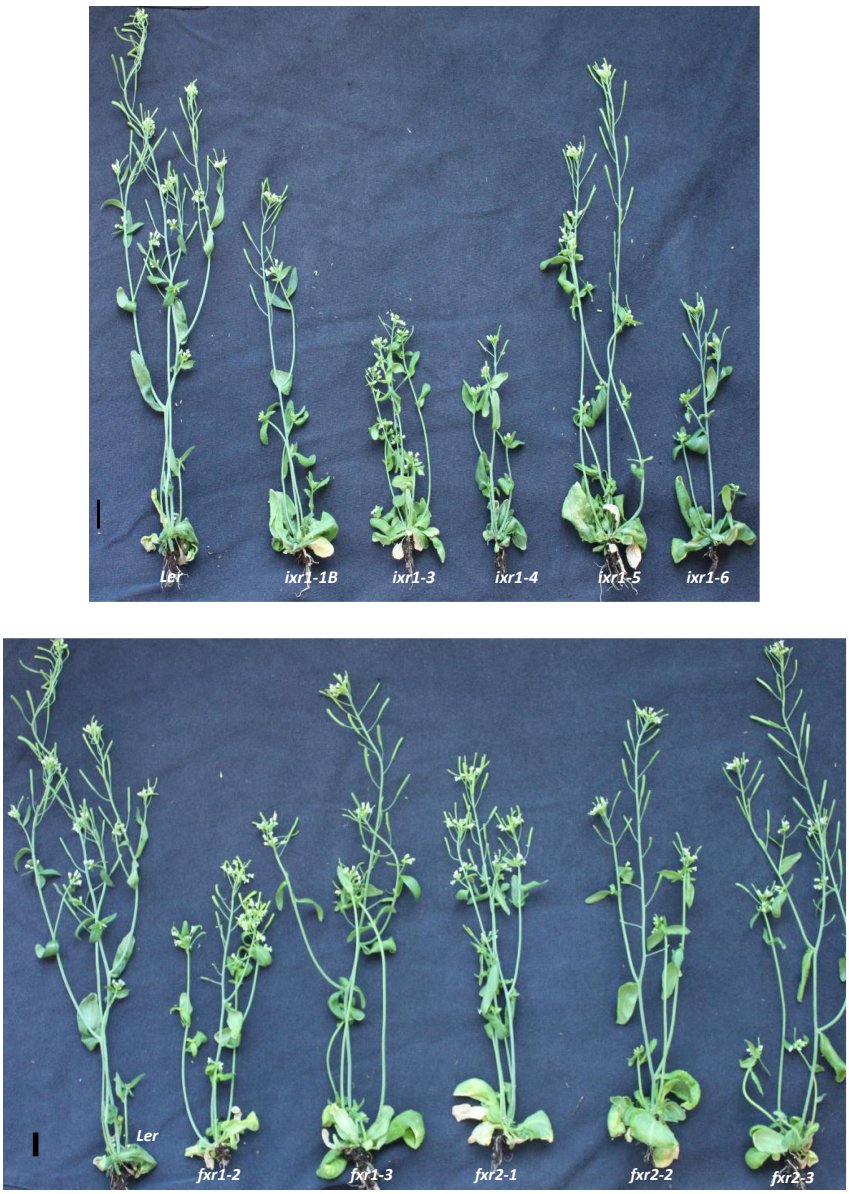

Figure 2.2.5C: Adult plant growth phenotypes of *ixr* and *fxr* mutants. Forty-five DAG isoxaben resistant mutants compared to *Ler* (top). From left to right: *Ler*, *ixr1-1B*, *ixr1-3*, *ixr1-4*, *ixr1-5*, and *ixr1-6* (bar = 1 cm). Forty-five DAG flupoxam resistant mutants compared to *Ler* (bottom). From left to right *Ler*, *fxr1-2*, *fxr1-3*, *fxr2-1*, *fxr2-2*, *fxr2-3* (bar = 1 cm).

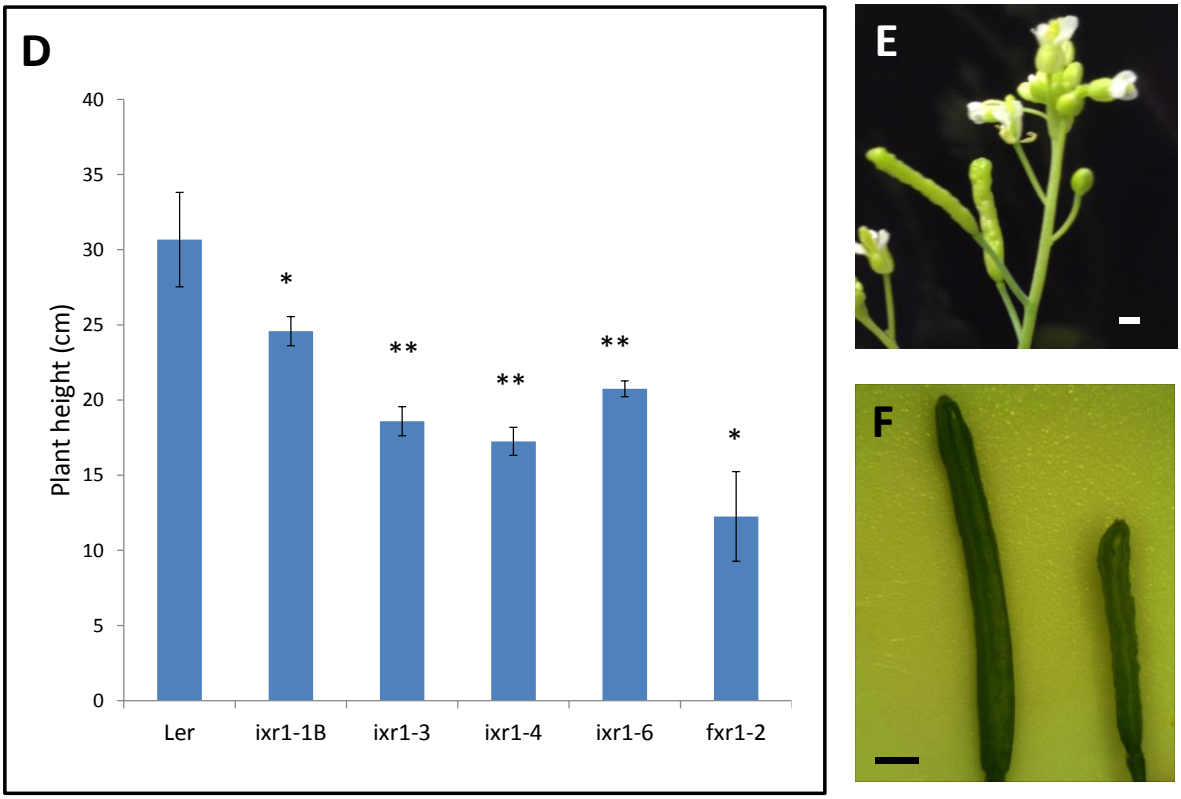

Figure 2.2.5: Quantification of growth differences of *ixr/fxr* mutants.

D) Heights of 45 DAG plants. Displayed are average values for significantly shorter mutants +/- standard deviation (n = 6, *p < 0. 01, **p <0. 001 using Student's t-test).

E) A photograph of the *fxr1-2* inflorescence (bar = 1 mm).

F) The siliques of *Ler* (left) and *fxr1-2* (right) compared. This illustrates clear irregularities in surface texture in the mutant along with a decrease in length (bar = 1 mm).

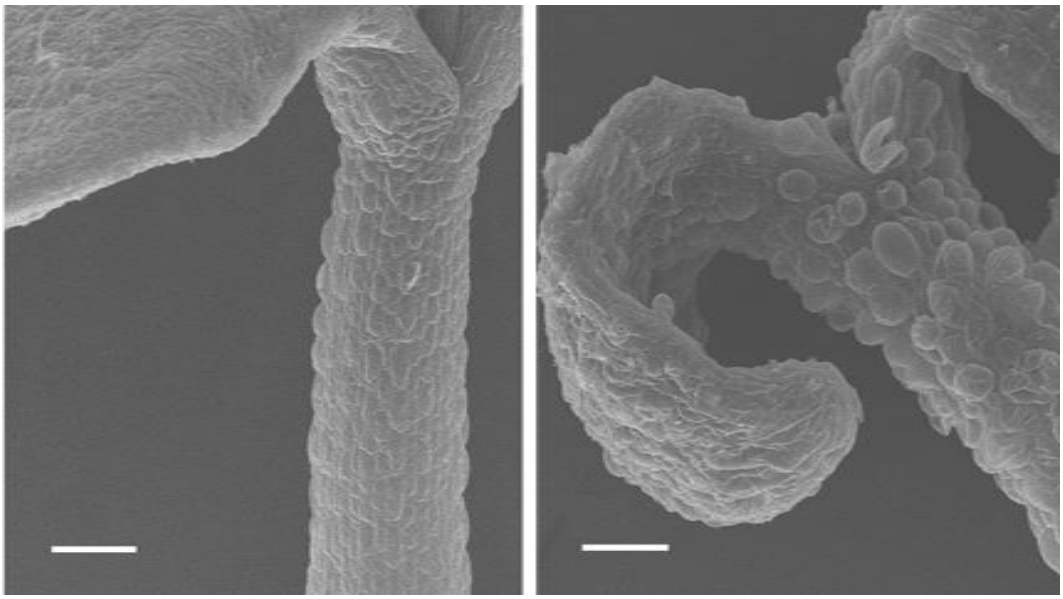

Figure 2.2.5G: SEM micrograph of wild-type and *ixr1-5* seedlings. The blistering observed in *ixr1*-5 cells are caused by underlying cellulose deficiency. This figure shows scanning electron micrographs of the upper hypocotyl from light-grown *Ler* (left) and *ixr1-5* (right) seedlings in the absence of CBIs. The swollen round cells of *ixr1*-5 are indicative of cellulose deficiencies (bar = 1 mm).

2.2.6 Etiolated hypocotyl length analysis reveals some *ixr*/*fxr* conditional phenotypes

When seedlings are grown in the dark, the cells of the hypocotyl undergo rapid elongation and consequently high rates of cellulose synthesis. Analysis of etiolated seedlings allows for the observation of mutant behaviour in situations where cellulose biosynthesis rates are at their highest. Measurements of the etiolated hypocotyl lengths of the mutant lines were taken and compared to their respective wild-types (Figure 2.2.6A). *ixr1-2, ixr1-3, ixr1-6* and *izr2-1* clearly display shortened etiolated hypocotyl lengths. Of these, the phenotype of *ixr1-6* is the most severe. In addition *ixr1-6* displays a blistering phenotype when grown in the dark. Figure 2.2.6B is a photograph of *ixr1-6* and *Ler* seedlings further illustrating the shortened etiolated hypocotyls phenotype compared to wild-type. The dark-grown hypocotyl lengths of *ixr1-4, ixr1-5, ixr1-7* and *ixr2-2* were significantly decreased in the presence of 10 nM of isoxaben. This conditional sensitivity implies that the CESA composition of the primary wall rosette is different or that it assumes altered conformational states in light and dark conditions. Indeed, evidence supporting distinct genetic pathways modulating hypocotyl growth in dark and light-grown *Arabidopsis* seedlings has been shown using T-DNA insertion lines of *cesA6* called *procuste1* (Desnos *et al.* 1996). The conditional cellulose deficiency of *procuste1* suggests that CESA6 is required for rapidly expanding cells such as hypocotyl cells in dark conditions. This observation also supports the model of CESA6-like subunits being interchanged depending on biological context. It also explains the low resistance of *ixr2* alleles.

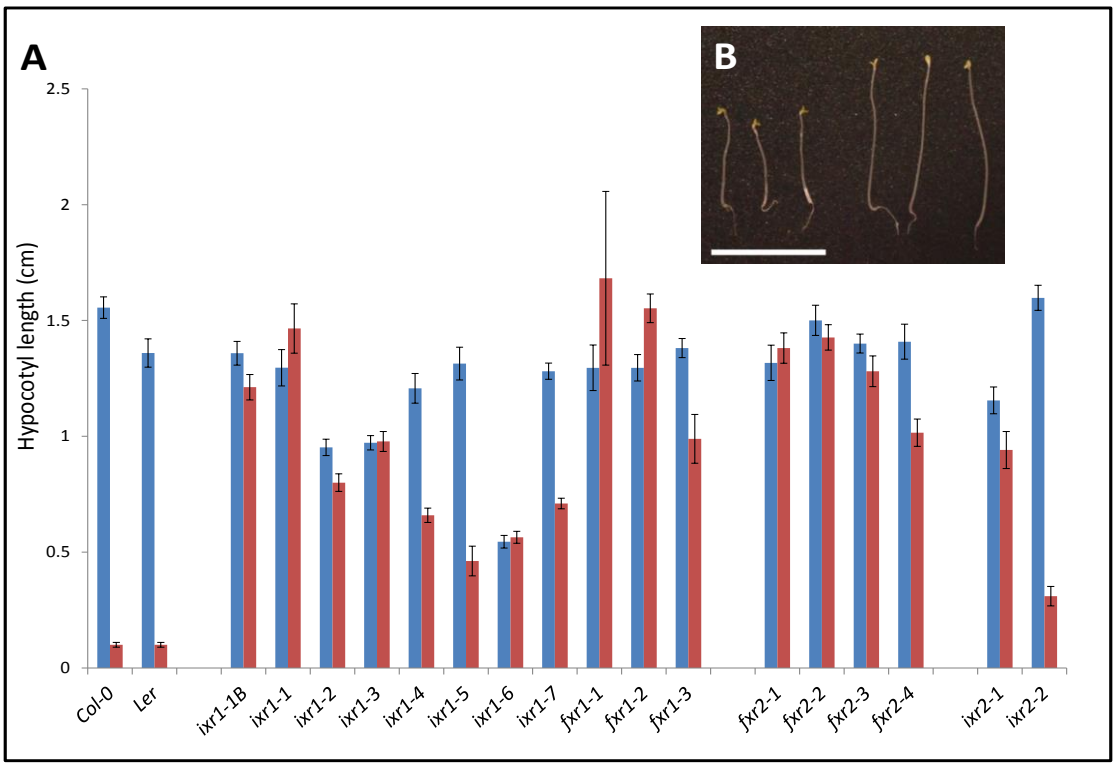

Figure 2.2.6: Comparison of hypocotyl lengths in wild-type and *ixr/fxr* alleles.

A) The etiolated hypocotyl lengths in the absence (blue bars) and presence (red bars) of 10 nM of isoxaben or flupoxam is shown. The seedlings were grown in the dark for 8 days in the presence and absence of CBI. Values are averages +/- standard deviation (n = 20).

B) A photograph of etiolated seedlings of *ixr1-6* (left) compared to *Ler* (right) (bar = 1 cm).

2.2.7 ^{14}C-glucose incorporation into cellulose is largely unaffected by IXR and FXR

In order to determine if the amino acid substitutions of the CBI resistance alleles affect the rate of cellulose synthesis, radioactive incorporation assays were performed. This assay indirectly measures the ability of the cellulose synthases to incorporate carbon-14 (^{14}C) labeled glucose into cellulose. This method measures the enzymatic activity of cellulose synthases. This is important because the presence of lower incorporation rates compared to wild-type in mutants reveal CESA regions involved in both herbicide resistance and cellulose biosynthesis. These SNPs represents regions where herbicide action and catalytic activity overlap.

The time course incorporation graph of wild-type (*Ler*) in the presence of isoxaben and flupoxam illustrates the similarities of the two CBIs (Figure 2.2.7A). Percent incorporation is the ratio of the emissions from the insoluble fraction and the total detected emissions. The incorporation results are expressed with respect to wild-type where 100% indicates that the mutant incorporated the same amount of ^{14}C-glucose are its respective wild-type (Figure 2.2.7B). In this assay only *ixr1-4* and *ixr1-5* showed a significant decrease in glucose incorporation compare to wild-type (Figure 2.2.7C). The result of isoxaben resistance causing a perturbation in the rate of incorporation of glucose into cellulose verifies the presence of a link between the two processes. It comes as no surprise that the SNPs responsible for decreased ^{14}C incorporation and lower cellulose synthase activity are found in the highly conserved QxxR region. This region has been implicated in glycan processing as the polymer emerges from the CESA complexes (Saxana *et al.* 2001). These two mutants confer low resistance to isoxaben and exhibit

severe cellulose deficient phenotypes. These two mutants likely allosterically alter the isoxaben binding site resulting in low resistance.

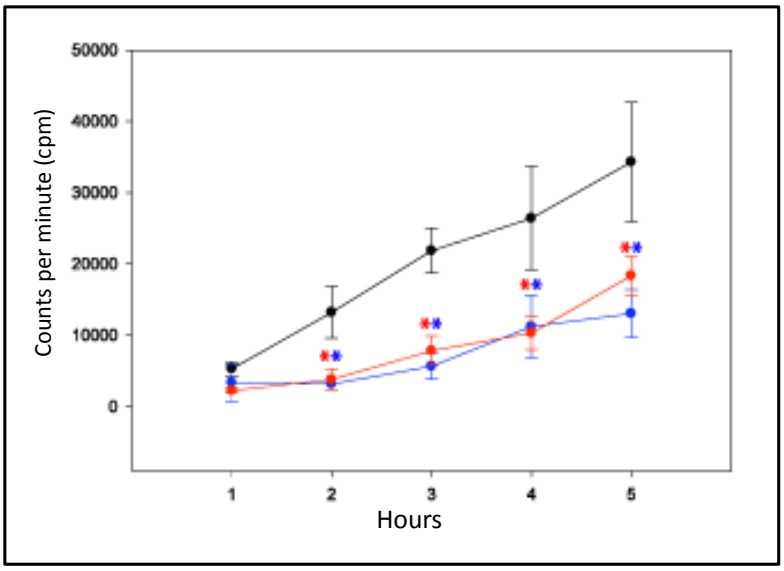

Figure 2.2.7A: Incorporation of labeled glucose into the cellulose fraction of the cell walls. The β-emissions from ^{14}C-glucose incorporated in to the acid-insoluble fraction is shown above illustrating the similar efficacy of isoxaben and flupoxam in inhibiting this process versus control. Five DAG etiolated *Ler* seedlings grown in the absence of CBI (black), 1 μM isoxaben and 1 μM of flupoxam. The vertical axis is expressed in counts per minute +/- standard deviation (n = 6, *p <0. 001 using Student's t-test) and measurements were taken once per hour for a total of five hours.

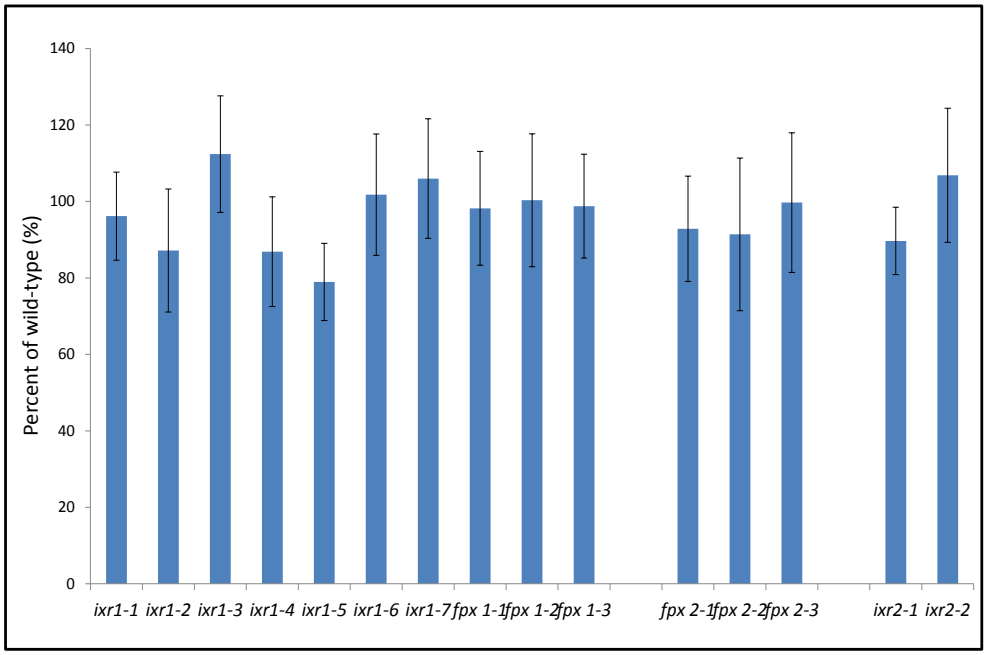

Figure 2.2.7B: Incorporation of labeled glucose into the cellulose fraction of *ixr/fxr* seedling cell walls relative to wild-type. A comparison of the ^{14}C-incorporation of etiolated seedlings is shown above. The vertical axis is expressed as percentage values of their respective wild-type +/- standard deviation (n = 6). Measurements were taken after the seedlings were incubated in ^{14}C-glucose for one hour. Most of the mutants show incorporation rates around 100% of wild-type.

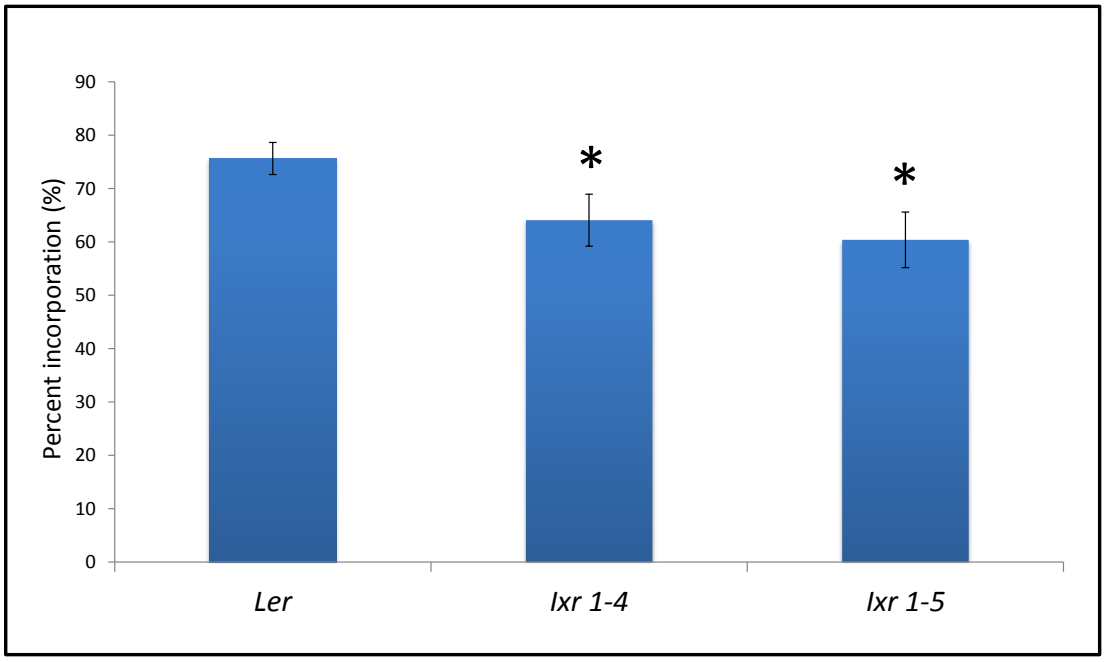

Figure 2.2.7C: Mutants with reduced glucose incorporation into the cellulose fraction of their cell walls. Two mutants, *ixr1-4* and *ixr1-5* show reduced radiolabeled glucose incorporation rates compared to wild-type. The vertical axis is expressed as the percentage of ^{14}C-glucose detected from both soluble and insoluble fractions +/- standard deviation (n = 6, *p < 0. 001 using Student's t-test).

2.2.8 X-ray diffraction (XRD) analysis shows reduced cellulose crystallinity in soluble domain mutants of IXR1

Since all the resistance alleles of isoxaben and flupoxam are found in the primary wall CESAs, it is important to examine the effects in the final glycan product. Perturbations in the cellulose biosynthetic pathway likely will cause defects in the structure of cellulose. The degree of cellulose crystallinity is an essential trait which determines many of its mechanical and chemical properties. In order to quantify the crystallinity of the cellulose produced by the CBI-resistant lines, x-ray diffraction was employed. The x-ray diffractor emits x-rays to the sample through a range of angles and the intensities of the diffracted photons in the direction of the detector are plotted as a function of angle of incidence (Figure 2.2.8A). An image of the x-ray diffractometer used for this study at the University of Toronto is provided in Figure 2.2.8B. Relative crystallinity index (RCI) is defined as: I_{002}-I_{am}/I_{002} x 100% where I_{002} is the characteristic maximal peak at $2\theta = 21.5^{o}$ for type I (Figure 2.2.8C) and 22.5^{o} for type II cellulose (Figure 2.2.8D) and I_{am} is the amorphous trough found around $2\theta = 18.5°$ (Segal *et al.* 1959). Washed senesced stem tissue of the CBI resistant alleles were compared against wild-type (Figure 2.2.8E). Resistance to CBIs appears to come at a cost to RCI. *fxr1-1* and *fxr1-3* were the only alleles which had RCI values similar to wild-type. The rest of the mutants had reduced crystallinity in their walls. The RCI seems to inversely correlate with the severity of cellulose deficient morphological phenotypes. The mutants with mild phenotypes show RCI values similar to wild-type and those with severe defects have significantly reduced RCI valves compare to wild-type. With this observation it is tempting to speculate that these morphological phenotypes are caused primarily by reductions in cellulose crystallinity. It appears that modification of CESAs which confers herbicide resistance

perturbs the cellulose biosynthetic pathway resulting in a reduction of crystallinity to varying degrees.

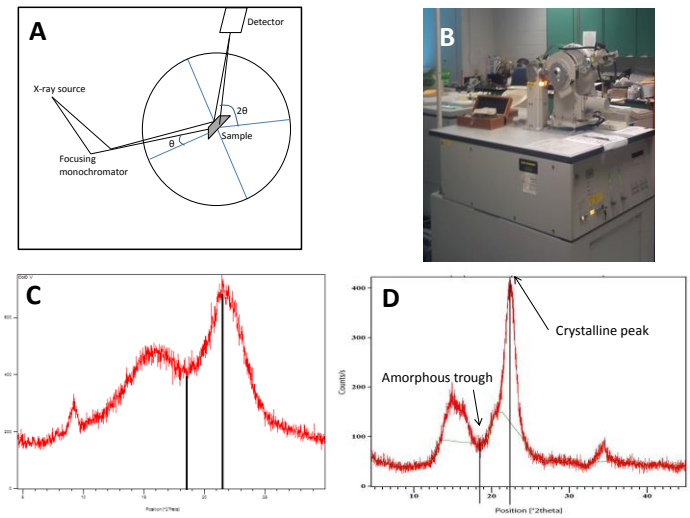

Figure 2.2.8:

A) A schematic of an x-ray diffractometer. X-rays are directed at rotating sample which diffract through the sample and reach the fixed detector. Crystalline cellulose diffracts x-rays at characteristic angles of incidence and this method can be used to quantify its crystallinity (Adapted from Segal *et al.* 1959).

B) A photograph of the x-ray diffractometer from the Department of Geology at the University of Toronto used in this study.

C) XRD spectrum of type-I cellulose from *Columbia* (*Col-0*) senesced stem tissue. The characteristic amorphous trough denoted by black vertical lines at $2\theta = 18.5^{o}$ and crystalline peak at $2\theta = 21.5^{o}$ are displayed. The vertical axis is expressed in counts per minute.

D) The XRD spectrum of commercially available type-II cellulose, Avicel. The crystalline peak is shifted from to $2\theta = 21.5^{o}$ to $2\theta = 22.5^{o}$ compared to type-I cellulose. The black vertical bars indicate the lowest point of the amorphous trough and the highest point of the crystalline peak. The crystalline peak is much more pronounced and consequently type-II cellulose has a higher RCI and is more crystalline.

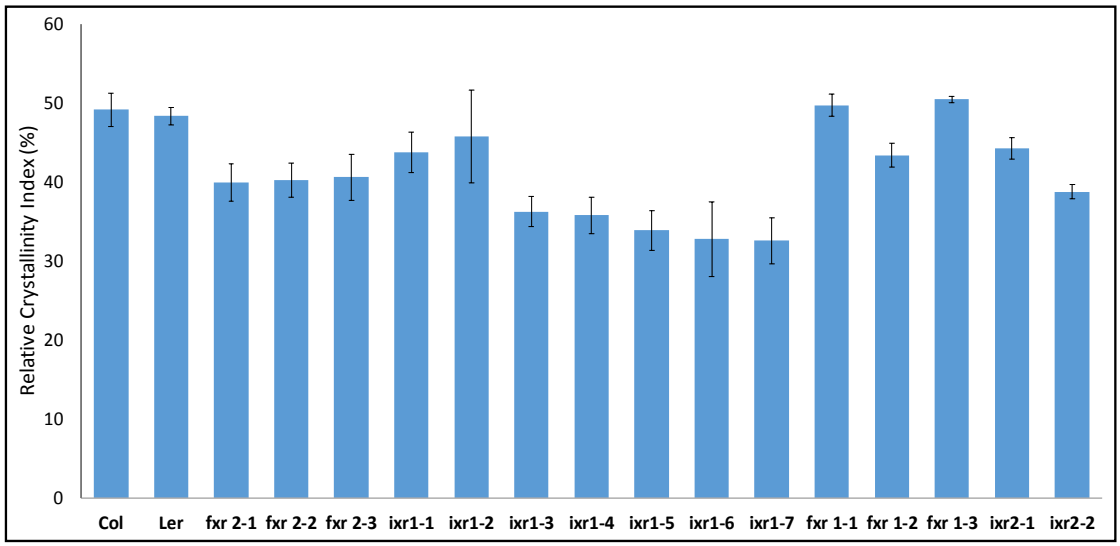

Figure 2. 2. 8E: The RCIs of washed senesced stem tissue for wild-type and the mutants. The first two columns on the left are wild-type and the mutants are grouped according to alleles from left to right are: alleles of CESA1, CESA3 and CESA6. Almost all of the mutants show decreased RCI values compared to wild-type. Values are averages +/- standard deviation (n = 3).

2.2.9 Sequential acid and enzymatic hydrolytic analysis reveal enhanced saccharification of *ixr* and *fxr* cell wall material

Cellulose crystallinity is a major factor contributing to biomass recalcitrance. Considering that all the mutants show decreased crystallinity, their sensitivity to acid and enzymatic hydrolytic schemes were examined. Isoxaben and flupoxam resistance alleles can potentially be used to decrease biomass recalcitrance as part of energy crop design. Senesced tissue of CBI resistant mutants was tested for wall hydrolysis sensitivity under sequential acid and enzymatic degradation schemes. The sugars for enzymatic hydrolysis were also quantified using the Glucose HexoKinase (HK) Assay Kit. The washed tissue was first macerated in water thoroughly then subjected to dilute sulfuric acid (0.2 M) at 80^{o}C for two hours. The sugars released were quantified using 0.2% anthrone. This tissue was then washed and subjected to cellulase digestion for two days. The remaining inaccessible crystalline cellulose was dissolved in boiling nitric and acetic acid and quantified using methods described by Updegraff 1969. The reducing sugar equivalents released at each step were quantified using 0.2% anthrone and are expressed as the percentage of the total sum from all steps (Figure 2.2.9A). What is immediately evident from this figure is that most of the cellulose remains inaccessible after sequential treatments of acid and hydrolytic enzymes. However, almost all of the CBI alleles show significant improvements in accessibility. The greatest improvements were observed after enzymatic hydrolysis with cellulase and cellobiase (Figure 2.2.9B).

It is clear that isoxaben and flupoxam resistance leads to changes in the wall resulting in greater sensitivity to enzymatic degradation. Despite the gains in glucose yields, the majority of the wall cellulose remains recalcitrant in almost all the mutants tested. Of the alleles which showed the most substantial improvements in accessibility,

ixr1-1, *ixr2-1*, *ixr2-2* and *fxr2-1* do not exhibit growth defects. Modifications to CESAs resulting in a substantial decrease in the cellulose RCI are typically associated with a smaller statured plant and significantly less biomass compared to wild-type. Upon consideration of the total glucose released per mg of tissue, *ixr1-1*, *ixr 2-2*, *ixr 2-1* and *fxr2-1* emerge as the most attractive for bioenergy crop considerations. The *cesA6* mutants released 80% more glucose and *ixr1-1* and *fxr2-1* both increased glucose yields by 60% compared to their respective wild-types (Figure 2.2.9B). Enhanced saccharification in *ixr1-2* has previously been described (Harris *et al.* 2009). The authors attribute this effect to reduced crystallinity in the cellulose enabling cellulases greater access and higher efficiency processing the *ixr1-2* cellulose. Although *ixr1-2* did release 25% more total accessible sugars compared to *Col-0* (Figure 2.2.9B), a large proportion of inaccessible cellulose remained undigested (Figure 2.2.9A).

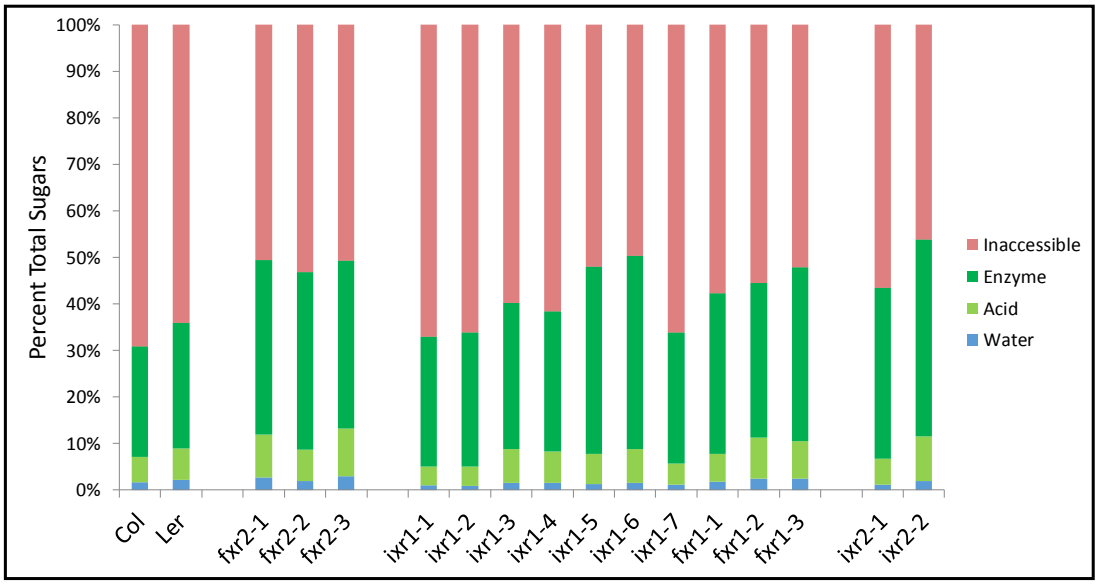

Figure 2.2.9A: Sugar released form *Arabidopsis* senesced stem tissue after sequential hydrolytic steps. Beginning with sugars released during maceration in water (blue), then after acidification to 0.2 M (light green), subsequent cellulase treatment (dark green) and the remaining cellulose treated with nitric acid (red). All values are averages (n = 3) and are expressed as a percentage of the total sugars released (See Figure 2.2.9S1).

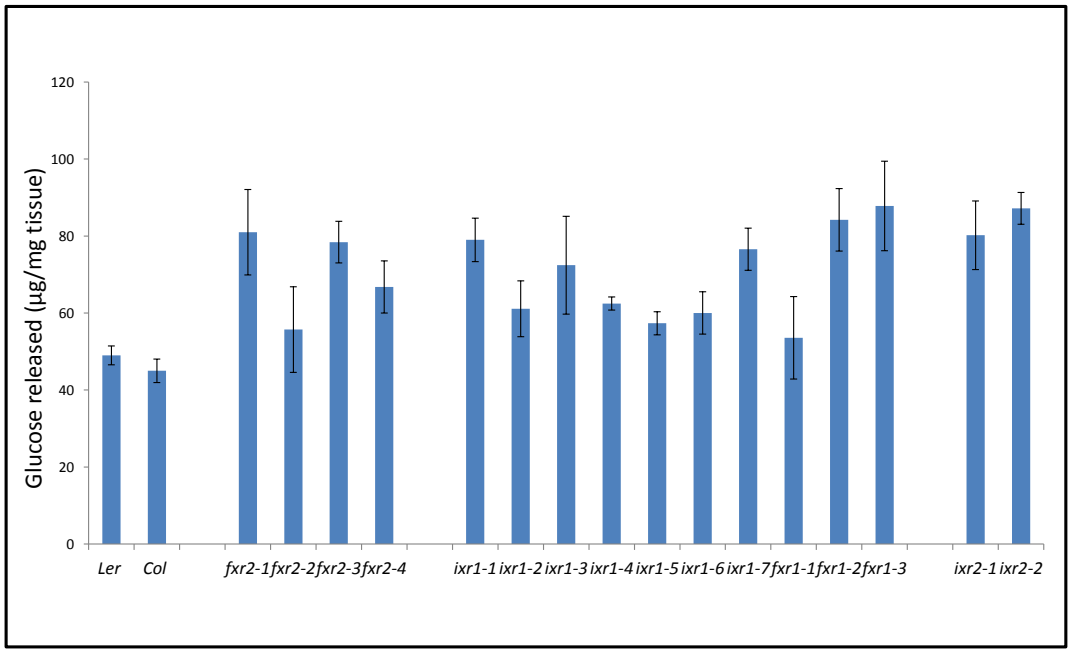

Figure 2.2.9B: Glucose released after enzymatic hydrolysis of *Arabidopsis* senesced stem tissue. The vertical axis is expressed in micrograms of glucose released per milligram of senesced tissue determined by the HK method. The values are averages +/- standard deviation (n = 3).

2.2.10 Phloroglucinol staining of *ixr/fxr* plants reveals ectopic lignin accumulation

Ectopic lignin as a result of cellulose deficiency has been reported in *pom1* (Zhong *et al.* 2002), *the1* and *cesA6* deficient mutants (Hematy *et al.* 2007). In addition, ectopic lignification has been reported in response to CBI application (Bischoff *et al.* 2009). Aberrant over-accumulation of lignin is indicative of cellulose deficiencies although not all cellulose deficiencies display ectopic lignin. The responsive up-regulation of lignin genes is likely a compensatory mechanism as the organism attempts to maintain structural integrity of the wall while cellulose deficient. Acidified phloroglucinol (1,3,5-trihydroxybenzene) or Wiesner's reagent specifically stains the lignin in plant cell walls to give a bright pink-red colour (Wiesner 1878). Etiolated seedlings were treated with Wiesner's reagent five days after germination and were visualized using a light dissecting microscope. Only *ixr1-4, ixr1-5* and *fxr2-4* displayed obvious ectopic lignin staining with phloroglucinol (Figure 2.2.10). Figure 2.2.10A is a light microscope image of a phloroglucinol treated *Landsberg erecta* (*Ler*) seedling root. Figure 2.2.10B and C are images of the treated roots of *ixr1-4* and *ixr1-5* respectively. Figure 2.2.10D, E and F compare Wiesner staining of the hypocotyl base of *Ler ixr1-4* and *ixr1-5* respectively. These images illustrate how perturbations of the QxxR region can result in ectopic lignification likely in response to cellulose deficiencies.

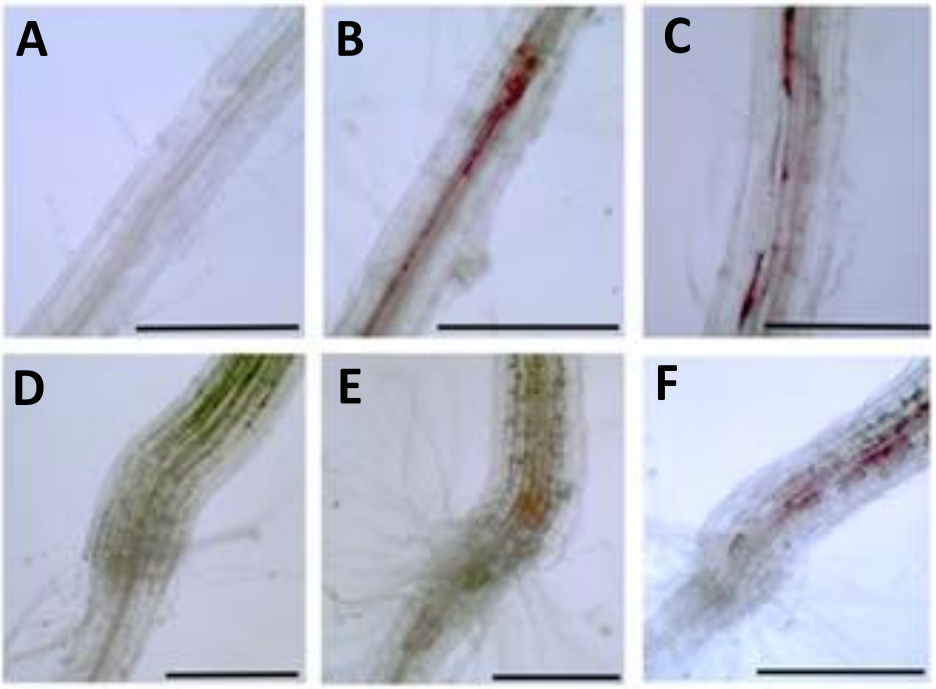

Figure 2.2.10: Lignin staining of wild-type and mutant roots and hypocotyls.

A) Light-microscope image of the root of a *Ler* seedling after phloroglucinol treatment showing no ectopic lignin (bar = 1 mm).

B) Image of the root of an *ixr1-4* seedling after phloroglucinol staining reveals large amounts of ectopic lignin surrounding the vascular tissue (bar = 1 mm).

C) Ectopic lignin surrounding the vascular tissue of the root in *ixr1-5* is seen but notably less than observed in *ixr1-4* (bar = 1 mm).

D) The base of the hypocotyl of a *Ler* seedling shows minimal staining after phloroglucinol treatment (bar = 1 mm).

E) The light-microscope image of the base of the hypocotyl of *ixr1-4* seedling after phloroglucinol treatment reveals ectopic lignin lining the vascular tissue of the hypocotyl (bar = 1 mm).

F) Phloroglucinol treatment of *ixr1-5* seedlings show strong ectopic lignin staining in the hypocotyl.

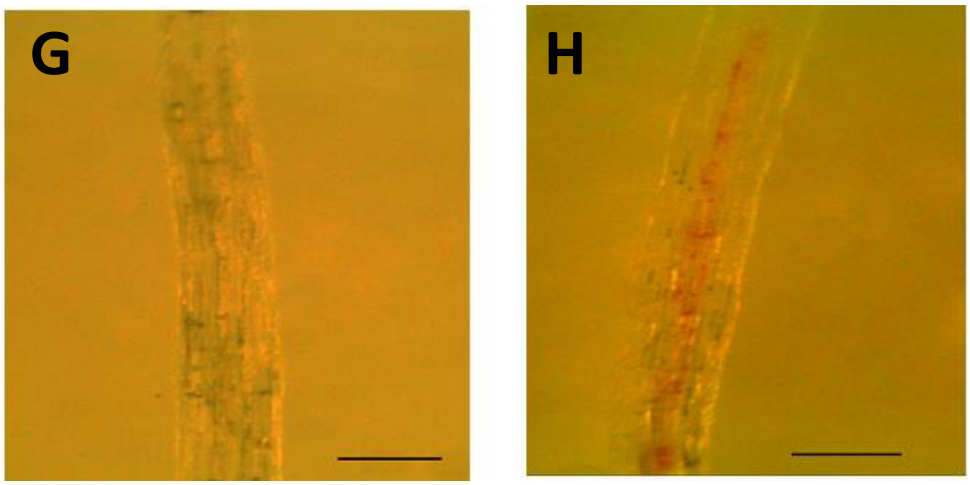

Figure 2.2.10: Lignin staining of *Ler* and *fxr2-4* hypocotyls.

G) The hypocotyl of a *Ler* seedling shows no staining after phloroglucinol treatment (bar = 1 mm).

H) The light-microscope image of a *fxr2-4* seedling after phloroglucinol treatment reveals ectopic lignin lining the vascular tissue of the hypocotyl (bar = 1 mm).

2.2.11 *ixr1-3;fxr2-3* double mutants provide genetic evidence for CESA1-CESA3 interaction in primary wall synthesis

In the search for further genetic evidence supporting the interaction of the primary wall CESAs, isoxaben and flupoxam resistance parents were crossed and the resulting F2 seeds were grown in the presence of both herbicides. Plants that were homozygous for both *ixr1-3* and *fxr2-3* displayed phenotypes not exhibited by either parent. The proportion of progeny resistant to both herbicides was much less than the 6.25% predicted by the Mendelian ratio for a dihybrid cross. Of the double homozygous mutants of *ixr1-3;fxr2-3* the survival rate on 10 nM of isoxaben and 10 nM of flupoxam was observed to be 0.69 % (n = 144, $p < 0.01$ by the Student's t-test). This is much lower than the expected rate of survival and is likely due to genetic complementation. The frequency of survival for homozygous double mutants of *ixr1-1;fxr2-3* was higher at 10. 2 % and is not a significant deviation from the expected ratio (n =137, p = 0. 06 by the Student's t-test). The few individuals who did survive displayed severe morphological deficiencies. Double homozygous *ixr1-1/3;fxr2-3* F2 plants resistant to 20 nM of both isoxaben and flupoxam were dwarfed and sterile due to fused carpels and collapsed siliques (Figure 2.2.11). The emergence of non-additive effects in the double homozygous progeny of two true breading parents is indicative of gene interaction and intergenic complementation.

The glycine-to-aspartate amino acid substitution of *fxr2*-3 1009 in CESA1 G(1009)D lies in the same conserved region as *ixr1*-3 in CESA3. It should be noted that both *ixr1-1;fxr2-3* and *ixr1-1B: fxr2-3* F2 double homozygous progeny displayed identical phenotypes as the *ixr1-3*: *fxr2-3* double homozygous F2s. This is important since *ixr1-1, ixr1-1B* and *ixr1-3* are substitutions of the same amino acid in CESA3 but

were isolated in independent screens. An introduction of a charged or polar side chain into this membrane spanning region likely causes distortions in the conformation of an inter-CESA junction by changing the hydrophobic profile. Interestingly, *ixr1-1/3*; *fxr2-1*F2 double mutant homozygous showed no complementation. Although *fxr2-1* harbors a substitution of the equivalent amino acid in CESA1 as *ixr1-1/3* do in CESA3, non-additive effects were not observed in complementation experiments. This may be due to the substitution resulting in the insertion of a basic residue in *fxr2-3*(G1013R) instead of an acidic one as in *ixr1-1/3* rather than the location. It would be interesting to see if a G994D substitution in CESA3 is able to confer resistance to isoxaben or flupoxam. This mutant would be particularly informative because crossing it to *fxr2-1* would create a situation where the modified amino acids are the same as in *ixr1-3* and *fxr2-3*. Complementation in this situation would further indicate inter-CESA interaction occurring through TMD7 in CESA1 and 3.

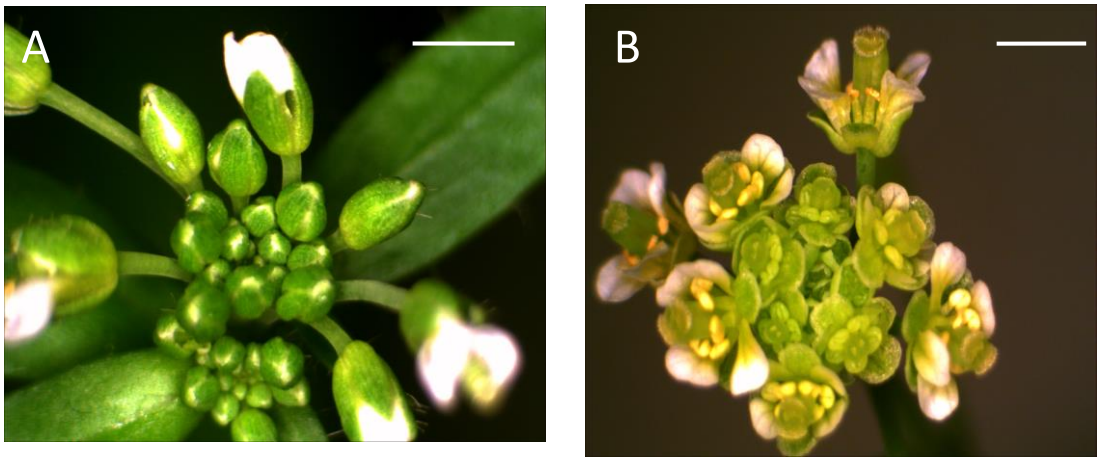

Figure 2.2.11: Comparison of the inflorescences in wild-type and double *ixr;fxr* mutant backgrounds.

A) Photograph of a typical inflorescence of *Ler* (bar = 1 mm).

B) The inflorescence of the *ixr1-1*; *fxr2-3* double mutant displays fused carpels and short undeveloped siliques (bar = 1 mm).

Figure 2.2.11C: A comparison of wild-type and double *ixr;fxr* mutant stature.

The *ixr1-1;fxr2-3* double mutant (right) is sterile and lacks all vigor. It is dwarfed when compared to *Ler* (left). Photograph is of 45 DAG plants (bar = 1 cm).

2.2.12 Chemical reduction of isoxaben yields active compounds

Isoxaben and flupoxam induce nearly identical phenotypes at the same concentrations in *Arabidopsis*. Alleles which confer resistance to these CBIs are restricted to the catalytic sub-units which constitute the primary-wall rosette complex. Moreover, alleles of both *ixr* and *fxr* can be found in *cesA3*. Despite these sibling-like similarities in the induced effects in plants, the chemical structures appear to be very distinct. Apart from the presence of aromatic and aliphatic groups, there is no apparent pattern to the three-dimensional spatial distribution of the steric bulk and functional groups. The similarities of the phenotypes induced by these two herbicides do not seem to be reflected in their chemical structures.

A possible explanation for this inconsistency may lie in the form the herbicide exists inside the reducing conditions of the cytoplasm. Flupoxam more than likely is able to remain unchanged long enough for it to reach its site of action. Isoxaben, however most likely does not. The O-N bond of the isoxazole ring in isoxaben is the weakest bond in the molecule with bond energy of only 200 kJ/mol (Eicher & Hauptmann 2003). This bond strength lies between the bond energies of Br-Br and the HO-OH in hydrogen peroxide (Figure 2.2.12A). At this point it is important to reiterate that the eukaryotic cytosol is a reducing environment and is actively maintained through thiol-disulfide exchange of glutathione (Lodish 2000). The hypothetical structure of the reduced-isoxaben (isxH) is given in Figure 2.2.12B. The formation of this compound is reasonable since methoxyphenyl pyrimidinol was found as a major metabolite in isoxaben treated soil (European Food Safety Committee 2010 and United States Environmental Protection Agency 2007) (Figure 2.2.12C). Reduced-isoxaben has been

found in concentrations as high as one-third of the applied dose of the parent molecule four months after soil treatment. The structure of the hypothetical product of isoxaben reduction (isxH) is compared to methoxyphenyl pyrimidinol a major metabolite and flupoxam (Figure 2.2.12B-D). All three have aryl groups bonded to an aromatic carbon flanked by two pyridine-like nitrogens. This creates a very flat structure with spatial and charge distribution features presumably resembling a β-glycan or cellobiose.

To test the validity of these hypothetical rearrangements, isoxaben was chemically reduced in the presence of excess sodium borohydride in tetrahydrofuran (THF). The resulting product migrated faster on thin layer chromatography silica solid phase in a mobile phase of 1:9 methanol and dicloromethane (DCM) (Figure 2.2.12E). This is consistent with the proposed chemical structure since isxH is more hydrophobic than isoxaben and should have a lower affinity for the polar solid phase and migrate faster. This faster-mobility, chemically distinct reduced-isoxaben induced the same cellulose deficiency effects in the same dose ranges as the parent molecule. Loss of anisotropy and severe cell wall defects were observed in wild-type (*Col-0* and *Ler*) exposed to the reduced-isoxaben. Furthermore, all of the *ixr* mutants were resistant to the reduced form of the herbicide. The effects of isxH on *Arabidopsis* seedlings were indistinguishable to the effects of the parent compound. This is strong albeit indirect evidence that supports the notion of a reduced and more hydrophobic metabolite of isoxaben being an active molecule of cellulose biosynthesis inhibition. The hypothetical structure of isxH was verified by ^{1}H NMR. The doublet peak at 6.24 and 6.25 ppm of the isoxazole aromatic proton is replaced with a weak alcohol peak at 6.21 ppm along with the appearance of the pyrimidinol aromatic proton peak further downstream than expected at 8.50 ppm (Figure

2.2.12F). The slightly higher ppm values for this proton can be explained by deshielding due to intermolecular hydrogen bonding with water molecules. The pyrimidinol proton peak is not split since there are no protons to couple with and appears as a singlet. Additionally, the weak amide peak at 11.75 ppm in the isoxaben spectrum is much further downfield than expected. The amide proton participates in intramolecular hydrogen bonding with the proximal methoxy-oxygen. This interaction significantly de-shields the amide proton which shifts the peak to the left as observed. This amide peak does not appear in the isxH spectrum due to the absence of the functional group. The functional group changes regarding protons from isoxaben to isxH involve the substitution of an amide and an alcohol. ^{1}H NMR is not particularly well suited to detect and characterize protons in these functional groups. This is because alcohol and amide protons are acidic enough that they readily exchange into their surroundings. This prevents high resolution characterization of their chemical properties by available techniques. This rapid acidic proton exchange gives rise to weak and unresolved peaks characterized by the absence of spin-coupling splitting pattern.

The proposed mechanism for the cleavage of the O-N bond under reducing conditions proceeds through the formation of an imine which opens the isoxazole ring (Figure 2.2.12I). The imine then nucleophillically attacks the amide carbonyl in a cyclization reaction forming a zwitter compound (J) which tautomerizes into compound K. Finally after a hydroxyl-shift and an intramolecular dehydration step the proposed structure of reduced-isoxaben (isxH) is formed (Figure 2.2.12L).

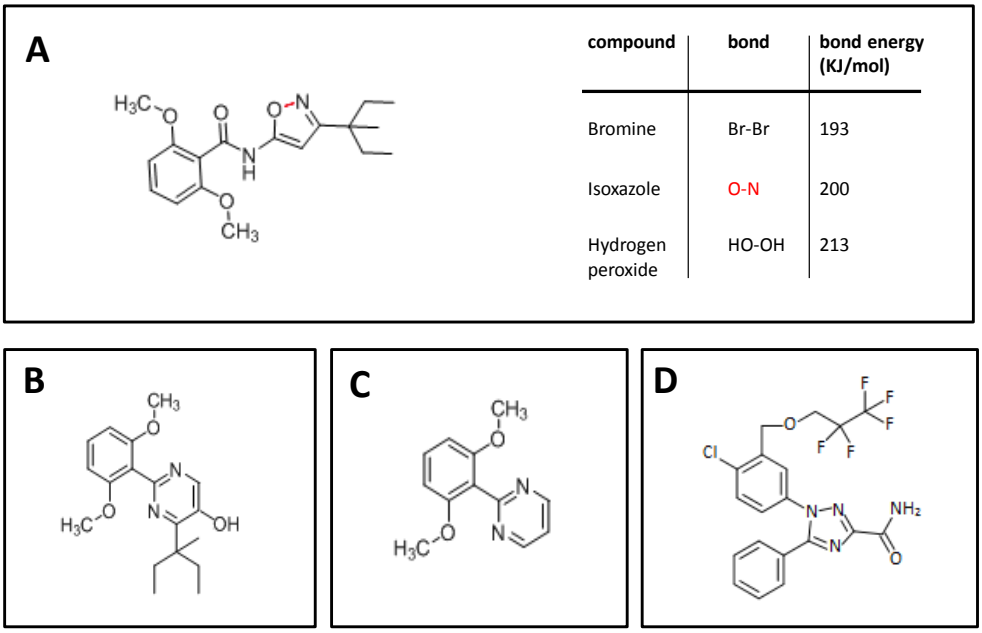

Figure 2.2.12: A comparison of the structures of isoxaben and related compounds.

A) The structure of isoxaben with the isoxazole bond highlighted in red. This bond can be broken by either chemical or enzymatic reduction. The bond energy of the N-O bond of isoxazole is between those of molecular bromine and the O-O bond of hydrogen peroxide (right). The values are from McMurry *Organic Chemistry* 5^{th}*ed*. (2000) and Eicher *et al*. *The Chemistry of Heterocycles* (2003).

B) The chemical structure of the hypothetical compound, isxH.

C) The chemical structure of methoxyphenyl pyrimidinol, a major environmental metabolite of isoxaben.

D) Flupoxam has a similar flat aromatic core with structures B and C.

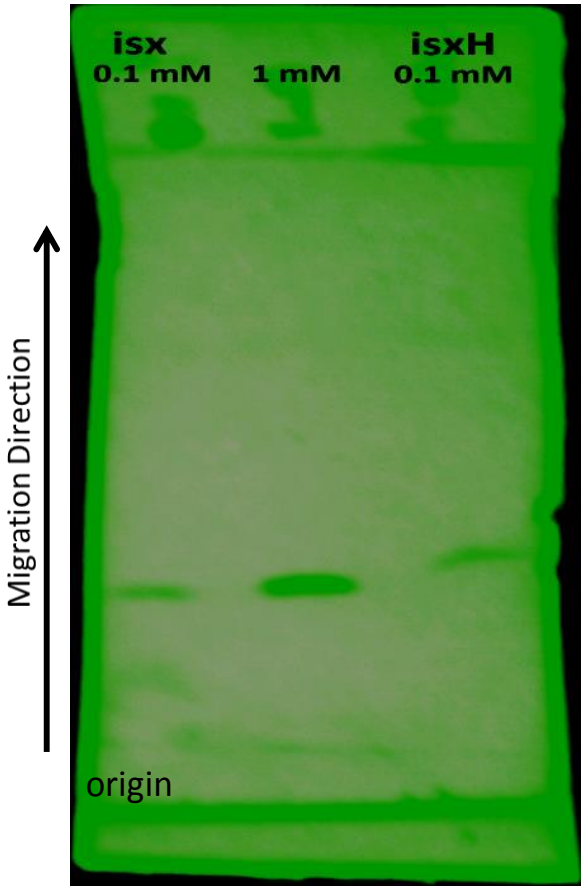

Figure 2.2.12E: Separation of isoxaben and isxH using thin layer chromatography (TLC). An image of a UV illuminated silica TLC plate loaded with 0.1 mM isoxaben (right), 1 mM isoxaben (center) and 0. 1 mM of isxH (right). The plate confirms that there is no remaining unreacted isoxaben.

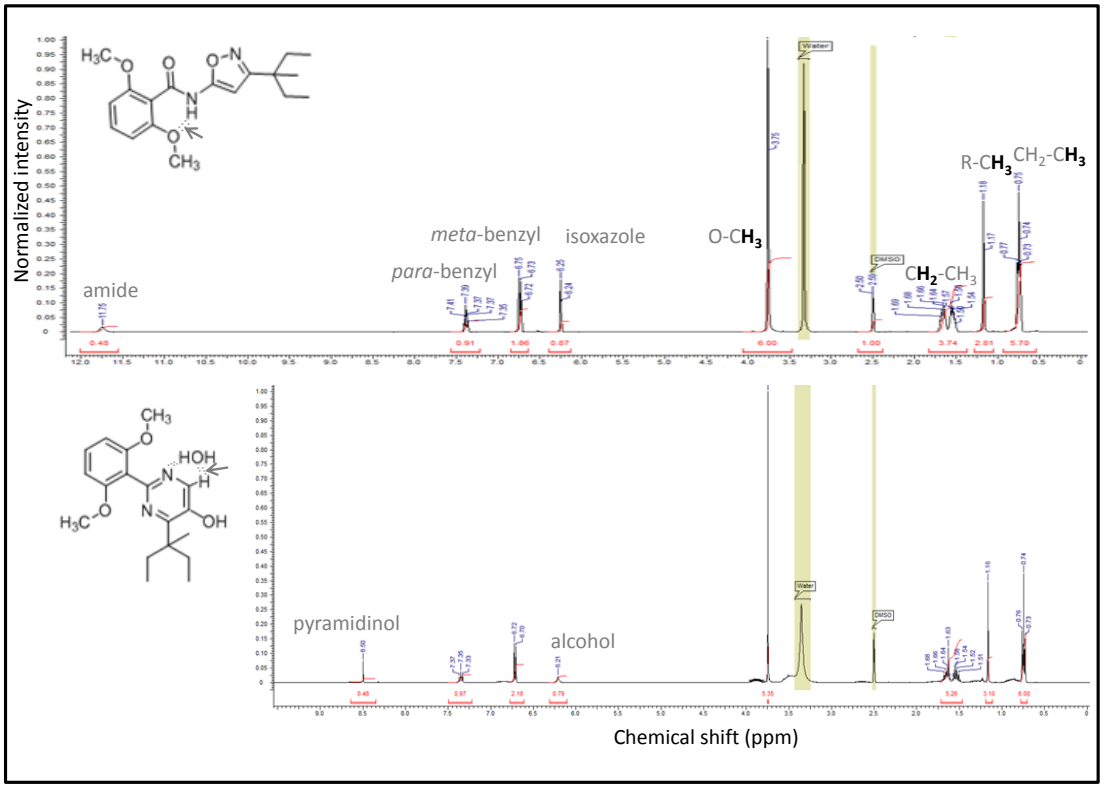

Figure 2.2.12F: Proton NMR spectra of isoxaben (top) and isxH (bottom). Along with the chemical structures are the relevant hydrogen bonds responsible for the downfield shifts of protons involved are shown (arrows).

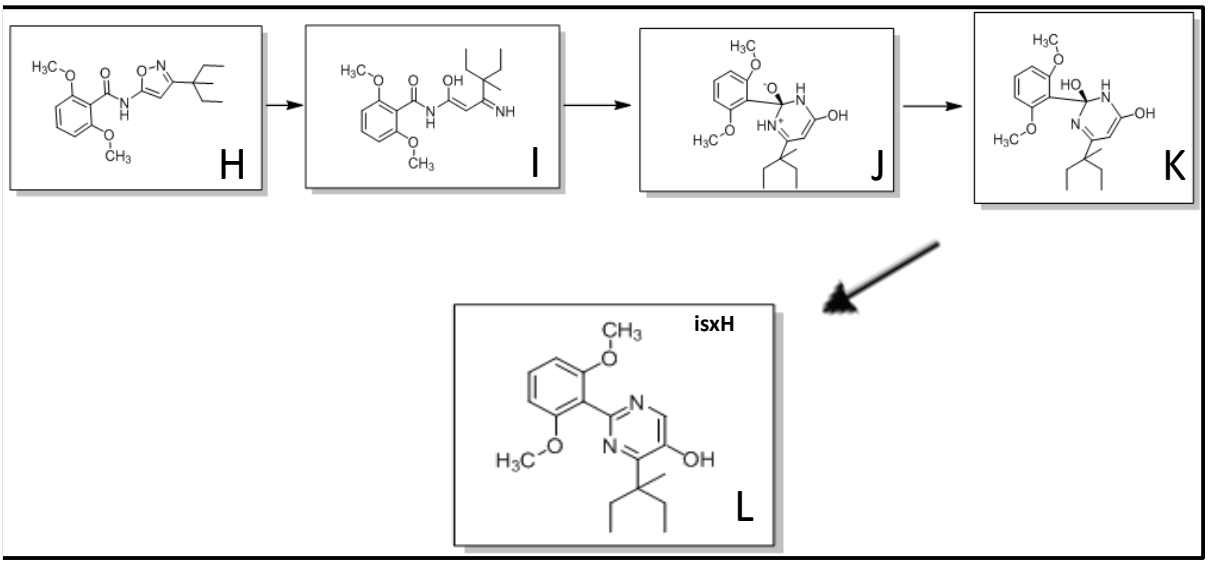

Figure 2.2.12: The chemical structures of isoxaben and its derivatives.

H) The chemical structure of isoxaben, the parent compound.

I) The product of reductive ring-opening is an open structure with the oxygen and nitrogen of the isoxazole forming an alcohol and an imine respectively.

J) Upon nucleophilic attack of the carbonyl by the imine a new six-membered ring forms.

K) A hydride shift produces a diol.

L) The hypothetical chemical structure of isxH.

2.2.13 2-(4-hydroxyphenyl)-5-pyrimidinol (pydA) is an inhibitor of glycan biosynthesis in *Arabidopsis* root hairs

To test the hypothesis of reduced-isoxaben and flupoxam sharing structural features, a compound with only the essential common features of both herbicides, 2-(4-hydroxyphenyl)-5-pyrimidinol (pydA) was acquired and tested on *Arabidopsis*. The chemical structure of pydA clearly illustrates the phenyl-aryl carbon-pyrimidine-like nitrogens common structural elements. Figure 2.2.13A shows the structure of 2-(4-hydroxyphenyl)-5-pyrimidinol (pydA) juxtaposed with the hypothetical structure of reduced-isoxaben (isxH) and flupoxam (fsx).

Etiolated Ler and Col seedlings incubated in pydA did not show a significant difference in crystalline cellulose production (data not shown). Light grown seedlings showed a dose dependent inhibition in root hair growth at high concentrations while at lower concentrations they displayed phenotypes associated with auxin imbalances (Figure 2.2.13C). The high concentration phenotype is strikingly similar to those of mutants deficient in CELLULOSE SYNTHASE-LIKE-D (CSLD) activity. Exposure to pydA produced root hair stumps in wild-type resembling the phenotype of CSLD3 loss-of-function mutants (Figure 2.2.13D). The mutant *kojak* in particular (Favery *et al.* 2001), exhibits similar phenotypes to those produced by pydA and CSLD3 is closely related to CESA6-like glycosyl transferases. CSLD3 and CESAs are phylogenetically the most closely related in *Arabidopsis* (Favery *et al.* 2001). The inhibitory action of pydA on root hairs must occur during the elongation phase since growth is initiated. *CslD3* has been implicated in root hair growth and has been shown to be co-transcriptionally regulated with *cesA3* and *cesA6*, however does not co-localize on the plasma membrane of root hair tip during elongation (Park *et al.* 2011). Furthermore no *ixr* was observed to be cross-

resistant to the effects of this compound. These observations provide indirect evidence that isoxaben and to a lesser extent flupoxam targets a protein or proteins similar in structure to CSLD3 but different enough for cross-resistance not occur. Mutagenesis studies screening for resistance to pydA would be the best approach to uncovering the target and genetic cause of its effects on *Arabidopsis*. Such a study would help elucidate the targets of pydA and provide insight in the connection with isoxaben and flupoxam and the CESA proteins. Mapping of resistance alleles to regions encoding *cslD3* would be an exciting finding and would be further evidence supporting the reduced-isoxaben hypothesis.

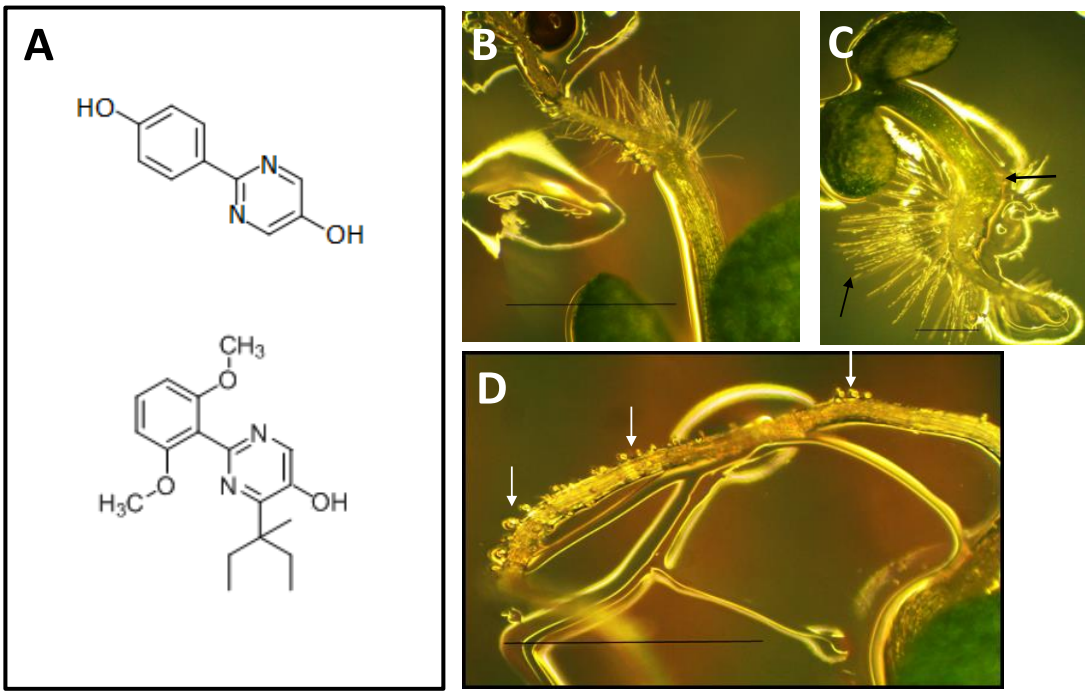

Figure 2.2.13: Assessment of the effects of pydA on seedling growth.

A) The chemical structures of 2-(4-hydroxyphenyl)-5-pyrimidinol (pydA) (top) and isxH (bottom).

B) Image of normal root hairs in a 10 DAG *Col-0* seedling in the absence of pydA (bar = 1 mm).

C) Exposure to low concentrations (1 µM) of pydA induces auxin-like effects such as blistering at the base of the hypocotyl (top arrow) and growth of root hairs predominantly only in one direction in *Col-0* (bottom arrow) (bar = 1 mm).

D) Higher concentrations (50 µM) of pydA results in complete loss of root hairs (bar = 1 mm). Arrows show stumps where root hair formation is incomplete.

2.2.14 CP-91149 treated *Arabidopsis* seedlings exhibit mild wall deficiencies and effects of auxin transport disruption

To further investigate the plausibility of the reduced-isoxaben hypothesis, an analogue of the hypothetical open chain compound (Figure 2.2.12I) was acquired and tested on *Arabidopsis* seedlings. The compound, CP-91149 has an indole carboxamide moiety resembling the carboxamide of isoxaben in its open chain reduced form (Figure 2.2.14A and B). Incidentally, this compound was previously described as an allosteric glycogen phosphorylase inhibitor and a promising antidiabetic agent (Rath *et al*. 2000). Glycogen phosphorylases catalyze the catabolism of glycogen to glucose-1-phosphate. This compound behaved like an auxin in the micromolar range which is not surprising since CP-91149 has an indole functionality (Figure 2.2.14B). In wild-type the compound had a stimulatory effect on root hair growth unsymmetrically along root, particularly at the base of hypocotyl and shortened thicker roots (Figure 2.2.14C and D). This effect was very similar to the effect of low concentrations of pydA (Figure 2.2.13C). Interestingly, *ixr1-4* displayed hypersensitivity compared to wild-type when treated with CP-91149 (Figure 2.2.14E). The amino acid substitution in this mutant occurs in the QxxRW sequence which is conserved amongst CESAs and CSLs proteins. Additionally, the homozygous double mutant *ixr1*-1;*fxr2-3* was hyper-sensitive to this compound and exhibited hypocotyl cell swelling similar to that seen in *ixr1-4* (Figure 2.2.14F). It is encouraging to see crude analogues of hypothetical structures from section 2.2.12 have such effects on glycan biosynthesis.

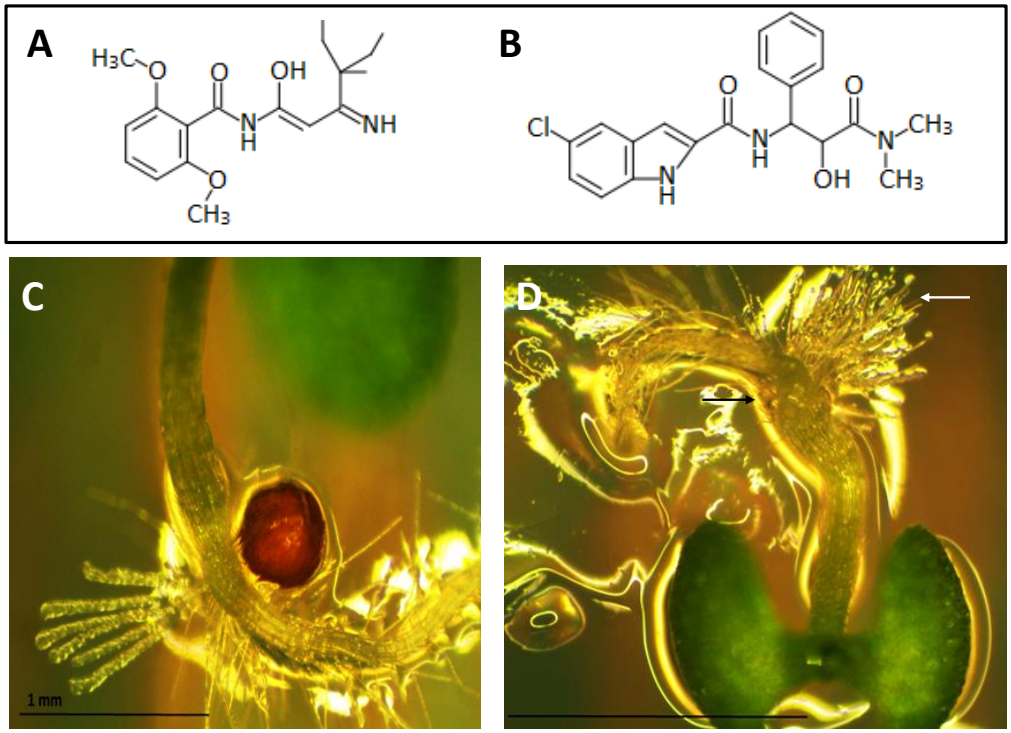

Figure 2.2.14: Effects of CP-91149 on seedling growth.

A) The chemical structure of the open chain isxH from Figure 2.2.12I.

B) The chemical structure of CP-91149 a glycogen phosphorylase inhibitor and an analogue of 2.2.12I.

C) A light-microscope image of the base of the hypocotyl of a *Col-0* seedling in the absence of CP-91149 (bar = 1 mm).

D) Wild-type seedlings treated with 10 μM of CP-91149 display blistering at the base of the hypocotyl (black arrow) and drastically asymmetric root hair growth (white arrow), effects similar to low doses of pydA (Figure 2. 2. 13C) (bar = 1 mm).

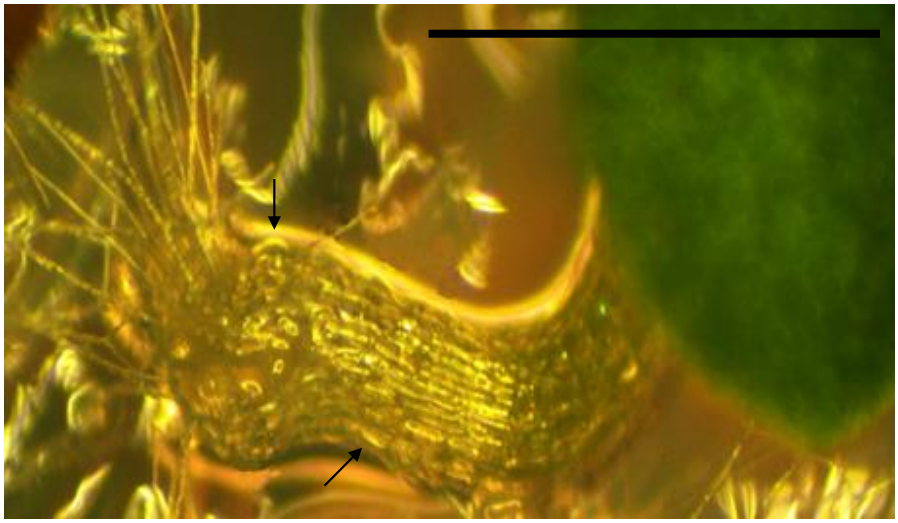

Figure 2.2.14E: *ixr1-4* 10 DAG seedlings are hypersensitive to the effects of CP-91149. They display more severe blistering in at the base of the hypocotyl compared to wild-type top arrow). Moreover, *ixr1-4* seedlings exposed to 10 μM of CP-91149 exhibit blistering throughout the hypocotyl not seen in wild-type (bottom arrow) (Figure 2.2.14D) (bar = 1 mm).

Figure 2.2.14F: Double mutant *ixr2-1*;*fxr1-1* seedlings display blistering in the hypocotyl (arrows) when subjected to CP-91149 at 10 μM concentrations similar to that seen in *ixr1-4* (bar = 1 mm).

2.3 Methods

2.3.1 Plant material and growth conditions

All *Arabidopsis* lines used were of the *Landsberg erecta* (*Ler*) ecotype and were generated in this study except: *ixr1-1*, *ixr1-2* and *ixr2-1* which were generated in the *Columbia* (*Col-0*) accession (Scheible *et al*. 2001 and Desprez *et al*. 2002). Moreover, *fxr1-1* also was created in the *Col-0* background, but was generated in a previous unpublished work along with *ixr1-1B* of the *Ler* ecotype. Seedlings were germinated and grown under continuous light (200 $\mu E/m^2/s$) or in the dark at 21°C on 0. 8% agar plates containing 2g/L of Murashige and Skoog (MS) mineral salts (Sigma-Aldrich, St. Louis, MO). Both MS and agar solutions were autoclaved at $121^{O}C$ for 20 minutes prior to use. Alternatively, plants were grown on a mixture of 70% sphagnum peat, 15% perlite and 15% vermiculite in growth chambers maintaining the following conditions: 21°C under long-day conditions (16 h light/8 h dark) at a light intensity of 200 $\mu E/m^2/s$. Flupoxam was a kind gift from Kureha Chemical Industry Co., Iwaki City, Japan and isoxaben, pydA and CP-91149 were obtained from Sigma-Aldrich. MS-Agar was directly inoculated with a 100 μM stock of the herbicide dissolved in anhydrous ethanol. *Ixr1-2*, *ixr1-2*, *ixr2-1*, *Ler* and *Col-0* seeds were obtained from the Arabidopsis Biological Resource Center at Ohio State University.

2.3.2 EMS mutagenesis and screening

EMS is an alkylating agent which induces transition mutations. Ninety-nine percent of the time, the nucleotide substitutions are generated through the formation of O^6-ethylguanine (Kim *et al.* 2005). This modified guanine nucleotide behaves like adenine

and favors base-pairing with thymine instead of with cytosine. Subsequent rounds of DNA replication results in the original G/C pair being replaced with an A/T pair (Kim *et al.* 2005). Forty-five thousand seeds of the *Landsburg* (*Ler*) accession were mutagenized by treatment with 0.3% EMS. The concentration of EMS used has been empirically determined to induce approximately 1000 mutations per genome in *Arabidopsis*. The EMS treated seeds were sown to generate a mutagenized M2 population of one million seeds. The mutagenized seeds were obtained as a generous gift from Dr. Sean Cutler at the University of California at Riverside.

Half of the M2 seeds were screened on isoxaben and the other on flupoxam. They were placed on 0. 8% agar plates containing 2 g/L Murashige and Skoog (MS) salts with either 20 nM isoxaben or flupoxam. Fourty-five thousand *Ler* seeds were treated with 0.3 % ethylmethane sulfonate (EMS) for 16 hours at room temperature. They were then extensively washed with water over the course of 10 hours and sewn onto soil to generate the M2 seeds. One million M2 EMS treated seeds were surface sterilized and screened for resistance on 20 nM flupoxam or 20 nM of isoxaben. Resistant mutants were isolated and transferred to MS. Plants were propagated and re-selected to confirm that the flupoxam resistance was heritable.

The genomic DNA of the retested M3 lines was extracted using the cetyl-trimethyl-ammonium bromide (CTAB) extraction method (Murray and Thompson 1980). *cesA1*, *cesA3* and *cesA6* genes were amplified by the polymerase chain reaction (PCR) and the purified products sent to The Centre for Applied Genomics (TCAG) at Sick Kids Hospital in Toronto for sequencing. The primers used to amplify the regions harboring the SNPs are given in Table 2.3.2.

Table 2.3.2: Primers used to amplify the regions containing the SNPs for each mutant. The primers amplify approximately a 1kb region containing the mutation.

Allele	**Gene**	**Primers**
ixr1-1, ixr1-1B, ixr1-3, fxr1-2 & fxr1-3	*cesA3*	5'-TCCTCAGGTTTGACACCTCTC-3' 5'-TGACACCAAGACAGAAGAACG-3'
ixr1-4 & ixr1-5	*cesA3*	5'-CCAGGGGAGGGGATTATTTA-3' 5'-CTACGCCACTCCACCTCATT-3'
ixr1-6	*cesA3*	5'-TACCTCGACAGGCTTGCTTT-3' 5'-TTGGTCAGAATGAAGAAGTCAAA-3'
ixr1-7	*cesA3*	5'-GGAATCTGATTTTGTCATTTGC-3' 5'-GTCCCAAAAATTGACCATGA-3'
ixr2-1 & ixr2-2	*cesA6*	5'-TAGCAACTATGCGAGTATC-3' 5'-ATCGAATCACAAGCAGTCTA-3'
fxr2-1, fxr2-2 & fxr2-3	*cesA1*	5'-CGCGAGTATTTGGTTCATTC-3' 5'-TTGGGTCCACATCTTCTTCC-3'
fxr2-4	*cesA1*	5'-GGTAAATACCATGAAGGGAAAG-3' 5'-CGGAAACTTCACATGGTCAG-3'

2.3.3 DNA purification using CTAB and DNA sequencing

Leaf tissue was ground in 150 µl of CTAB using a drill-press with a homogenizing bit in a sterile eppendorf tube. Cetyltrimethyl Ammonium Bromide (CTAB) buffer consisted 100 mM Tris HCl pH 8.0, 1.4 M NaCl, 20 mM EDTA, and 2% w/v CTAB (adapted from Murray and Thompson 1980). The homogenizing bit was then rinsed with another 150 µl of CTAB to clear left over tissue debris into the eppendorf tube. The tissue suspension was then incubated for one hour at 65°C. Following incubation, an equal volume of chloroform was added and the solution was vortexed thoroughly and centrifuged for 3 minutes at 20 000 *g*. The aqueous phase was removed and an equal volume of 2-propanol was added and the tube was inverted several times to precipitate DNA. The tubes were then centrifuged for 10 minutes at 20 000 *g*. The DNA pellet was washed with 70% ethanol; air dried and dissolved in sterile 10 mM Tris buffer pH 8.0.

The isolated genomic DNA of the selected mutant lines were used as templates for polymerase chain reaction (PCR). Primer sets were used to amplify *cesA1*, *cesA3* and *cesA6*. Unless otherwise stated the annealing temperature and time used was 55°C for 30 seconds with extension for 1 min. The enzyme used was ExTaq polymerase from TaKaRa. The sequences of the primers used to amplify the regions harbouring the mutations are given in Table 2.2.2. The PCR products were purified using the QIAquick PCR Purification Kit. Fifty nanograms of PCR product was placed in seven microliters of milliQ water along with approximately 5 pmols of the forward or reverse primer in 0.7 µL. The samples were then sent to The Centre for Applied Genomics in Toronto, Canada for direct PCR sequencing.

2.3.4 ^{14}C-glucose incorporation in to cellulose

Five milligrams of homozygous seeds were weighed out on a microbalance Mettler Toledo AB204-S scale in sextupilicates. Seeds were surface sterilized in a chlorine gas chamber and transferred to six well plates containing 5 mL of 0.5x liquid Murashige and Skoog (MS) media (Sigma-Aldrich; St. Louis, MO) and 0.5% w/v glucose. Seeds were then stratified at 4^{o}C for 3-4 days. After this, plants were grown on an orbital shaker in the dark at medium speed. After five days of growth, seedlings were washed three times in 5 mL glucose free medium and suspended in 2 mL of 0.5x MS containing 0.5 Ci/mL ^{14}C-glucose (American Radiolabelled chemicals; St-Louis, MO). Seedlings were then incubated for 1 hour in the dark on an orbital shaker. Following treatment, seedlings were washed three times with 5 mL of glucose free medium. These were then transferred to glass tubes and incubated in 5 mL anhydrous ethanol at 80^{o}C for 20 min. This was repeated three times. Seedlings were then incubated in 3 mL chloroform: methanol (1:1) for 20 min at 45^{o}C. Finally, seedlings were incubated in 5 mL of acetone at room temperature for 15 min. The acetone was aspirated and the tissue was allowed to dry for two days before being weighed. Material was then treated according to Updegraff (1969) with minor modifications. One mL of Updegraff solution (nitric acid: acetic acid: water 1:8:2) was used to hydrolyze the cell wall material in a boiling water bath for one hour. Soluble and insoluble fractions were separated using an aspirator. The insoluble fractions were retained on Whatman 25 mm GF/A glass microfilters and tubes were washed once with 1 mL of water. The flow through and 1 mL water wash were combined to represent the soluble fraction. Both soluble and insoluble fractions were transferred into separate scintillation vials to which 5 mL of Ultima Gold High Flash Point Scintillation Liquid

Cocktail (Perkin Elmer; Waltham, MA) was added. Beta emissions were quantified using a Perkin Elmer Tri-carb 2800 liquid scintillation detector (Waltham, MA). Data is presented as percent incorporation ([insoluble/ (insoluble + soluble)]*100).

2.3.5 X-ray diffraction

Dried and processed senesced plant material was loaded onto an aluminum sample holder with a glass background. This was in turn placed into a PANalytical Phillips PW3170 X-ray diffractor at the Department of Geology, University of Toronto. Material was pressed by hand using a scupula to generate an even surface. Protocols were run with start angle of $2\theta = 4.5°$ and an end angle of 30°. The scan speed was run at 0.008 °2θ/s, an intensity of 40 kV and 40 mA. Data was calculated using the equation for Relative crystallinity index (RCI) used by Segal *et al*. (1959) where $RCI=I_{002}-I_{am}/I_{002} \times 100$. I_{002} is the maximal peak around $2\theta = 21.5^{o}$ for type I and 22.5^{o} for type II cellulose. The I_{am} is the amorphous trough found around $2\theta= 18\text{-}20°$ (Segal *et al.* 1959). An average of 10 peaks was taken at the amorphous trough and the crystalline peak areas. Results indicated are a product of n = 3, with each replicate containing plant material pooled from 6 plants.

2.3.6 Acid and enzymatic hydrolysis of plant biomass

The senesced above ground tissue (>95% stem) was ground using a Thomas Scientific Mill (model 3383-L10) and passed through a 60 gauge screen after being baked at $65^{o}C$ for 24 hours. Two hundred milligrams of dry tissue were placed in glass test tubes then filled with 10 mL of water. The tubes were vortexed then left at room temperature overnight to allow the tissue to macerate. Once the majority of the tissue had sunk to the

bottom of the tube, the water was aspirated and a fresh 10 mL of water was added. The tubes were vigorously vortexed before being placed in a water bath set at 80°C for 1 hour. The water was removed by aspiration and 10 mL of 70% ethanol were added to each tube. The tubes were vortexed then placed at 80°C for 1 hour. The ethanol was removed by aspiration and replaced with 5 mL of acetone. The tubes were vortexed and allowed to sit at room temperature for 15 minutes before the acetone was removed by aspiration. The tissue was allowed to dry for 2-3 days at room temperature. Ten milligrams of this tissue were placed in 1.5 mL screw-cap microcentrifuge tubes in triplicates.

Water Soluble

To each screw cap tube containing 10 mg of prepared tissue, 0.8 mL of water were added. After being vortexed the tubes were placed at room temperature overnight. The tubes were centrifuged at 14 000 *g* for 5 minutes and 50 µL of the supernatant were placed into separate wells of a 96-well spectrophotometric plate. One hundred microlitres of 0.2 % anthrone in H_2SO_4 (conc.) were added to the wells and mixed. The plate was placed on a heat block set at 100°C for 5 min then placed at 4°C for 10 min. Absorbance at 620 nm was determined using a BIO RAD xMark™ Microplate Absorbance Spectrophotometer (#168-1150). The reducing sugar equivalents were determined by converting the absorbance readings to corresponding sugar quantities according to a glucose standard curve (Yemm & Willis 1954).

Acid Hydrolysis

Fifty microlitres of water were added to the tubes to replace the water taken for the above assay. In addition, 0.2 millilitres of 1 M H_2SO_4 were added to bring the volume to 1 mL and the concentration to 0.2 M. These tubes were vortexed then

placed at 80ºC for 2 hours. The tubes were allowed to cool to room temperature then centrifuged at 14 000 *g* for 5 min. Fifty microlitres of the supernatant from each sample were assayed for their soluble reducing sugar content using 0. 2% anthrone in the manner described above.

Enzymatic Hydrolysis

The dilute acid was then aspirated and 1 mL of water was added to each tube. After vigorous vortexing the tubes were centrifuged at 14 000 *g* for 5 min. The water was aspirated and replaced with 0.9 mL of 50 mM sodium citrate (pH= 4. 8). Twenty microlitres of 0.1x Celluclast (Sigma) and 80 µL of 0.1x Novozyme 188 (Sigma) were added to each tube to bring the final volume to 1 mL. The activities for 1x were determined to be 111 FPU/mL and 500 U/mL respectively (Ghose 1987). After vortexing, the tubes were placed in a water bath set to 50ºC for two days vortexing periodically throughout. The tubes were then centrifuged at 14 000 *g* for 5 min and 5 µL of the supernatant were placed into 45 µL of water in a 96-well spectrophotometric plate. The reducing sugars were then quantified using 0.2% anthrone as described above.

Inaccessible Cellulose

The supernatant was then removed by aspiration and replaced with 1 mL of Updegraff solution. This solution is a 1:8:2 mixture of nitric acid (conc.), glacial acetic acid and water. The tubes were placed in a boiling hot water bath for 1 hour. The tubes were allowed to cool then centrifuged at 14 000 *g* for 5 min. The supernatant was removed by aspiration and replaced with 0. 2 mL of 72% (v/v) H_2SO_4 and placed at room temperature for 1 hour. After the entire pellet had dissolved, 0.8 mL of water was added and the tubes were vortexed. Five microlitres of the supernatant was placed into 45 µL of

water in a 96-well spectrophotometric plate and assayed with 100 µL of 0.2 % anthrone as previously described.

2.3.7 Phloroglucinol staining of lignin

Seedlings on MS Agar plates were stratified for 4 days at 4ºC. They were then exposed to 200 µE/m^2/s for 10 hours at 20ºC. The plates were then left vertically in the dark for 8 days. The seedlings were then placed in a solution of 1% (w/v) phloroglucinol in 95% (v/v) ethanol. An equal amount of 50% (v/v) HCl was added to visualize the staining. The samples were mixed and allowed to sit for 5 minutes. The stained seedlings were then examined under a dissecting light microscope equipped with an Amscope MD900E camera (Irving, CA). The seedlings were examined for ectopic lignin staining and were compared against wild-type controls (n = 9).

2.3.8 Sample preparation for scanning electron microscopy

Five day old seedlings were immersed for 30 seconds in pure anhydrous ethanol. They were then fixed in a solution consisting of 50% ethanol, 5% acetic acid, 3.7% formaldehyde for 24 hours. After this incubation, the tissue was dehydrated in a series of ethanol exchanges of increasing concentrations of ethanol (+5 %/hour). The tissue was then stored in100% ethanol for 24 hours prior to being critically point dried in carbon dioxide using Autosamdri-815 drier and then gold sputter coated using a Balzer Sputtering device. Samples were visualized using a Hitachi S2300 scanning electron microscope at the Department of Cell and Systems Biology, University of Toronto.

2.3.9 isxH preparation and ^{1}H NMR characterization

One hundred milligrams of isoxaben was dissolved in 100 mL of THF along with 0.5 grams of sodium borohydride. The solution was stirred at room temperature for 3 hours. The reaction mixture was quenched with distilled water. The solvent was evaporated off and the remaining compound was reconstituted in ethanol and analyzed by TLC. Five microliters of the isxH solution was placed on a silica plate and the TLC was run using a 1:9 methanol: DCM mobile phase. The silica plate was visualized under UV light at a wavelength of 254 nm.

Nuclear Magnetic Resonance (NMR) was performed on a Varian 400 MHz spectrometer. All ^{1}H NMRs were recorded for 64 transients at 400 MHz. Spectra were processed and integrated using ACD/NMR Processor Academic Edition. ^{1}H NMR peaks were referenced to 2.50 ppm for measurements performed in Dimethyl Sulfoxide-D6 (d_6-DMSO).

Analytical grade Isoxaben was purchased from Sigma-Aldrich. ^{1}H-NMR of isoxaben (400 MHz, d_6-DMSO); δ 0.75 (m, 6H), 1.8 (d, 3H, J= 4.00 Hz), 1.57 (m, 4H), 2.5 (d, 1H, J= 1.9 Hz), 3.76 (d, 6H, J= 4.30 Hz), 6.25 (d, 1H, J= 4.70 Hz), 6.74 (m, 2H), 7.39 (m, 1H), 11.75 (s, 0.5H).

Ten milligrams of crude isxH was dissolved in 1 mL of d_6-DMSO and filtered through a pipette filled with cotton to remove undissolved material. ^{1}H-NMR of reduced isoxaben (400 MHz, d_6-DMSO); δ 0.74 (m, 6H), 1.16 (s, 3H), 1.63 (m, 5H), 3.75 (s, 5H), 6.21 (s, 1H), 6.71 (d, 2H, J= 8.60 Hz), 7.35 (t, 1H, J=8.60 Hz), 8.50 (s, 0.5H).

2.4 Discussion

Cellulose is synthesized by large multimeric membrane-bound complexes. These complexes are composed of an estimated 36 catalytic glycosyl transferase subunits whose crystal structure remains to be determined. There have been significant advances using various different indirect approaches in an attempt to elucidate this process. These include but are not limited to the study of conditional *cesA1* mutants (Arioli *et al*. 1998); the use of molecular fluorescence techniques to track the movement of CESA particles as they move and are distributed throughout the cell (Wrightman & Turner 2010) and forward chemical genetic studies to investigate the effects of perturbations on cellulose synthesis (Scheible *et al.* 2001). This study employed a chemical genetics approach using the chemical herbicides isoxaben and flupoxam. The two herbicides cause many similar effects including anisotropic expansion of cells, reduced cellulose content of the walls and synthesis, detachments of the plasma membrane from the cell wall, increased pectin accumulation, wall thinning, and ectopic lignin (Vaughn & Turley 2001). Both herbicides inhibit the incorporation of glucose into cellulose at nanomolar concentrations and are putative CBIs (Figure 2.2.7A). Although the exact mode of action is not known, the picture of how these molecules work is materializing. Modification of CESA3 G(998)D, CESA3 T(942)I and CESA6 R(1064)W have previously been described and as *ixr1-1 ixr1-2* and *ixr2-1* respectively (Scheible *et* al. 2001 and Desprez *et al*. 2002). These mutants provide genetic evidence for its mode of action. Since no cross-resistance allele has been observed for isoxaben and flupoxam it seems plausible that they may disrupt the rosette complex on separate binding sites.

A screen of 1 million EMS treated seeds on 20 nM of CBI isolated twelve novel alleles. No genes other than primary wall *cesA*s were identified and interestingly, certain amino acid residues were hit multiple times. In this screen, substitutions resulting in S(377)F of *ixr1-6* (CESA3) and S(307)L of *fxr2-4* (CESA1) were both isolated twice independently in separate pools. Furthermore, the G(1013)R substituted in CESA1 (*fxr2-1*) is the same residue as the G(998)D in CESA3 of *ixr1-1* described Heim *et al*. 1989 (Figure 2.2.1B). Glycine 998 of CESA3 is the site of substitution for three independently generated alleles across both eco-types all of which conferring high levels of resistance (*ixr1-1, ixr1-1B* and *ixr1-3*). This site is in the C-terminal end of TMD7 suggesting that the CBIs act within the membrane. This is reasonable considering isoxaben and flupoxam both are relatively hydrophobic having log K_{ow} values of 3.94 and 3.27 respectively (agrochemicals.iupac.org). The substitution of S(10002)F in *ixr2-2* (CESA3) is the same residue as S(983)F in CESA3 of *fxr1-3*. These data indicates that the mutagenesis screen was saturated and primary *cesA* genes exclusively harboring resistance is genetic evidence supporting the notion that isoxaben and flupoxam act by binding and disrupting the primary wall CESA complex. The lack of cross-resistance suggests that they do so by binding different sites.

The mutations discussed in this study show varying degrees of relative resistance to the CBIs (Figure 2.2.4 A and B). For flupoxam resistance on CESA1, the introduction of charge appears to confer the greatest resistance. *fxr2-2* P(1010)L does not introduce a charge and is not as resistant as *fxr2-1* G(1013)R or *fxr2-3* G(1009)D (Figure 2.2.4B). This trend is best illustrated when *ixr1-1* G(998)D and *ixr1-3* G(998)S are juxtaposed. Both carry substitutions at the same site but for different residues. Glycine and proline

are known to be important in determining tertiary structure and suggests alterations of the herbicide binding site as the mode of resistance. *Ixr1-1* is highly resistant and displays no cellulose deficiencies, contrasted to *ixr1-3* which is less resistant and exhibits many cellulose deficient phenotypes. Resistance seems to favor amino acid substitutions that are predicted to be at the cytosol-membrane interface. This is the case for all alleles of *fxr1, ixr1-7, fxr2-4, ixr1-1, ixr1-3* and *ixr2*-2.

All *fxr1* alleles result in amino acid substitutions on CESA3 of serine residues within the C-terminal TMD (Figure 2.2.3B). Of the seventeen CBI resistant mutants discussed in this study, seven involve the substitution of a serine/threonine residue, five of which are in CESA3. In addition, the L797F substitution of *ixr*1-5 introduces a bulky residue immediately adjacent to a serine and possibly results in blocking access to neighboring residues. The significance of this bias for substituting out serine/threonine in *ixr* and *fxr* is a matter for speculation. One hypothesis is that these residues are involved in inter-CESA interactions through hydrogen-bonding. Based on the non-polar to polar substitutions providing the greatest resistance and the non-polar nature of the CBIs, it can be reasonably speculated that flupoxam and isoxaben occupy sites defined by CESA1-CESA3 and CESA3-CESA6 membrane-cytosol interfaces respectively. The single amino acid substitutions of *ixr* and *fxr* may result in slight conformational changes in the topology of the CBI binding site, reducing affinity for the herbicide. Since most of the CBI resistant mutants do not exhibit obvious cellulose deficiencies, modification of the binding site is possible without significant perturbation of the underlying process. Indeed, the mutants displaying the highest level of CBI resistance display wild-type plant height, RCI, and ^{14}C-glucose incorporation phenotypes (Figure 2.2.4A-B, Figure 2.2.5C,

Figure 2.2.7B and Figure 2.2.8E). This indicates that isoxaben and flupoxam act allosterically or through another protein and do not directly bind the catalytic center. Nevertheless, modifications at or near putative catalytic residues are represented in the examined collection of mutants. For instance, the R(806)K substitution of *ixr1-4* is contained within the highly conserved QxxRW domain and results in moderate resistance to isoxaben accompanied by short stature, reduced RCI and ^{14}C-glucose incorporation into cellulose (Figure 2.2.7C) all of which are symptoms of cellulose deficiencies. *ixr1-6* possesses moderate isoxaben resistance from the substitution of S(377)F in CESA3 which is immediately upstream of a catalytic aspartate. This mutant displays reduced dark-grown hypocotyl lengths (Figure 2.2.6), reduced plant height (Figure 2.2.5D) and reduced RCI (Figure 2.2.8E) all of which are indicative of decreased cellulose content in the walls (Sethaphong *et al.* 2013). Interestingly, reduced dark-grown hypocotyl lengths have also been observed in *procuste1* (*cesA6*) (Fagard *et al.* 2000). A possible explanation for the conditionally reduced functionality in the cellulose synthase machinery is variation in the conformational states or CESA composition of rosettes. Indeed, two distinct genetic pathways have previously been implicated hypocotyl cell elongation in *Arabidopsis* seedlings (Desnos *et al.* 1996).

The alternate explanation for the disproportionate substitution of serine residues of primary wall CESAs giving rise to *ixr* and *fxr* is they are sites of phosphorylation. Moreover, the isoxaben/flupoxam mode of action would then perturb the phosphorylated state of CESAs promoting rosette dissociation. With the removal of a potential phosphorylation site, these IXR/FXR proteins many not assume conformations and/or phosphorylation states sensitive to the CBIs. The phosphorylation of CESA7 results in its

targeted degradation *via* the proteasome (Taylor 2007). Although many of the serine residues within the CESAs are predicted to be phosphorylated, the serines/threonine substituted in *ixr* and *fxr* mutants are not (Nuhse *et al.* 2004 and Taylor 2007). It has been suggested that phosphorylation of CESA1 differentially affects a polar interaction with microtubules which in turn alters the properties of the microfibril such as: length, quantity within a subset and orientation within the membrane (Chen *et al.* 2010). The role of phosphorylation in isoxaben and flupoxam resistance merits further investigation. Although there is no evidence to suggest that the residues substituted in this study are phosphorylated, the possibility of isoxaben and flupoxam acting by perturbing the phosphorylated state of CESAs cannot be discounted. The most attractive model for flupoxam and isoxaben action is by the disruption of an inter-CESA interaction most likely at the membrane-cytosol interface. The role phosphorylation plays in the post-translation regulation of the primary wall CESAs and perturbation by isoxaben and flupoxam is an intriguing topic for future research.

In order to determine the effect of these mutations on the enzymatic synthesis of β-(1-4)-glucan, ^{14}C-glucose incorporation in to cellulose was investigated. Only *ixr1-4* and *ixr1-5* exhibited a significant decrease in the incorporation of radiolabelled glucose into crystalline cellulose *in vivo* (Figure 2.2.7B and C). These mutants also display decreased plant height (Figure 2.2.5D) and *ixr1-5* additionally exhibits an incompletely penetrant blistering phenotype in the absence of isoxaben (Figure 2.2.5G). Since most of the mutations did not display drastic reduction in enzymatic glucose incorporation, some other aspect of the cellulose synthase must be perturbed. To this end, the senesced stem tissue of the mutants was assessed for alterations in cellulose crystallinity using XRD.

Given that *ixr 1-2* T(942)I in CESA3 has been described to have reduced crystallinity and enhanced fermentable sugar release (Harris *et al*. 2009), it seems reasonable that mutations identified in this study should have a similar effect on the cell wall (Figure 2.2.9B).

The x-ray diffraction results agreed with previous findings of an RCI value ranging from 47-50% in wild-type (Harris *et al.* 2008). All of the flupoxam and isoxaben alleles tested in this study had significantly lower RCI values than wild-type with the exception of *fxr1-1* and *fxr1*-3 (Figure 2.2.8E). The *cesA1* mutants all uniformly had approximately a 15 % drop in crystalline cellulose. The decreases in RCI were the result of increases in the amorphous scattering zone around $2\theta = 18°$ more than from decreases in the crystalline peak around $2\theta = 22.5°$ (Figure 2.2.8S1). It has been hypothesized that amino acid changes close to site of cellulose extrusion may modify the angles required for proper cellulose crystallization (Harris *et al*. 2009). Decreases in crystallinity generally correlate with increases in wall degradation sugar yields. Lower crystallinity allows for more of the glucan surfaces to be made accessible to cellulase enzymes increasing their efficacy.

Finally, investigation of analogues of isoxaben and possible metabolism products where explored. The presumption of an isoxazole ring-opening event occurring under reducing conditions prompted the prediction of potential active metabolite structures. Based on these structures, similar commercially available compounds were acquired and tested on *Arabidopsis* for cellulose biosynthesis inhibitory effects. Of these, CP-91149 treatment induced effects on *Arabidopsis* seedlings similar to that of exogenous auxin exposure. The other, 2-(4-hydroxyphenyl)-5-pyrimidinol (pydA) caused root hair growth

inhibition in *Arabidopsis* seedlings. This effect was similar to those mutant lines that have lost the function of CSLD3, one of the closest relatives to CESAs (Favery *et al.* 2001). Perhaps differential chemical functionalization of pydA is what determines specific targeting of particular CESAs and CSLs. The investigation of additional phenyl pyrimidinol compounds is necessary to establish a structure-function relationship within the CBI and further resolve the nature of the CBI-synthase interaction. The notion of having a chemical tool box containing a generic CBI core structure with the option of tuning the efficacy and specificity through chemical modification is attractive. This represents a directed approach to novel CBI development. Further characterization of the reduced-isoxaben particularly *in planta* is necessary to unveil the mode of action. Structurally linking these to other CBIs would broaden our understanding of not only how the herbicides work but about the underlying mechanics of cellulose biosynthesis.

Chapter 3: Forward Genetic Analysis of Wall Hydrolysis Sensitivity

3.1 Introduction

Plant biomass is derived from solar power via photosynthesis and is the raw material for a stable, environmentally benign source of energy. However, much of the plant's biomass resists degradation because the tight association of cellulose with other wall polymers such as hemicellulose and lignin occludes hydrolytic enzymes from their targets. In addition, the cellulose microfibrils are highly crystalline themselves rendering it resistant to most degradation schemes. As a result the biochemical conversion of cell walls to a more versatile carbon source remains a costly and energy inefficient process. This recalcitrance has led to the development of a variety of strategies to deconstruct the plant cell walls through a combination of acid, thermal and enzymatic hydrolysis. Pre-treatments with dilute acid are sufficient to hydrolyze hemicellulose which can enable access to microfibrils for cellulases. Dilute acid is not severe enough to hydrolyze the highly crystalline cellulose. Increasing acid concentrations or carrying out acid treatments at high temperature and pressure improves sugar yields from cellulose but are both increasingly hazardous and expensive. Enzymatic approaches are not yet a mature technology being plagued with long digestion times and high cost. The lack of a cost-competitive and environmentally benign strategy for the conversion of cell wall polymers into fermentable sugars is an opportunity to apply genetic and genomic approaches to modify the cell wall to be more amenable to saccharification. In the previous chapter the effects of particular modifications to well-known cell wall synthesis enzymes, the primary wall CESAs were discussed. Although this approach did yield desirable results,

it depends on a prior molecular knowledge of the genes and the resulting strategies are homogeneous, predictable and represent only a small subset of possible approaches. Forward genetic screens for digestibility have the potential to uncover novel processes that could improve saccharification. Forward genetic screens for mutants with improved saccharification from biomass were performed in the model-plant, *Arabidopsis.* Mutants that showed improved sugar release compared to wild-type plants under mild acid hydrolysis conditions were selected and characterized. The mutants that gave the best saccharification phenotypes carried modified genes that would not be thought to have any obvious role in cell wall biology. The perturbation of starch metabolism and polar auxin transport interestingly improved sugar release from vegetative tissues. In the case of auxin transport perturbation, the effect could be translated to the biomass crop, *Zea mays*. These results indicate that many unknown processes influence cell wall integrity which in principle expands the potential genotypes that may contribute to improving industrial processing of plant biomass (Stamatiou *et al*. 2013).

3.2 Results

3.2.1 Forward genetic screen on fresh leaf tissue identifies sixty-three *responsive to acid hydrolysis* (*rah*) mutant lines

Twenty-two thousand *Col-0* seed were treated with 0.3% EMS then the M2s were screened for sensitivity to acid hydrolysis. The screen involved taking leaf disc punches from the third and fourth leaves twenty-one days after germination and subjecting them to dilute acid at room temperature (Figure 3.2.1A). The top panel shows the 96-well format in which the plants where grown. Leaves 3 and 4 are identified in the middle panel. They were hole-punched and the leaf punches subjected to 1 M H_2SO_4 for 1 hour at room

temperature. The reducing sugar equivalents were detected using 0.2% anthrone solution (bottom panel). Anthrone solution is extremely acidic and in the presence of reducing sugars forms furfuralic compounds whose absorbance maxima at 620 nm is proportional to the amount of sugars present (Yemm & Willis 1954). Sixty-three lines reproducibly released greater than 50% more reducing sugar equivalents than *Col-0* and were organized into groups based on the amount of sugar released (Figure 3.2.1B). These mutants, referred to as the *responsive to acid hydrolysis* (*rah*) were part of a collaborative project with Dr. Peter McCourt's research group at the University of Toronto and is published in Plos One (Stamatiou *et al*. 2013). The fresh leaf tissue type and this method of hydrolysis allowed high throughput screening and was employed because of its rapidity and simplicity. Although these properties are ideal for screening a large mutant population, examination of more relevant tissue types for cellulosic biofuel production were necessary to further validate this approach.

A

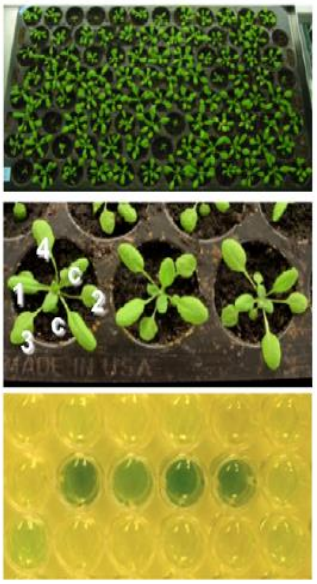

B

Absorbance (620nm)

0.130 – 0.200		0.201 – 0.270		0.271– 0.340	0.341– 0.390
# of mutants	30	23		8	3
rah34	*rah49*	*rah12*	*rah27*	*rah4*	*rah1*
rah35	*rah50*	*rah13*	*rah28*	*rah5*	*rah2*
rah36	*rah51*	*rah14*	*rah29*	*rah6*	*rah3*
rah37	*rah52*	*rah15*	*rah30*	*rah7*	
rah38	*rah53*	*rah16*	*rah31*	*rah8*	
rah39	*rah54*	*rah17*	*rah32*	*rah9*	
rah40	*rah55*	*rah18*	*rah33*	*rah10*	
rah41	*rah56*	*rah19*	*mur11-1*	*rah11*	
rah42	*rah57*	*rah20*			
rah43	*rah58*	*rah21*			
rah44	*rah59*	*rah22*			
rah45	*rah60*	*rah23*			
rah46	*rah61*	*rah24*			
rah47	*rah62*	*rah25*			
rah48	*rah63*	*rah26*			

Figure 3.2.1: High throughput acid hydrolysis screen isolates 63 *rah* mutants.

A) Three-week old *Arabidopsis* plants grown in 96-well flats at 22°C under a 16 h/8 h light/dark cycle (top). Leaf 3 or 4 was excised from 21 day-old plants using a hole punch and subjected to acid hydrolysis using 1 M H_2SO_4 (middle). Cotyledon (c) and leaf numbers are indicated. Results of the colorimetric anthrone assay illustrates that *rah* mutants release more sugars and turn a blue/green colour. Yellow indicates baseline levels of sugar release (bottom) (Stamatiou *et al.* 2013).

B) From the screen, 63 *rah* mutants were isolated and organized into 4 categories of low to high yielding sugar mutants (Stamatiou *et al.* 2013).

3.2.2 Enzymatic digestion of *rah* senesced tissue

The sixty-three mutants were further screened for enhanced degradation susceptibility against enzymatic hydrolytic schemes. Three separate types of digestion screens were performed. Each successive screen encompassed an additional degrading enzyme targeting another recalcitrant contributing wall polymer. Before the dried senesced tissue could be subjected to hydrolysis it had to be ground and washed. The washing of the tissue is necessary to remove residual sugars which would otherwise obscure those released from wall hydrolysis. One of the major obstacles to cellulose degradation schemes is its occlusion by other cell wall polymers. To address this issue, enzymatic hydrolysis strategies were developed utilizing xylanases and peroxidases in co and pre-treatments targeting hemicellulose and lignin respectively. These wall polymers are known to be in tight association with cellulose and their degradation will aid in its accessibility. An enzymatic hydrolysis protocol for the digestion of *Arabidopsis* biomass was developed and the optimal enzymatic ratios were empirically determined. Cellulase, cellobiase, xylanase and peroxidase were used in genetic screening procedures resulting in the discovery of a genetic mutant, *rah9* which releases three times more glucose than *Col-0* and clearly stands out (Figure 3.2.2A). A close up of enzymatic hydrolysis results for the mutants focused on in this study is given in Figure 3.2.2B.

It was experimentally determined that 80 international units (IU) of Novozyme 188 (cellobiase) with 15 filter paper units (FPU) of Celluclast (cellulases) are the optimal amounts per gram of senesced *Arabidopsis* tissue (Figure 3.2.2S1). One FPU is defined as the concentration of enzyme that produces 2 mg of glucose in one hour in 0.5 mL at pH 4.8 (Ghose 1987). One IU of Novozyme 188 is defined as the amount of enzyme

required to convert one micromole per minute of paranitrophenol-β-D-glucopyranose into paranitrophenol at pH 4.8 and 50^{o}C. The first of three enzymatic screens used only Celluclast to target the cellulose microfibrils and Novozyme 188 to hydrolyze the cellobiose products. Cellobiases break the β-glycosidic bonds of the disaccharide to release monomers of D-glucose. The action of Novozyme 188 produces the desired monosaccharide and more importantly clears the cellobiose which otherwise accumulate and retard cellulase action by feedback inhibition (Mandenius *et al.* 1987). The amount of cellulose hydrolyzed was quantified by indirectly measuring the glucose released into the supernatant. The glucose content was determined using the Glucose (HK) Assay Kit (Sigma). This kit contains hexokinase (HK), glucose-6-phosphate dehydrogenase (G6PDH), ATP and NAD. In the presence of glucose from the sample, the components of the kit undergo a coupled enzymatic reaction producing NADH in molar equivalents to the glucose in the sample. NADH has an absorption maximum at 340 nm and can be quantified spectrophotometrically (Figure 3.2.2S2). This detection method is preferred over the reducing-sugar quantification using 0.2% anthrone because the hexokinase kit is specific for glucose and uses milder conditions (pH 7, 20^{o}C). The anthrone method detects all reducing sugars with varying sensitivities (Figure 3.2.2C). As the anthrone reagent is not specific and has different sensitivities for every sugar tested, it is not ideal for detecting specific products from a mixture of sugars. Due to this inherent ambiguity, sugar readings using anthrone will be expressed as 'glucose equivalents'. Since glucose is the expected product, all readings were calibrated using glucose as the standard. Incidentally, anthrone is the least sensitive at detecting glucose compared to any of the sugars tested (Figure 3.2.2C).

The second screen incorporated xylanases from *Thermomyces lanuginosus* which are commercially available from Sigma. This study determined the activity of the stock powder to be 6400 U/g using xylan from birch wood (Sigma X0502) as the substrate, D-xylose as the standard and quantified using 0.2% anthrone. One unit is defined as the amount of protein required to form one micromole of xylose in one minute at pH 4.8 and 50^{o}C. It was determined that in the presence of the predetermined amounts of Celluclast and Novozyme 188, 115 U/g of xylanases for *Arabidopsis* senesced tissue was optimal. The xylanases target the β-(1-4)-xylose linkages of xylan, a major constituent of hemicellulose. This allows for greater access to the cellulose and facilitates hydrolysis by the cellulases. *Col-0* releases approximately two-fold more glucose per mg of tissue when treated with the hydrolytic scheme supplemented with 115 U/g of xylanases (Figure 3.2.2B).

The final screen incorporated all the enzymes in the concentrations used in the second screen subsequent to tissue pre-treatment with lignin peroxidase. Calibration determined that the most glucose was released from *Col-0* tissue after it was pre-treated with 0.04 U/g of lignin peroxidase for 2 hours. One unit corresponds to the amount of enzyme required to oxidize 1 micromole of 3,4-dimethoxybenzyl alcohol per minute at 30^{o}C and pH 3 (Sigma). It should be noted that the activity of the peroxidase was the only enzyme in the hydrolysis assays that was not experimentally determined. The activity was assumed to be 2.18 U/mg which was provided by the manufacturer (Sigma). The peroxidase pre-treated tissue of *Col-0* released 16% more glucose compared to the same tissue from screen two. The addition of xylanases and lignin peroxidases to the

cellulase hydrolytic schemes resulted in an increase of glucose liberation by greater than 58% for *Col-0* senesced tissue.

Every *rah* mutant released 50% more reducing-sugar equivalents from their leaf discs under dilute acid conditions than *Col-0*. Despite this pre-selection, the vast majority of them failed to release more glucose than the control when subjected to enzymatic hydrolysis (Figure 3.2.2D). Only six of the mutants released 50% more glucose than *Col-0* in the first enzymatic hydrolysis scheme. Two of these mutants along with three others met the greater than 50% of *Col-0* cut-off in the xylanase assay. Ten mutant lines released 50% more glucose than *Col-0* in the peroxidase assay. The inability to transfer the acid and enzymatic hydrolysis digestion results for the *rah* mutants can be partly attributed to difference in the quantification methods and types of tissue used between the two protocols. The acid hydrolysis screen was conducted on fresh tissue and quantified by the anthrone assay which detects all reducing sugars. Whereas the enzymatic hydrolysis method used senesced tissue and was quantified using the HK kit which is specific for glucose. Nevertheless, the possibility remains that enzymatic and acid hydrolytic sensitivity requires different and even mutually exclusive wall properties. This would preclude the existance of a wall composition or conformation ideal under both schemes.

Figure 3.2.2A: Enzymatic hydrolysis of senesced stem tissue from *rah* mutants. All *rah* mutants are arranged on the horizontal axis with *Col-0* at the far right and the sugar release is expressed in micrograms of glucose released per milligram of washed tissue determined by the glucose hexokinase (HK) method. The values are averages +/- standard deviation (n = 3). The glucose released from cellulase treatment (white), cellulase+xylanase (grey) and cellulase+xylanase+peroxidase (black bars) are shown.

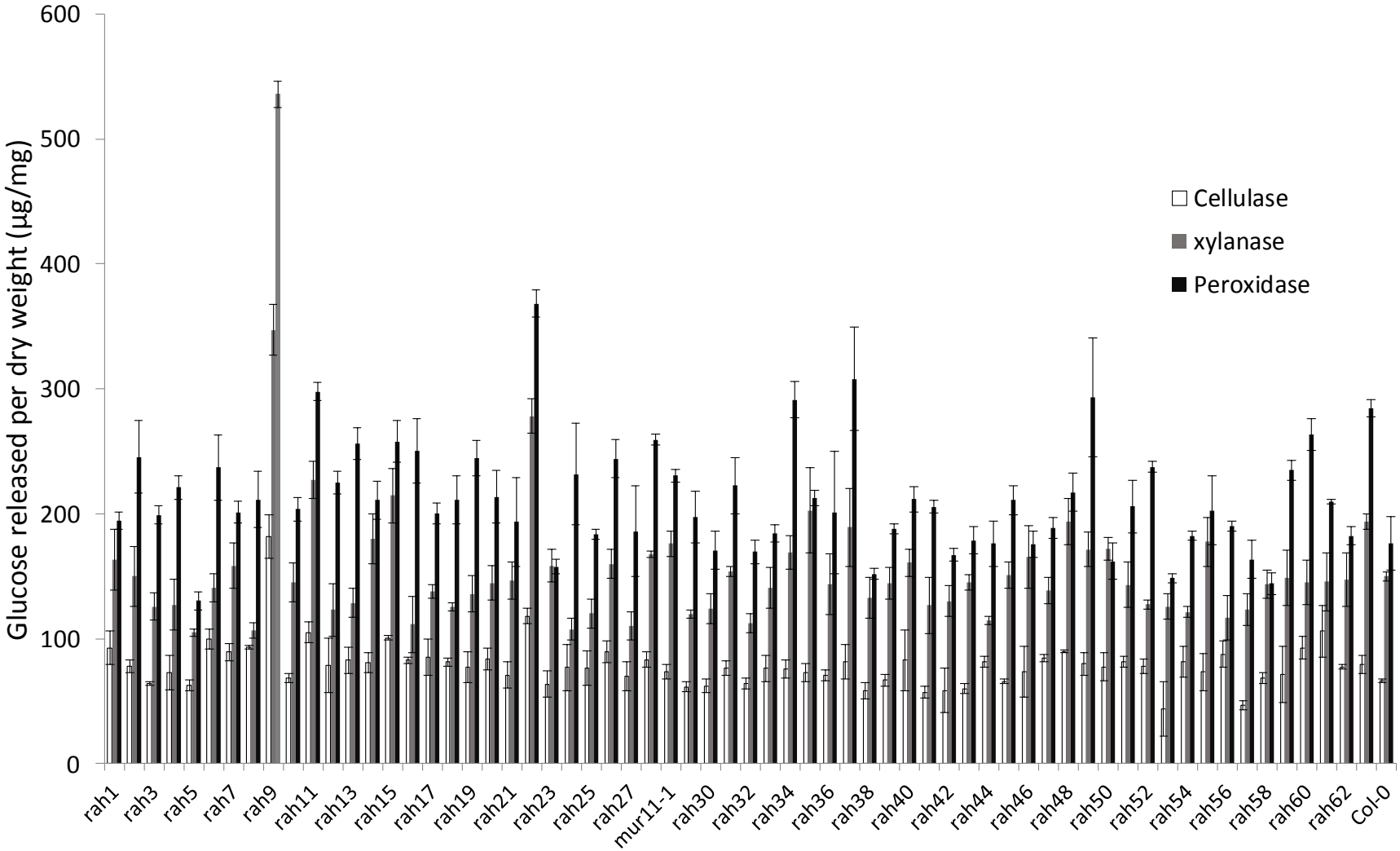
Glucose released per dry weight (µg/mg)
600
500
400
300
200
100
0
Cellulase
xylanase
Peroxidase
rah1
rah3
rah5
rah7
rah9
rah11
rah13
rah15
rah17
rah19
rah21
rah23
rah25
rah27
mur11-1
rah30
rah32
rah34
rah36
rah38
rah40
rah42
rah44
rah46
rah48
rah50
rah52
rah54
rah56
rah58
rah60
rah62
Col-0

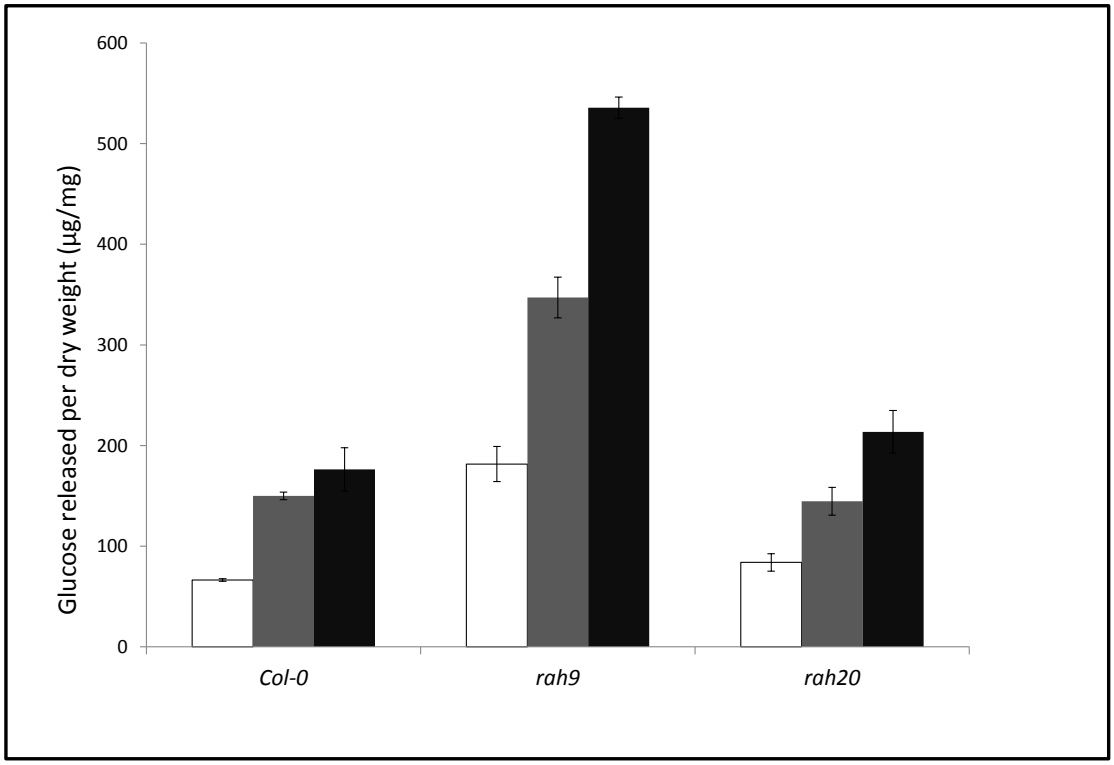

Figure 3.2.2B: Glucose released from *rah9* and *rah20* after enzyme hydrolysis. Senesced stem tissue was subjected to cellulase (white), cellulase+xylanase (grey bars), and cellulase+xylanase+peroxidase treatment (black bars). The values are averages +/- standard deviation (n = 3) and are expressed as micrograms of glucose released per milligram of tissue determined by the HK method.

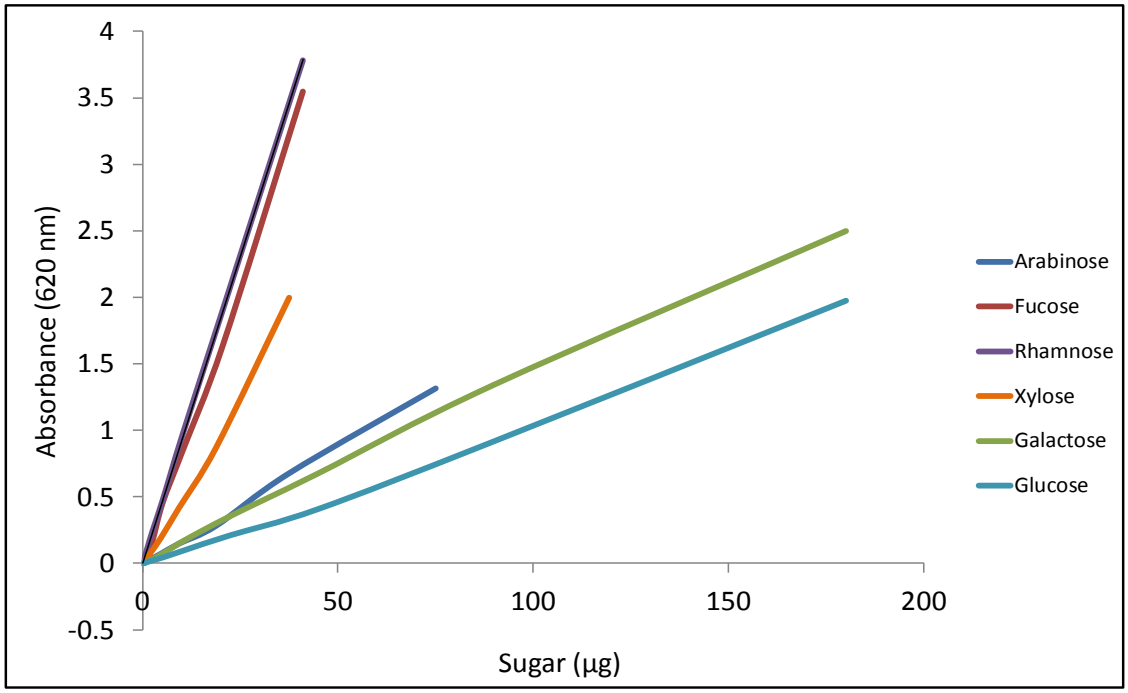

Figure 3.2.2C: Wall relevant sugar standards quantified by the anthrone method. All the sugars are detected by anthrone with differing absorbance slopes at 620 nm. Anthrone is most sensitive in detecting the deoxysugars followed by the aldopentoses and is least sensitive in quantifying aldohexoses such as glucose.

Figure 3.2.2D: Clustered heatmap of sugar content as measured by the anthrone method. The data shown of the 63 *rah* mutants include: acid hydrolysis of fresh leaf tissue using 1 M H_2SO_4, acid hydrolysis of senesced stem tissue using 0.2 M H_2SO_4, glucose content (HK method) of cellulase, cellulase+xylanase and cellulase+peroxidase digested senesced tissue and starch staining of 14 day-old seedlings. Values are percentages relative to wild-type (See Table 3.2.2S1). The mutants are grouped according to sugar release profiles. Yellow indicates high levels of sugar; black, low levels of sugar (Stamatiou *et al.* 2013).

3.2.3 *Starch excess 4* (*sex4*) and *rah9* show enhanced saccharification under enzymatic schemes

Of the sixty-three *rah* mutants none released more glucose than *rah9*. This particular mutant released approximately 2.5 times more glucose than *Col-0* and released the most sugar in every enzymatic hydrolysis scheme. This line was backcrossed to the *Ler* ecotype and an F2 mapping population was generated. Bulk segregant and map-based cloning analysis revealed that the enhanced glucose-release phenotype was closely linked to the *ciw4* simple sequence length polymorphism (SSLP) marker (Figure 3.2.3A). This shows a 4% agarose gel loaded with 100 ng of PCR products amplified using primers specific for polymorphic regions of the *Arabidopsis* genome. *Col-0*, *Ler* then the pooled DNA of the F2s displaying the hyper-saccharification phenotype (Bulk) were loaded for every PCR marker. Since the mutant was generated in the *Col-0* background, the underlying mutation is expected to be flanked by *Col-0* polymorphic markers. Figure 3.2.3A shows the PCR products amplified off of the Bulk DNA displaying a *Col-0* SSLP, indicating linkage of the hyper-saccharification phenotype and the region of DNA flanking the *ciw4* marker. Further phenotypic analysis of individual F2s established a recombination frequency of 2.0% at *ciw4* corresponding to a map distance of approximately five hundred thousand bases in *Arabidopsis* (Lukowitz *et al.* 2000) (Figure 3.2.3B). In the course of characterizing the phenotypes of the mutant, it became clear that Lugol's iodine solution stains *rah9* very strongly in both fresh and senesced tissue, where this is not observed in *Col-0*. Light microscope images of senesced tissue Lugol staining are shown in Figure 3.2.3C. Lugol's solution is used as a quick qualitative test for the presence of amylose, a major component of starch. The long helical

polysaccharides of starch enclose the iodine molecules forming a complex which turns the solution from a transparent yellow to a dark blue (Rundle & French 1943).

Recognizing that the *starch excess 4* (*sex4*) gene is only 450 kb downstream of *ciw4*, the *sex4* locus in *rah9* was sequenced. In collaboration with Peter McCourt's lab at the University of Toronto, *rah9* was found to carry a slice-site mutation at the beginning of intron 8 of *sex4* (At3g52180). Typically the first two and last two bases of each intron follow the GT-AG rule. In *rah9* the conserved GT bases have been changed to AT probably leading to aberrant pre-mRNA splicing. *Sex4* has 13 exons and 12 introns and the addition of the 8th intron to exon 7 most likely results in the introduction of a premature stop codon producing a protein with its C-terminal truncated to half its normal length. SEX4 is a laforin-like phosphoglucan phosphatase which removes phosphate groups from phosphoglucans in starch polymers (Kotting *et al*. 2009). Since dephosphorylation of phosphoglucans is required for starch metabolism, it accumulates in great quantities in the stem tissue and leaf tissue of *rah9*.

The hyper-saccharification phenotype was also observed in the T-DNA insertion *sex4 knock-out* (*sex4KO*) line (SALK_102567). This finding supported the assertion that enhanced scarification is mainly due to starch accumulation caused by the loss of function of SEX4. Senesced tissue of *rah9* and *sex4* showed wild-type level saccharification following α-amylase pre-treatment (Figure 3.2.3D and Figure 3.2.3S3). It is worth nothing that the products of the α-amylase digestions were not detected by the glucose HK assay kit, indicating that product of the scheme was not monomeric glucose and were most likely α-linked gluco-oligomers of short lengths. To determine if starch accumulation alone was responsible for the hyper-saccharification phenotype, the

cellulase hydrolysis product was made into alditol-acetate derivatives and subsequently analyzed by gas chromatography (GC) (Figure 3.2.3E, F and G). The peaks are compared to the alditol-acetate derivatives of the standard monomeric sugars found in plant walls (Figure 3.2.3E). Two prominent peaks in the *rah9* chromatogram that are absent in *Col-0* adjacent to glucose were immediately obvious. Since *rah9* is a phosphoglucan phosphatase loss of function mutant, it is likely that C-3 and C-6 phosphorylated glucoses are responsible for the two peaks at 27 minutes in Figure 3.2.3G. As described above, glucose-6-phosphate (G6P) is an intermediate in the HK-glucose detection kit, which explains *rah9* scoring highly in glucose detection assays while releasing wild-type levels of glucose observed by GC.

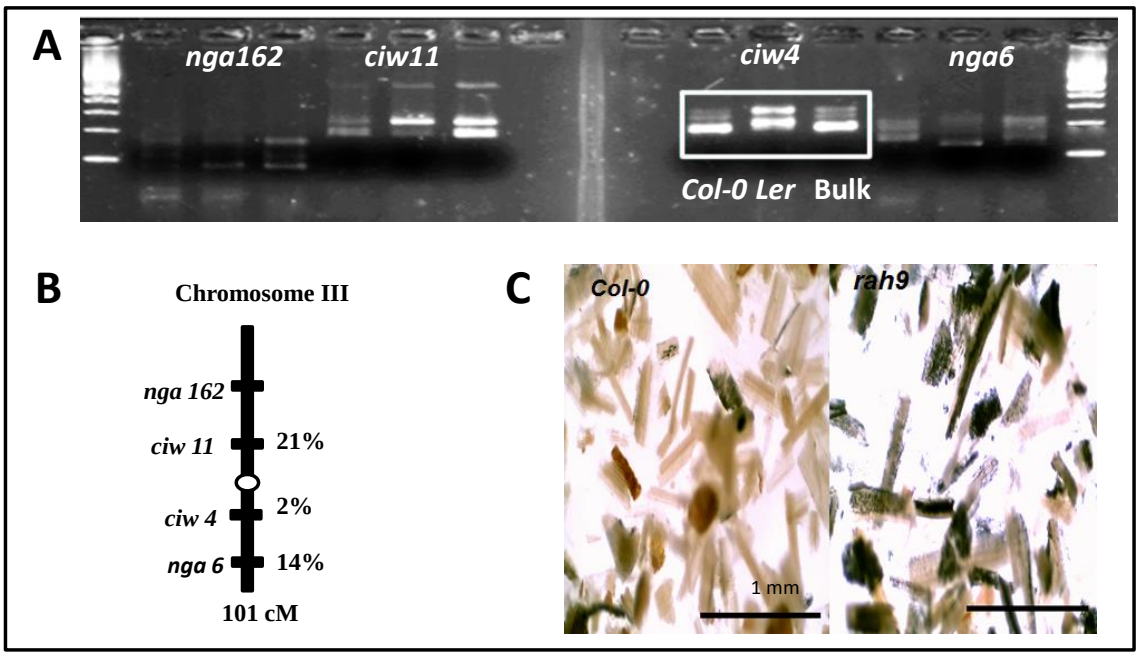

Figure 3.2.3: Mapping of *rah9*

A) A 4% agarose gel of SSLPs in chromosome 3 used in the bulk segregant mapping mutants of *Arabidopsis thaliana*. The lanes are loaded in the order: *Col-0*, *Ler* and the bulk mixture of selected F2 DNA (See Figure 3.2.3S4). The bulk lane is more similar to *Col-0* for the markers: *ciw11*, ciw4 (box) and *nga6*. The far left and far right lanes are filled with 100 bp ladder.

B) A diagram of Chromosome 3 along with the markers used in A (Adapted from Lukowitz *et al.* 2000). The recombination frequencies on the right are expressed as the percent of *Ler* alleles present per chromosome in the pool of bulk DNA.

C) Lugol staining of *Col-0* (left) senesced stem tissue is juxtaposed with *rah9* (right). The dark staining of *rah9* indicates the presence of a substantially greater amount of starch in compared to wild-type (bars = 1mm).

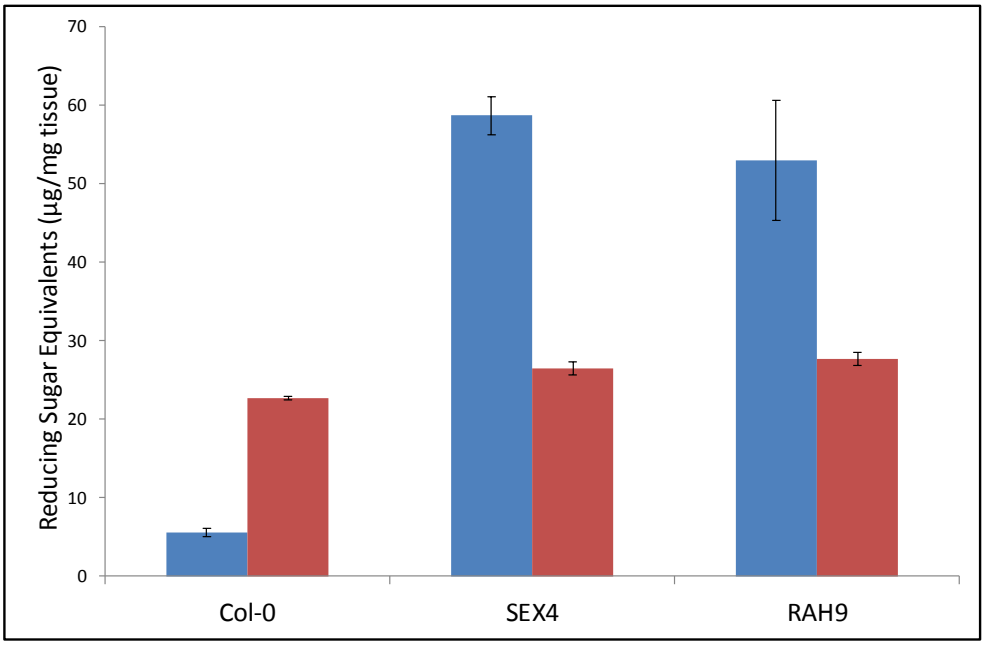

Figure 3.2.3D: Sugar released by *rah9* after amylase pre-treatment. Glucose equivalents of the sugars released after amylase treatment of senesced stem tissue (blue bars) are compared to those released during subsequent acid hydrolysis in 0.1 M sulfuric acid (red bars). Values are averages +/- standard deviation (n = 3) determined by the anthrone method. Tissue from both mutants also showed wild-type levels of saccharification during cellulase digestion following amylase pre-treatment (Figure 3.2.3S3).

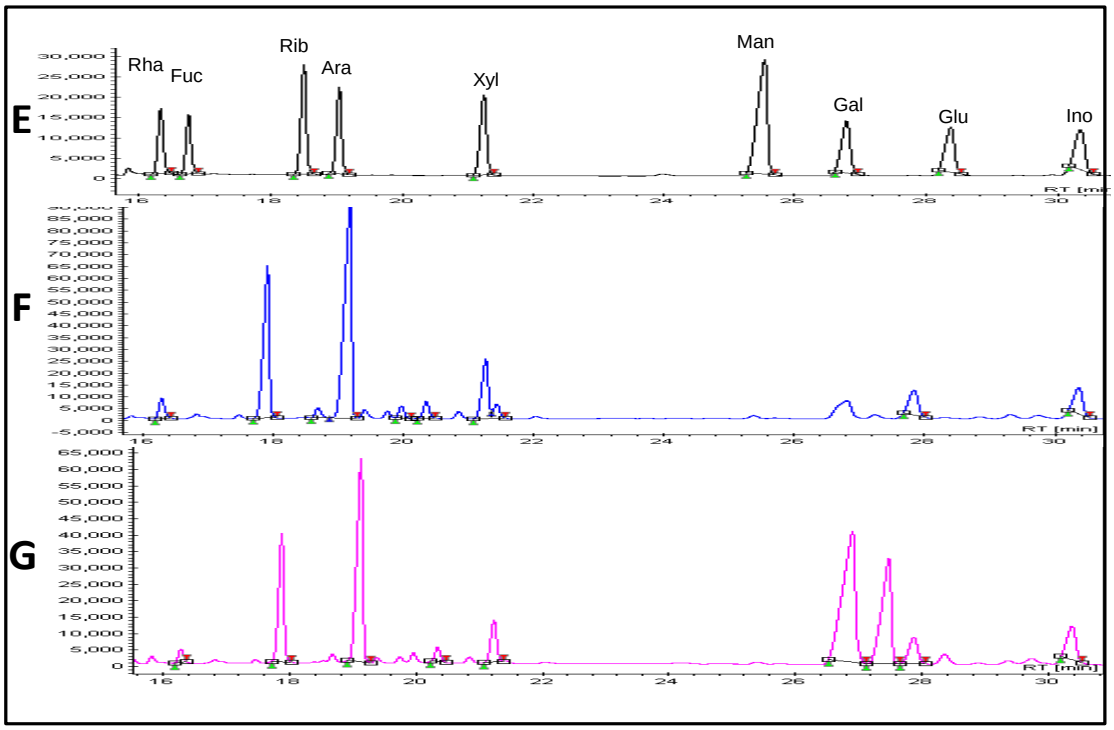

Figure 3.2.3: Gas Chromatography of *rah*9 derivatized sugars.

E) Chromatogram showing the standard peaks for wall sugar alditol acetate derivatives. The peaks are in order from the left are: rhamnose, fucose, ribose, arabinose, xylose, mannose, galactose, glucose and inositol. The standard peaks show the separation and intensity for fifty micrograms of each sugar. Inositol is used as an internal standard as it is not naturally present in cell walls.

F) Gas chromatogram of the derivatized cellulase digestion products of *Col-0* senesced tissue.

G) The chromatogram of the cellulase digestion products of *rah20*. There are two large peaks between the retention times of 26-28 minutes not present in wild-type. Compared to the standards the peaks are most likely a modified aldohexose. Phosphorylated glucoses are likely candidates for the identity of these peaks because of their roles in starch metabolism.

3.2.4 PINOID (PID) and RAH20 show that polar auxin transport perturbation is a potential strategy to enhance saccharification

Amongst the lines which showed improved sugar release in all the schemes tested, one line stood out because of distinct morphological features, *rah20*. During reproductive growth it showed an incompletely penetrant pin-shaped inflorescence phenotype. This phenotype had been previously described in certain mutants with perturbations in the polar transport of the plant hormone auxin (Okada *et al*. 1991). Subsequent molecular analysis of *rah20* identified a mutation in the *pinoid* (*pid*) gene resulting in a D223N substitution yielding a loss-of-function mutant (Stamatiou *et al*. 2013). PID encodes a serine-threonine protein kinase that is thought to play a role in the cellular localization of the PIN-FORMED (PIN) efflux auxin carrier (Christensen *et al*. 2000). Interestingly, mutations in other genes that result in a pin-shaped phenotype such as loss of function alleles of *pin1* (Okada *et al*. 1991) also show an improved saccharification phenotype (Figure 3.2.4). Sugar release was measured using the anthrone method from ground, senesced stem tissue from *Arabidopsis* pin-shaped inflorescence mutants after being subjected to 0. 2 M acid hydrolysis for one hour. The top right inset shows representative pin-shaped inflorescence in *Arabidopsis* juxtaposed to wild-type.

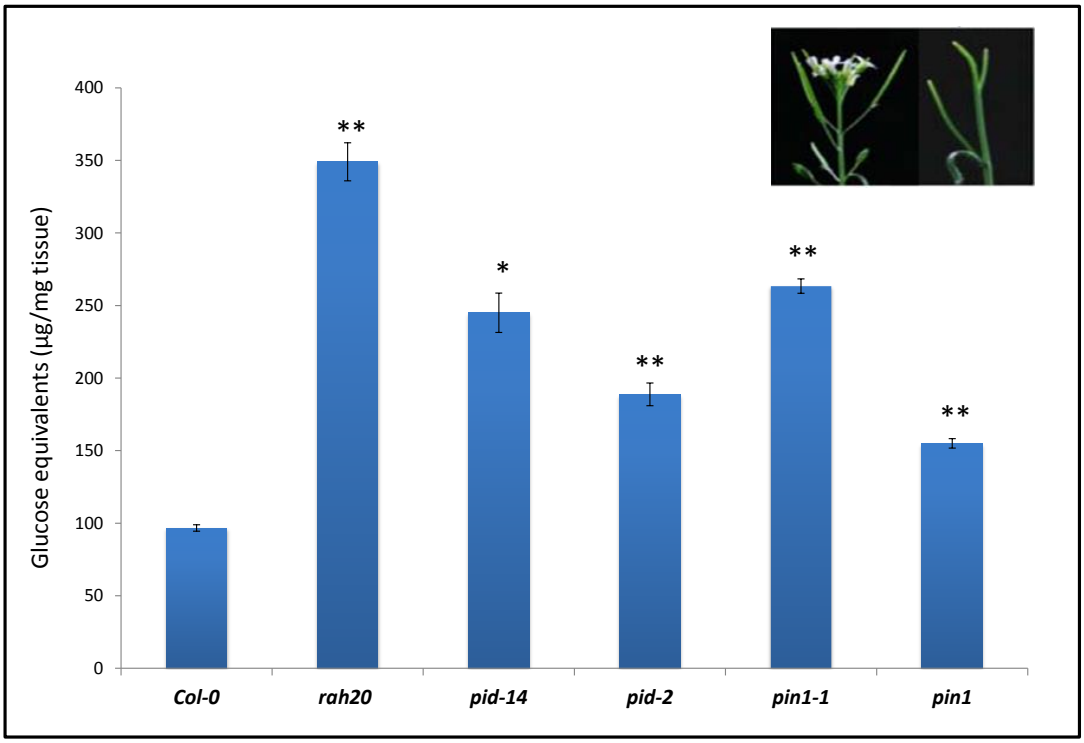

Figure 3.2.4: Acid hydrolysis of auxin transport mutants. Sugar released from the ground, senesced stem tissue of *Arabidopsis* pin-shaped inflorescence mutants subjected to 0.2 M acid hydrolysis. Values are averages expressed as micrograms of glucose equivalents released per milligram of tissue +/- standard deviation ($n = 3$, $*p < 0.01$, $**p < 0.001$ using Student's *t*-test) determined with 0.2% anthrone. Inset shows a representative pin-shaped inflorescence (right) in *Arabidopsis* compared to wild-type (left).

3.2.5 Enhanced saccharification of PINOID extends to monocots such as *Zea mays*

Many current agriculturally significant crops and potential future bioenergy crops fall in the commelinoids clade of monocots which have a different type of primary wall as discussed earlier in section 1.1.1. Considering the differences in the composition of dicot and monocot primary walls, enhancement of saccharification in *Arabidopsis* may not transfer to commelinoids. Therefore, strategies to enhance hydrolytic sensitivity and saccharification must be empirically verified with a member of the commelinoid family to ensure transferability to crops in the field such as maize.

A monocot orthologue of *pid* known as *barren inflorescence 2* (*bif2*) in maize has been previously described (McSteen *et al.* 2007). Mutants with barren inflorescence phenotypes were tested for enhanced response to acid hydrolysis. The downstream target of *bif2* is a basic helix-loop-helix transcription factor called BARREN STALK1 (BA1) (Skirpan *et al.* 2008) which was also tested. Consistent with the results from *Arabidopsis*, both *bif2* and *ba1*maize inflorescence mutants show an improved saccharification phenotype (Figure 3.2.5). Sugar release was measured using the anthrone method from ground stems and leaves of three month-old maize inflorescence mutants, *bif2* and *ba1*. The tissue was then subjected to 0.2 M H_2SO_4 for one hour. The inset above shows a representative maize inflorescence mutant compared to *Col-0*. These data denotes the relevance of auxin polar transport perturbation for enhanced saccharification to industrially significant crops, many of which are monocotyledonous commelinids such as maize.

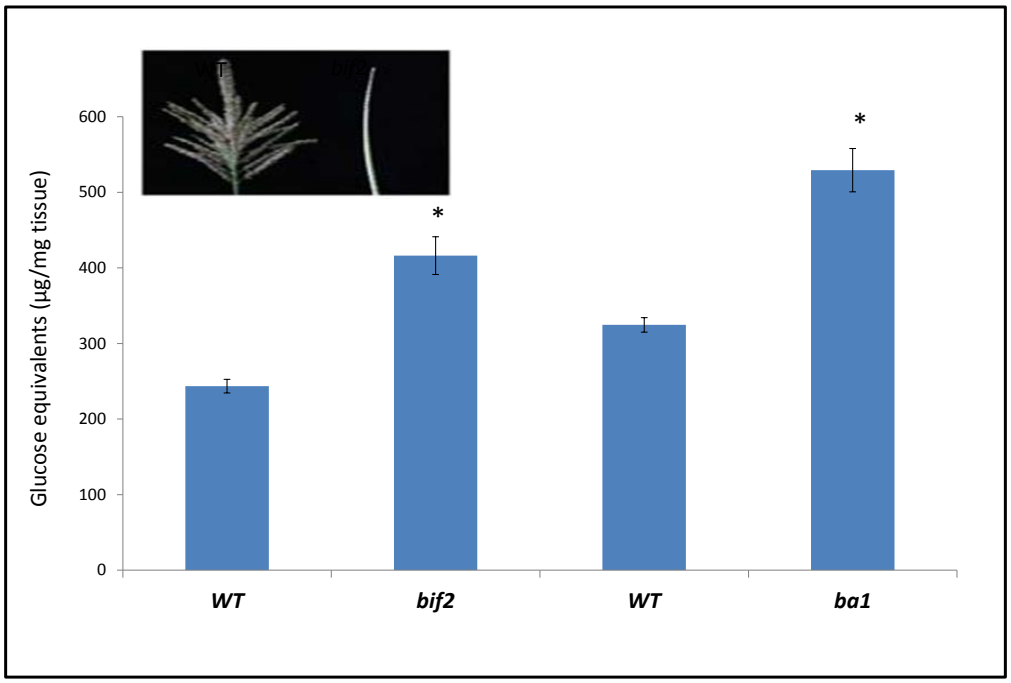

Figure 3.2.5: Acid hydrolysis of *bif2* and *ba1* in maize. Sugar release measured using anthrone method from ground, stems and leaves of 3 month-old maize inflorescence mutants, *bif2* and *ba1*, subjected to 0. 2 M H_2SO_4 acid hydrolysis. Graph shows glucose equivalents per mg dry tissue determined using 0.2% anthrone. Values are averages +/- standard deviation (n = 3, *p < 0. 0001 using Student's t-test). Inset shows a representative maize *bif2* inflorescence mutant (right) compared to wild-type (left).

3.2.6 Phenocopying *pid* with N-1-naphthylphthalamic acid (NPA)

The connection between auxin transport and increased sugar release was further probed using a specific inhibitor of auxin transport, N-1-naphthylphthalamic acid (NPA) (Katekar & Geissler 1980). Application of varying concentrations of NPA to wild-type *Arabidopsis* seedlings resulted in a 1.5 to 2 fold increase in the release of sugars relative to untreated plants (Figure 3.2.6A). Wild-type *Arabidopsis* seedlings were grown on MS media supplemented with NPA for 28 days after germination (DAG). The chloroform-methanol washed tissue was subsequently subjected to 0.2 M H_2SO_4 and the released sugars were quantified using anthrone. The ability to chemically perturb auxin transport allowed for further analysis in to *Zea mays* (maize). Application of NPA to two different cultivars of maize also resulted in a significant increase in saccharification (Figure 3.2.6B). The two maize cultivars were grown for 4 weeks and then treated with 120 mM NPA for 2 weeks. The stems and leaves of the plant were then subjected to 0. 2 M H_2SO_4 acid hydrolysis and the sugars released were measured using the anthrone method.

Together, these results show that genetic or chemical inhibition of auxin transport can enhance saccharification from plant biomass and specifically in industrially relevant plants. Further studies with the application of auxin polar transport inhibitors on bioenergy crop candidates such as *Miscanthus* and switchgrass are necessary to further validate this promising strategy and implement it into commercially viable biofuel production.

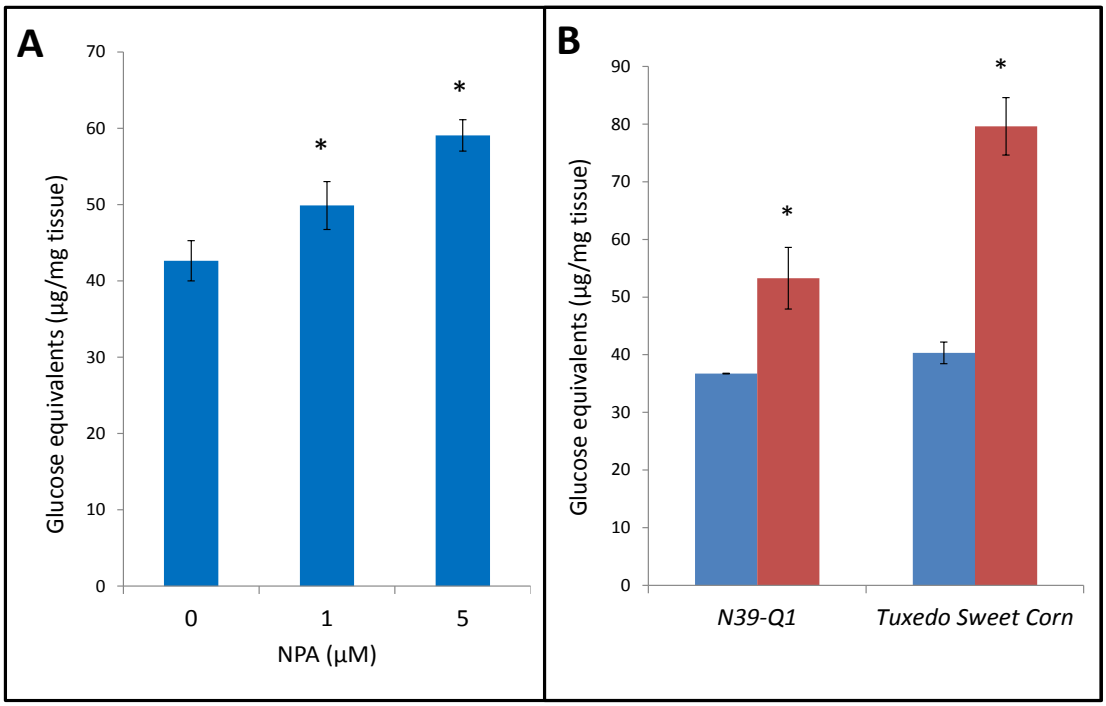

Figure 3.2.6: Effects of NPA treatment on *Arabidopsis* and corn sugar release.

A) Wild-type (*Col-0) Arabidopsis* 28 day-old seedlings grown on MS media supplemented with 0, 1 or 5 micromolar concentrations of NPA. Graph shows glucose equivalents detected per milligram of dry tissue. Values are averages +/- standard deviation ($n = 4$, $*p < 0.01$ using Student's *t*-test).

B) Two maize cultivars were grown for 4 weeks and then treated with 120 µM of NPA. Stems and leaves of 6 week-old plants were subjected to mild acid hydrolysis (0.2 M of H_2SO_4) and the sugars released were measured using the anthrone method. Untreated (blue bars) tissue is compared with NPA treated tissue (red bars). Graph shows glucose equivalents detected per milligram of dry tissue. Values are averages +/- standard deviation ($n = 3$, $*p < 0.01$ using Student's *t*-test).

3.2.7 Translating *pid* phenotypes to potential bioenergy crops with NPA

The next logical step in utilizing auxin transport perturbation for biofuel production, NPA was tested on potential energy crops. Chemically induced enhancement of saccharification coupled with the biomass production potential of *Miscanthus sinensis* and *Panicum virgatum* (switchgrass) offer promising strategy for cost-effective cellulosic biofuel production. Following the success of the application of NPA on maize, the treatment was employed on *Miscanthus sinensis* and switchgrass. Both of these organisms are monocots and like maize and belong to the *Poaceae* or 'grass' family of plants. *Miscanthus* and switchgrass were grown up for four weeks then treated with 120 μM of NPA for two weeks. The tissue was then washed with chloroform: methanol (1:1 v/v) and the saccharification was compared to the untreated using the anthrone method.

In case of *Miscanthus*, three varieties responded with significant improvement to acid catalyzed saccharification after NPA treatment (Figure 3.2.7A). The varieties were *Miscanthus sinensis* goliath, gracillimus and graziella. Soluble sugar yield increased 21% for acid hydrolyzed NPA treated tissue in the three varieties mentioned. Switchgrass was also put through the NPA regiment and similar to maize and *Miscanthus*, treatment resulted in an average increase in saccharification yield of 16% (Figure 3.2.7B). Unfortunately the genetic tools are not currently available to introduce *pid* into *Miscanthus* and switchgrass genetically. Nevertheless, the result of NPA enhancing saccharification in *Miscanthus* and switchgrass illustrates the potential of forward genetic high-throughput screens in *Arabidopsis*. It allows for the discovery of connections almost impossible to have been made analytically. Knowledge gained from high throughput in *Arabidopsis* can indeed be transferred to monocots with similar effects.

This is particularly advantageous when the species of interest is not traditionally viewed in the molecular context. Strategies can be developed in organisms with well-developed resources then transferred to organisms of interest regardless of the available genetic tools for the target organism.

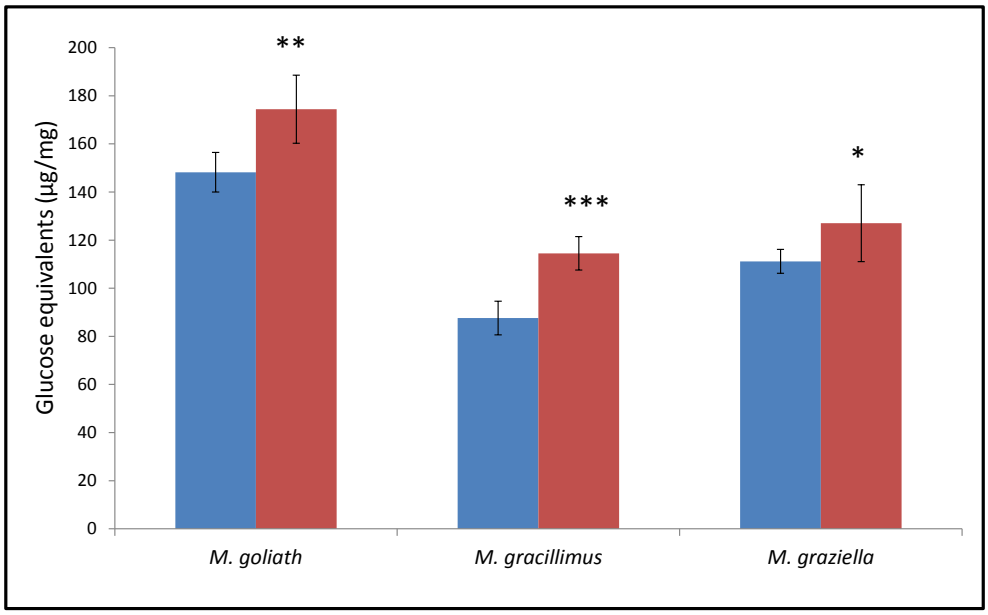

Figure 3.2.7A: Effects of NPA on acid hydrolytic sensitivity in *Miscanthus.*

Sugar release after acid hydrolysis of four week-old *Miscanthus* tissue untreated (blue bars) and treated with 120 µM NPA (red bars) is shown above. NPA treatment significantly increases sugar release measured by the anthrone method. Values are averages +/- standard deviation (n = 9, *p < 0. 05, **p < 0. 01, ***p < 0. 00001 using Student's t-test) expressed as glucose equivalents per milligram of tissue.

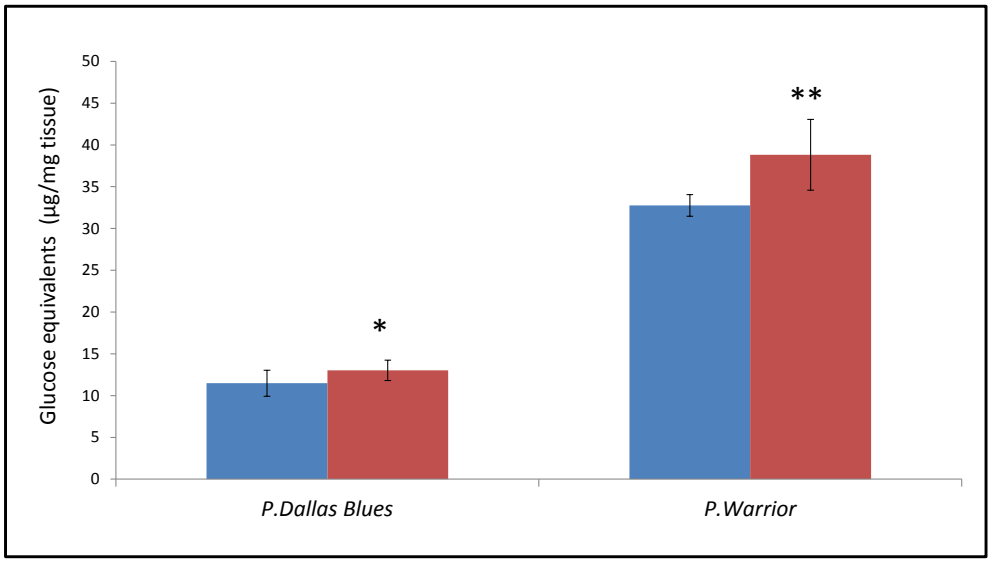

Figure 3.2.7B: Effects of NPA on acid hydrolytic sensitivity in switchgrass. Sugar release after acid hydrolysis of four week-old switchgrass tissue treated with 120 µM NPA (red bars) and without NPA treatment (blue bars) is displayed. Although not as sensitive as *Miscanthus*, NPA treatment also significantly increases sugar release in switchgrass measured by the anthrone method. Values are averages +/- standard deviation (n = 9, *p < 0. 05, **p < 0. 005 using Student's t-test).

3.2.8 Stacking *pid* with *ixr/fxr* using NPA enhances saccharification additively in some mutants

To determine if NPA application could further enhance the saccharification yields of cellulose synthase mutants, *ixr* and *fxr* mutants were grown in the presence of 5 μM concentrations of NPA (Figure 3.2.8). Compared to wild-type, NPA treatment did indeed result in greater sugar release of 28 DAG *Arabidopsis* stem and leaf tissue. The saccharification enhancement of NPA is more pronounced in the *Ler* eco-type compared to *Col-0*. *Ixr1-1*, *ixr2-1* and *fxr1-1* all were generated in the *Col-0* background and show the least sensitivity to NPA treatment in regards to saccharification. Interestinly, many of the mutants, particularly those harboring serine substitutions released considerably more sugars compared to wild-type by water maceration when treated with NPA (Figure 3.2.8S1). This indicates a preponderance of loosely associated wall glycans and residual sugars.

As mentioned previously, *Ler* carries a nonfunctional version of the *erecta (er*) gene which codes for a putative transmembrane receptor-like protein kinase (Kelko *et al*. 1996). This is interesting because NPA chemically phenocopies *pid*, which codes for a serine/threonine protein kinase (Christensen *et al*. 2000). An interaction between the functions of the two kinases cannot be discounted and warrants future investigation.

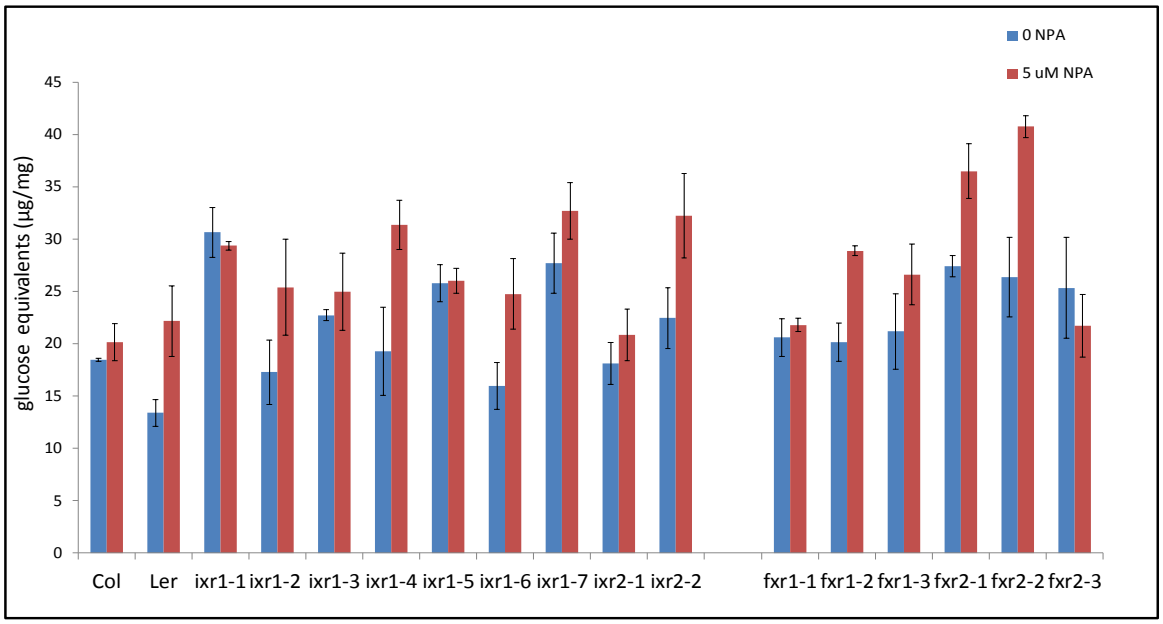

Figure 3.2.8: Enhancing hydrolytic sensitivity of *ixr* and *fxr* with NPA treatment. Treatment with 5 µM NPA (red bars) increases sugar yields when compared to untreated (blue bars). Sugars were quantified by the anthrone method and values are averages +/- standard deviation (n = 3) expressed as micrograms of glucose equivalents released per milligram of dry tissue. NPA treatment enhances the increased saccharification observed in the *ixr* and *fxr* lines.

3.3 Methods

3.3.1 Plant materials and growth conditions

Arabidopsis thaliana ecotype *Columbia* M2 seeds mutagenized by ethyl methane sulfonate (EMS) were purchased from Lehle Seeds (Round Rock, TX). EMS mutant alleles and T-DNA insertions lines were provided by the *Arabidopsis* Biological Resource Centre (Ohio State University, Columbus, USA). Seeds were surface sterilized in 50% bleach, 0. 01% Tween-20 for 5 min, rinsed 5 times with sterile water and stratified in dark at 4ºC for 4 days to synchronize germination. Seeds were plated on 0.5x strength Murashige and Skoog (MS) agar plates and sealed with surgical tape under continuous light at room temperature. Plants were grown to senescence (approximately 8 weeks) by sowing them onto mixture of sphagnum peat moss, perlite and vermiculite (Promix) and incubated in a growth chamber under continuous illumination (200 $mE/m^2/s$) at 21ºC. The maize mutants, *bif2-N2354* (stock #108A) and *ba*l (stock #318B) in the *W23/M14* genetic background, were obtained from the Maize Genetics Cooperation Stock Center (Stamatiou *et al.* 2013).

3.3.2 Acid sensitive mutant screen

The M2 generation of EMS-mutagenized *Arabidopsis* (Col-0) seeds were chilled for 4 days at 4ºC and sown onto 0.5x MS plates placed vertically under continuous light conditions at room temperature. After 7 days, the seedlings were transferred to soil in 96-well flats. Leaf 3 or 4 was excised from 21 day-old plants using a hole punch and placed abaxial side up in a 96-well plate corresponding to the same coordinates as the flat. The hole punch produced a disc of uniform in size and weight when avoiding the midvein to

reduce thickness variability. Samples were submerged in 200 ml of1 M H_2SO_4 and incubated at room temperature for 1 hour. A 50 ml aliquot was removed and incubated with 100 ml of 0.2% anthrone (Sigma-Aldrich, A91205) in concentrated (18 M) H_2SO_4. The samples were incubated at 100^{o}C for 5 minutes, cooled and the absorbance was read at 620 nm (Dische *et al*. 1962). Approximately 22,000 seedlings from 32 pools were screened from which 63 *responsive to acid hydrolysis (rah*) mutants were identified as having an absorbance reading greater than two standard deviations from wild-type (Stamatiou *et al.* 2013).

3.3.3 Genetic Mapping of mutants

Mapping of an unknown mutation in *Arabidopsis* involves backcrossing a parent that is homozygous for the mutation with a different eco-type. In this case *rah9* was created in a *Col-0* background and is crossed with *Ler* (Figure 3.3.3). The resulting F1 is allowed to self-pollinate and undergoes homologous recombination via crossing-over during meiosis which effectively shuffles *Col-0* and *Ler* DNA markers. The resulting F2 progeny will have undergone an additional round of recombination and one-quarter of them will be homozygous for the mutation of interest according to Mendelian segregation for a monohybrid cross. Those 25% are selected by screening for the clear phenotype (enhanced saccharification). The DNA of the individuals homozygous for the desired mutation is collected and mixed creating a bulk segregant pool. Every individual in this pool possesses the mutation on pieces of DNA flanked by markers of its parent (*Col-0*). The closer the mutation is to the marker, the lower the probability of a crossing-over event happening between them. Analysis of the genetic markers in search of *Col-0*

polymorphism clustered regions amongst the pool leads to the location of the mutation. The proximity of a particular marker to the causative mutation is expressed as a recombination frequency. This is simply the number of heterozygous individuals (possessing both *Col-0* and *Ler* markers) in the pool for a particular marker. The lower the recombination frequency, the closer the marker is to the site of mutation.

Genetic mapping was accomplished using an F2 population derived from a cross between the *rah* mutants (*Col-0*) and *Landsberg erecta* (Ler). F2 seedlings were scored for enzymatic hydrolysis sensitivity as determined by the HK method (Figure 3.2.3S4). Genomic DNA was isolated from individual *Ler* backcrossed F2 plants from a mapping population showing the mutant phenotype and assigned to a chromosome using published simple sequence length polymorphism (SSLP) markers (Lukowitz *et al.* 2000). New molecular markers were developed using the Monsanto *Col-0* and *Ler* polymorphism database. The cloned *rah* genes were amplified by PCR using X-Taq DNA polymerase with proofreading activity (Takara). Sequencing reactions were performed by The Centre for the Analysis of Genome Evolution and Function (CAGEF) at the University of Toronto. Second generation mutants from two independent crosses were used for sequencing and verifying lesions (Stamatiou *et al.* 2013).

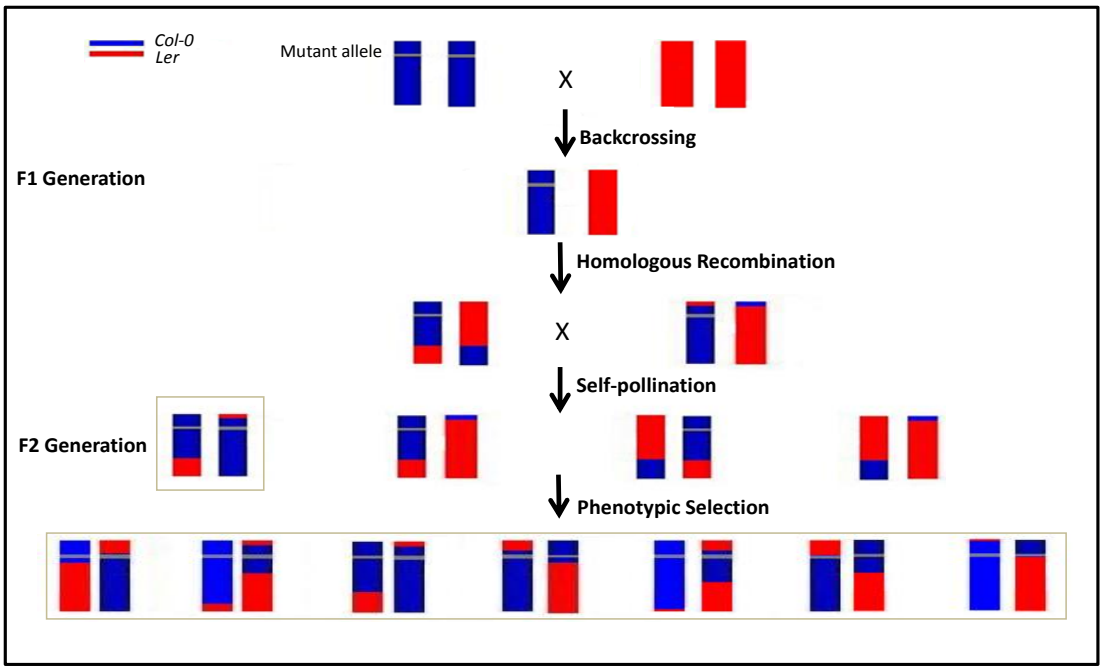

Figure 3.3.3: A diagram illustrating the shuffling of genetic markers through segregation and homologous recombination. This mixing of DNA is utilized in mapping an unknown mutation in *Arabidopsis*. The blue regions represent DNA containing *Col-0* markers and red denotes regions of *Ler* descent. Since the *rah9* mutant originated from a *Col-0* background, the site of the mutation will be flanked by *Col-0* markers. The causative mutation lies in a genomic region of low recombination and thus clustering of *Col-0* polymorphisms (blue).

3.3.4 Enzymatic digestion of plant biomass

The senesced above-ground tissue (>95% is stem tissue) of *Arabidopsis* was prepared by initially drying it at 65^{o}C for 2 days. The tissue was then ground using a Thomas Scientific Mini-Mill (Model 3383-L10) and passed through a 60 mesh screen. Approximately 100 mg of this ground tissue was then macerated in 10 mL of water at 20^{o}C in glass test-tubes for three hours. The water was aspirated away and replaced with fresh 10 mL of water after which the tubes were placed in a water bath set at 80^{o}C for one hour. The water was then exchanged with 10 mL of 70% ethanol and placed back in 80^{o}C for an additional hour. The tissue was then rinsed twice with 5 mL of acetone, and the ground and washed tissue was oven dried at 65^{o}C for 2 days. Cellulase (Celluclast, Sigma-Aldrich, C2730) and Cellobiase (Novozyme 188, Sigma-Aldrich, C6105) had activities empirically determined to be 111 filter paper units (FPU)/mL and 500 U/mL respectively (Figure 3.3.4S1). Cellulase activities were determined using the filter paper assay (Ghose 1987), where the glucan products were quantified using 0. 2% anthrone according to a glucose standard (Figure 3.3.4S2). The cellobiase activity was determined by assaying the p-nitrophenol formation from pnitrophenyl-1,4-β-glucoside (Sigma-Aldrich, N7006) by measuring the absorbance at 400 nm. Triplicates of 15 FPU/g tissue of cellulase and 80 U/g of cellobiase were used on 5 mg of tissue in 200 mL of 50 mM sodium citrate, pH 4.8 in 1.5 mL microcentrifuge tubes. The samples were incubated in a water bath set at 50^{o}C for 24 hours then heat inactivated at 100^{o}C for 5 min. Once cooled on ice, the samples were centrifuged at 12 000 g for 5 min and the supernatant was retained. The free glucose in the supernatant was measured using a glucose hexokinase assay kit (Sigma-Aldrich, GAHK20). Digestion of the same plant material with xylanase

(Sigma-Aldrich X2753) was done by incubating 5 mg of washed milled tissue in 50 mM sodium citrate buffer (pH 5.0) containing 0.57 U of xylanase, 0.077 U of cellulase and 0.4 U Novozyme 188 for 24 hours at 50ºC. The reactions were terminated by heating at 100º C for 5 min. Samples were then centrifuged and the supernatant was assayed for the presence of glucose using the Glucose Hexokinase Assay Kit. In cases where lignin peroxidase (Sigma-Aldrich, 42603) was used, it was done prior to using the above enzyme mixtures by incubating the tissue in 50 mM sodium citrate buffer (pH 3) containing 0.00436 U peroxidase, 0.3% hydrogen peroxide for 2 hours at 30ºC.

3.3.5 Positional cloning and bulk segregant analysis of *rah9*

Two hundred back-crossed F2 seeds (*rah9 x Ler*) planted in a 96-well tray. DNA from each F2 was extracted 28 days after germination. The plants were allowed to fully senesce before the tissue was processed for enzymatic hydrolysis in the manner described in section 3.3.4. Glucose levels of the F2s were quantified using the glucose-(HK) assay. Aliquots of the previously CTAB extracted DNA from each homozygote displaying the phenotype enhanced glucose release were combined as described in section 3.3.3. Mapping primers given in Lukowitz *et al.* (2000) were used on the pool to amplify 22 uniformly distributed regions of the *Arabidopsis* genome known to contain distinguishing SSLP markers between *Col-0* and *Ler*. The PCR products were resolved using gel electrophoresis in 0.5x Tris-Borate-EDTA buffer with 0.5 μg/mL ethidium bromide. The 4% agarose gel was run at 100 V for 45 min at room temperature. The gels were visualized by illuminating at 302 nm using a transilluminator.

3.3.6 Aldol acetate derivatization for gas chromatography

The monosaccharide hydrolysis products of stem tissue were quantified using gas chromatography (GC) of alditol acetates and was carried out with modification to the previously described method (Reiter *et al.* 1997). The sugars from the supernatant of the cellulase enzymatic hydrolysis scheme were analyzed. Three technical replicates were performed for select *rah* mutants. The released monosaccharides in the supernatant were converted into alditol acetates and quantified by a Varian model 3900 using a Supelco glass capillary column (SP-2330). The samples form the enzymatic hydrolysis for select *rah* mutants were treated with cellulse and cellobiase and were prepared using the procedure described in section 3.3.4. Sample analyzed by GC were treated with cellulase and cellobiase.

Two hundred microliters of the enzymatic hydrolysis aqueous product was added to 100 μL of 9M ammonia in a glass test tube and vortexed briefly. To each sample 1 mL of 2% $NaBH_4$ dissolved in dimethylsulfoxide (DMSO) was added and incubated for 90 minutes at 40^{o}C. Two hundred and fifty microliters of glacial acetic acid were added and the tubes were vortexed. Then 250 μL of 1-methylimidazole and 4 mL of acetic anhydride were added to each tube and left at room temperature for 10 minutes. Eight milliliters of double-distilled water was added and the tubes were mixed by inversion thoroughly and placed at room temperature for 30 minutes. The alditol acetate products were extracted by adding 1.5 mL of dichloromethane (DCM) and inverting the tubes 30 times and placed at 4^{o}C overnight. The DCM layer was extracted with long Pasteur pipets and transferred to small disposable test tubes. The samples were heated to 55^{o}C until the DCM had completely evaporated. The alditol acetate products were

resuspended in 200 μL of DCM. The samples were then washed by adding 1 mL of double distilled water and vortexing vigorously for 10 seconds. The organic phase was then transferred to GC vials and stored at -20ºC.

3.3.7 Lugol amylose staining

Senesced tissue and fresh leaf tissue were treated with Lugol`s stain for the presence of starch. Lugol`s stain was made my mixing 6.6 g/L and 3.3 g/L (2:1) of potassium iodide and iodine respectively. The samples were placed in the solution and allowed to sit for 5 minutes. The samples were washed with water then examined under a dissecting light microscope equipped with an Amscope MD900E camera (Irving, CA). The seedlings were examined for ectopic lignin staining and were compared against wild-type controls (n = 9).

3.3.8 Amylase digestion of plant biomass

Five milligrams of milled and washed senesced *Arabidopsis* stem tissue was weighed out in triplicate in 1.5 mL microcentrifuge tubes. The tissue was macerated in 940 μL of 0.1 M sodium acetate, pH 5 for several hours. The starch was then gelatinized by incubating the tubes at 80ºC for 30 min. The tubes were cooled on ice, and then 30 μL of a tenfold dilution of α-amylase (Sigma-Aldrich A7595, undiluted activity: 250 U/mL) was added. In addition, 15 μL of pullulanase M1 (Megazyme 699 U/mL) and 15 μL of pullulanase M2 (Megazyme 250 U/mL) were added to bring the total liquid volume to 1 mL. The samples were vortexed then placed in an incubator set at 37ºC for 16 hours. The tubes were placed at 100ºC for 5 min, cooled to room temperature then centrifuged at 12 000 *g*

for 10 min. The reducing sugar equivalents present in the supernatant were quantified using 0.2% anthrone.

3.3.9 Acid hydrolysis of plant biomass

Five milligrams of washed tissue were macerated with 0.8 mL of ddH_2O water in microcentrifuge tubes. Once the tissue has sunk to the bottom, 0. 2 mL of 1 M H_2SO_4 was added and the tubes were placed at 65^oC for one hour. The tubes were then centrifuged at 13 000 *g* for 5 min and 50 µL of the supernatant was assayed for sugar content using 0.2% anthrone.

3.3.10 N-1-naphthylphthalamic acid (NPA) treatment of monocot plants

Polar auxin transport inhibition was carried out as described (Wu & McSteen 2007). The two maize cultivars, Syngenta hybrid N39-Q1 and Tuxedo Sweet Corn, were grown in a greenhouse at 24^oC with a 12 hour day/night cycle. The plants were grown four weeks before NPA treatment followed by a two week watering regime using 120 mM NPA (ChemService, West Chester, Pennsylvania, USA) or DMSO alone (solvent) applied every two days in a volume of 150 mL for each pot (3.5" x 3.5"). Plants were fertilized once a week with 150 mL of 20-20-20 fertilizer (5 g per gallon) with or without NPA. After 2 weeks of treatment, above ground tissue (mostly leaves and stems) was collected and destained in chloroform: methanol (1:1 v/v). The tissue was thoroughly dried in an oven and milled to a 60 mesh size. Acid hydrolysis was performed as described above (Stamatiou *et al.* 2013).

3.4 Discussion

The objectives of this study were to develop a simple, high throughput forward genetic screen to identify informative genotypes displaying improved sugar release under mild acid treatment. The enzymatic digestion schemes were developed to characterize the senesced tissue degradability of the screened mutants. The two lines with the most obvious phenotypes were chosen to be examined for this study. Several additional *rah* lines were cloned and characterized and are described in Stamatiou *et al.* (2013). The remaining uncloned lines from this screen release more sugar than wild-type under acid and/or enzymatic schemes and potentially harbour novel saccharification enhancement strategies. Furthermore, the low frequency of mutant identification (0.3%) and the small number of allelic members within the *rah* pool suggests the screen was not saturated and that more genetic variation remains to be discovered (Stamatiou *et al.* 2013).

In the enzymatic schemes, the *sex4* mutant released the most sugar. The identification of mutants that overaccumulate starch in vegetative tissues presents an unconventional approach to enhance the fermentable sugars yields for biofuel production. Starch is much easier to access and takes less energy to hydrolyze compared to lignocellulose. The conversion of sugars derived from starch for ethanol production through fermentation has been practiced for thousands of years in beer and wine making. Unlike reproductive tissues such as corn kernels and rice grains, starch levels in stems and leaves were considered unsubstantial and vegetative tissues are not regarded as useful starch based feed stocks. However, this study shows that genetically increasing vegetative starch levels can contribute to the overall fermentable sugar yields during acid pretreatment and enzyme hydrolysis. Since starch metabolism is far removed from wall

polymer biosynthesis, in principle its genetic manipulation should be a stackable trait with genetic strategies to reduce lignocellulosic recalcitrance. It was shown by Stamatiou *et al*. (2013) that disruption in starch metabolism does not always result in enhanced saccharification suggesting that different forms of starch have varying degradability and a complex relationship between starch metabolism perturbation and saccharification exists.

The second strategy to enhance saccharification uncovered by this study was in the disruption of polar auxin transport. A loss-of-function mutant of *pid* displayed enhanced sugar release and the pin-formed phenotype. Although, auxin and cellulose synthesis are both essential for cell expansion and growth, the understanding of relationship between the two pathways is tentative. Recently, a weak allele of *cesA3* carrying the amino acid substitution (P578L) was found to cause PIN localization defects and resistance to isoxaben (Feraru *et al*. 2011). In addition, the isoxaben resistant allele, *ixr1-1* was found to have increased tolerance to NPA compared to wild-type (Tegg *et al.* 2013). This study found *ixr1-1* to be insensitive to the saccharification enhancing effects on NPA (Figure 3.2.8) in agreement with the observation of Tegg *et al.* (2013). These results suggest a close linkage between auxin transport and cell wall synthesis.

This study showed that pinoid and other pin-shaped inflorescence mutants have increased sugar release again compared to wild-type (Figure 3.2.4) which suggests a role for auxin in influencing sugar accessibility. Interestingly, this association has been observed to be limited to perturbations in the auxin pathway which results in mutants that display a pin-shaped inflorescence phenotype (Stamatiou *et al.* 2013). This suggests that aberrant inflorescence development may be associated with cell wall integrity deficiencies. Alternatively, auxin transport may influence the accumulation of cytosolic

sugars although *rah20* tested negative for starch in amylase assays and Lugol's staining experiments (data not shown). Currently, the underlying mechanisms connecting auxin to increased saccharification are a matter of speculation.

PINOID is a threonine/serine kinase known to act on PIN proteins (Christensen *et al*. 2000). *Rah20* is a loss-of-function mutant of PID and the only one displaying pin-formed inflorescences detected in this screen. The pin-formed phenotype of *pin1* is completely penetrant resulting in infertility, unlike *rah20* which is incompletely penetrant allowing for reproduction. As a result propagation of pin-formed lines may be less than ideal. However, this may prove to be advantageous with respect to preventing contamination amongst neighboring commercially grown transgenic crops. The results found in *Arabidopsis* were shown to transfer in maize. The maize ortholog, *barren inflorescence 2* (*bif2*) was shown to display similar morphological and saccharification sensitivity phenotypes. Treatment of NPA and *pin* mutants showed abnormally high radial proliferaton along with extensive xylogenesis in the xylem vascular tissue (Gälweiler *et al*. 1998). The aberrant auxin transport in *rah20* may enhance saccharification by altering hemicellulose composition in vascular cells. The altered hemicellulose content may either permit accessibility to a greater extent or the higher yields are accounted for by more accessible hemicellulose itself.

Auxin transport was also inhibited chemically by NPA in this study. It was shown that treatment of wild-type *Arabidopsis,* maize, *Miscanthus* and switchgrass plants with the polar auxin transport inhibitor, NPA, also results in increased saccharification. In applying the strategy of polar auxin transport disruption to enhance saccharification yields, chemically induced phenotypes using compounds such as NPA offer alternatives

to transgenic plants. Chemical application should allow for finer tuning of dose and greater temporal and spatial control application. NPA is already a component of approved and agriculturally relevant preemergence herbicides and its application for saccharification enhancement should be compatible with currently existing practices, infrastructure and equipment. Finally, the ability to increase saccharification using NPA in maize, switchgrass and *Miscanthus* shows that forward genetic screening using *Arabidopsis* can be applied to develop chemical leads useful in biomass pretreatment processing for cellulosic biofuels.

Chapter 4: Conclusion

4. 1 Summary and Future Directions

The plant cell wall is comprised of a variety of polymers forming a heterogeneous network highly resistant to hydrolysis. Cellulose microfibrils form the core of the walls and are the targeted polymer in cellulosic processes. Despite the abundance and indispensability of cellulose in nature, details about its biosynthesis and degradation remain scarce and interpretive. Generally, biological processes are studied by searching for genetic mutants who have lost the ability to perform a normal function. Since proper cellulose deposition is usually required for cell viability, more indirect approaches are necessary. The resistance to putative CBIs such as isoxaben and flupoxam was examined. All known alleles of isoxaben and flupoxam resistance cluster to loci encoding CESA1, CESA3 and CESA6. Details uncovered concerning the mode of action of isoxaben are certain to disclose information about cellulose synthase. Comprehensive knowledge of CESAs and wall synthesis will undoubtedly expose opportunities to enhance digestibility and reduce biomass recalcitrance. In addition, a deeper understanding of the biological processes involved in the biosynthesis and degradation of cellulose will be essential for future sustainable energy crop engineering.

One unconventional approach to enhance saccharification yields explored in this study was perturbing starch metabolism resulting in ectopic starch deposition in vegetative tissue. The starch accumulation was the result a deficient splice variant allele of *sex4* which encodes a phosphoglucan phosphatase. The examination of the phosphorylation status of the components of wall polymers with radiolabeling assays promises to provide insight on the broader effects of *sex4* and other phosphorylation

perturbations on the cell wall. Given the promiscuous nature of phosphatases, it is reasonable to speculate that SEX4 acts on many different phosphoglucans. SEX4 deficiency could result in the overabundance and accumulation of a variety of phosphoglucans and may have implications for cell wall integrity. It is likely that the absence of the dephosphorylating action of SEX4 has far reaching regulatory consequences which may result in aberrant wall formation. It would be very exciting for cellulosic biofuel development if a link between starch metabolism deficiency and cell wall digestibility were made. This link would potentially enable the advent of energy crops which accumulate starch while possessing cell walls that are highly susceptible to hydrolysis.

A major finding of this study is the clustering of *ixr* and *fxr* alleles to *cesA1*, *cesA3* and *cesA6*. Furthermore, *fxr* is only found on *cesA1* and *cesA3* whereas *ixr* is only observed in *cesA3* and *cesA6*. The locations of the amino acid substitutions leading to flupoxam resistance are highly localized. These locations of the substitutions suggest that CESA1 and CESA3 interact through TMD6-8 and that flupoxam binds and disrupts this interaction causing cessation of cellulose biosynthesis via rosette disassembly. Deciphering the mode of action of isoxaben however, is less straight forward. Isoxaben has been documented to cause a broad range of effects and resistance alleles to its CBI effects are not as localized as they are for flupoxam resistance. Alleles of *cesA3* which confer resistance to isoxaben act through two probable mechanisms. The first is by directly modifying the binding site of isoxaben and lowering the binding affinity. In this case the single amino acid substitution would result in localized changes in the spatial conformation of the CESA. The second is by decreasing the binding affinity

allosterically. Single amino acid substitutions leading to global changes in CESA conformation alter the binding affinity indirectly. The first case of alleles should be characterized by high resistance to their respective CBI and mutants should exhibit few morphological deficiencies. Allosterically acting alleles however would likely be characterized by lower CBI resistance and a greater preponderance of growth and reproductive defects. Despite these differences, the distinction between a direct binding-site modification resulting in weak resistance and an allosteric one causing high resistance remains arbitrary. For example, *ixr1-1* likely results in a direct modification of the isoxaben binding site. This mutant displays no obvious growth or fertility defects and confers an exceptionally high degree of resistance to isoxaben. In contrast, *ixr1-6* confers relatively low resistance and displays many cellulose deficiency phenotypes. This mutant is probably an example of an allosteric modifier of the binding site. Interestingly, *ixr1-3* must directly modify the CBI binding site since it is at the same site as *ixr1-1*. However, *ixr1-3* harbors a different amino acid substitution and behaves like an allosteric modifier with growth defects and comparably lower resistance. This is an example of a direct modification of the site of action additionally causing global effects diminishing CESA function. The CBI resistance and morphological consequences of *cesA6* mutants are diluted by its lower representation in primary wall rosettes. This further hampers the classification of *cesA6* resistance alleles. Based on the broad ranges of resistance and scattered locations of substitutions of *ixr* alleles, it is probable that most are allosteric modifiers of the isoxaben binding site.

Homozygous double mutants of *ixr1-3; fxr2-3* exhibit reversion to wild-type sensitivities to both herbicides with 0.7% escaping with obvious primary wall

deficiencies. Further detailed studies of this mutant effect are required to fully characterize the effects the simultaneous expression of these two alleles have on CESA interaction and cellulose biosynthesis. The G1009D substitution is only four amino acids from the G998S of *ixr1-3* when aligned according to sequence similarity (Figure 2.2.3A). This may suggest that this conserved region is important for inter-CESA associations within the membrane. Interestingly, homozygous double mutants of *ixr1-1/3;fxr2-1* did not exhibit any reversion phenotypes suggesting the requirement of acidic sides for complementation. A revealing experiment to perform in future studies involves site-directed mutagenesis to create CESA3 (G994S) and CESA1 (G1013D) lines. These are the equivalent substitutions defining *fxr2-3* and *ixr1-3* when in CESA1 and CESA3 respectively. It would be interesting to see if either modification results in CBI resistance. Subsequent crossing and selection for double homozygotes would create a mirror of the genetic situation of *ixr1-3;fxr2-3*, where the substitution in CESA1 resulting from *fxr2-3* is placed in the equivalent position in CESA3 and vice versa.

An interesting feature of isoxaben and flupoxam is that they cause similar effects at the same concentrations. Resistance to either CBI is restricted to modifications of primary wall CESAs and their targets overlap in *cesA3*, which harbours both *ixr* and *fxr* alleles. Despite these striking similarities, cross-resistant lines remain elusive. The absence of a single allele conferring resistance to both herbicides leads one to conclude that the two CBIs have unique targets within the same complex. These targets must also be separated by a distance large enough that allosteric effects of an amino acid substitution conferring resistance to one herbicide does not affect the binding site of the other. Since these herbicides act by disrupting inter-CESA interactions, resistance can

only be harbored in those subunits which directly interact. Alleles for isoxaben resistance were not found in *cesA1* nor were alleles for flupoxam found in *cesA6*. This suggests that CESA1 and CESA6 do not directly interact. Resistance to both herbicides can be found in *cesa3* alleles indicating that it is the central subunit and mediates the association of CESA1 and CESA6 in the primary wall synthase complex (Figure 2.2.3D). This model of the rosette predicts a CESA1:CESA3:CESA6-like stoichiometric ratio to be 2:3:1.

In order to further investigate the nature of the interaction between isoxaben and its target, a one step reduction of isoxaben was performed with excess amounts of sodium borohydrate in tetrahydrofuran (THF). This reduced-isoxaben (isxH) compound behaved much like isoxaben in *Arabidopsis* seedlings although TLC and ^{1}H NMR verified that isxH is indeed a distinct compound from the starting material. With the structure of isxH in mind, a chemical analogue of isxH, pydA was tested on *Arabidopsis* seedlings. This lead to the observation that pydA causes root hair growth inhibition in *Arabidopsis*. PydA appears to phenocopy the effects of the *kojak* mutant and it is tempting to speculate that CSLD3 is the target. A forward genetics screen for resistance to pydA would be a useful experiment to investigate this possibility. Alleles of pydA situated in CSLD3 would provide compelling evidence to support this speculation.

Exploration of additional analogues of isxH, particularly phenyl-pyrimidinol derivatives shows promise in the discovery of a wide range of CBIs and other wall glycan biosynthesis inhibitors (GBI). This structure may represent a class of CBIs and the potential diversity may allow for the tuning and targeting of specific CESAs and CSLs. Subtle chemical structural differences may correspond to large changes in efficacy and/or specificity. Although the preliminary results regarding isxH and pydA are exciting, more

validation is required. The metabolic profile of isoxaben and isxH *in planta* through HPLC analysis of fractionated plant cell extract compared against isx and isxH would be informative data.

These isxH analogues can be applied late in an energy crop grow season as part of a pretreatment regiment in order to decrease recalcitrance. Additionally, wall hydrolysis sensitive isxH-analogue resistance traits can be stacked with starch over-accumulating genes to increase overall fermentable sugar yields. This study has brought forth the frame work for a novel glycan biosynthesis inhibitor (GBI) toolbox along with attractive stacking options for energy crop design. Alternatively, GBIs and their corresponding set of resistance alleles can potentially be applied as novel weed management systems in current commercially relevant crops. Examination of patterns in the chemical structures of active GBI compounds may reveal novel structure-function relationships in CESAs and CSL proteins. The greater the number of characterized GBIs and CBIs, the clearer the perspective is on their targets. Similarly, increasing the pool of unique resistance alleles to a particular inhibitor better defines the nature of inhibitor binding and action. Resolving the nature of the interaction between GBIs and their targets is proposed to be approached both from the perspective of the target enzyme and the small molecule.

Another approach to enhancing saccharification was in the inhibition of polar auxin transport as a result of deficiencies in the threonine/serine protein kinase, PID. This effect was extended to the more agriculturally relevant commelinoids by chemically phenocopying *pid* with NPA, revealing a link between auxin transport disruption and saccharification enhancement. The apparent requirement of the pin-formed phenotype for enhancement of sugar release in auxin mutants suggests that there is connection with

aberrant inflorescence development and saccharification. Reversible PIN1 phosphorylation at conserved serines in the hydrophilic loop mediated by PID is required for proper localization, making it essential for proper auxin transport (Huang *et al.* 2010). Other proteins directly involved in cellulose synthesis may also be phosphorylated by PID or a similar kinase, influencing their function and determining localization. Indeed, the phosphorylation status of the primary wall CESAs have been suggested to play a role in the regulation of cellulose biosynthesis (Chen *et al.* 2010 and Taylor 2007). A disproportionate number of serine substitutions conferring isoxaben and flupoxam resistance were observed in this study. In addition, it was observed by this study and Tegg *et al.* (2013) that *ixr1-1* was resistant to many of the effects of NPA, providing a possible link between auxin transport and isoxaben resistance (Figure 3.2.8). Furthermore, a *cesA3* mutant that restored PIN localization was also resistant to isoxaben (Feraru *et al.* 2011). These results suggest that isoxaben resistance is tied to polar auxin transport which influences saccharification through complex mechanisms. Isoxaben and flupoxam are putative CBIs and likely interact with the cellulose synthases complex at the CESA3-CESA6 and CESA1-CESA3 subunits respectively. The internalization and sequestration of CESA complexes upon exposure to isoxaben by Scheible *et al.* (2001) could be related to the phosphorylation states of the CESAs. The regulation of these states could be disrupted by isoxaben and flupoxam acting as specific auxin mimics.

Future studies should be directed towards examining the sensitivity of *pid* and related kinase mutants to isoxaben and flupoxam and their gene interactions with the *ixr* and *fxr* alleles. The evidence for a direct relationship between isoxaben and flupoxam resistance and polar auxin transport are mounting and provide a tool to view cellulose

biosynthesis from the perspective of auxin regulation. This link will enable connections between two essential pathways providing invaluable knowledge facilitating the advent of novel cellulosic bio-energy technologies.

Elucidating the cellulose biosynthetic pathway is a challenge relying on innovative, indirect and novel approaches for glimpses at the underlying mechanism. It is a complicated and dynamic process which is constantly adjusting to environmental stimuli. Both cellulose and auxin are ubiquitous and essential plant compounds so it comes as no surprise that they should meet in this study. Polar auxin transport mutants were found to release greater amounts of fermentable sugars compared to wild-type. Additionally, isoxaben produces effects similar to IAA in very low doses. It is becoming apparent that auxin affects cellulose deposition or even synthesis but the mechanistic details remain obscure. The isoxaben resistant allele, *ixr1-1* was found to have increased tolerance to NPA, a polar auxin transport inhibitor compared to wild-type (Tegg *et al.* 2013). Characterization of the *ixr* and *fxr* mutants on NPA may prove to further link these CBIs and polar auxin transport. Additionally, a weak allele of *cesA3* carrying the amino acid substitution (P578L) was found to cause PIN localization defects and resistance to isoxaben (Feraru *et al*. 2011). The disproportionate number of serine substitutions amongst the *ixr* and *fxr* may indicate the involvement of CESA phosphorylation in the mode of action. It is possible that the primary wall CESAs are phosphorylated by a PID-like kinase whose action regulates its activity and determines its possible conformations. Removing or blocking these phosphorylation sites may prevent the CESA from assuming the conformation necessary for CBI binding.

Although attractive, these notions are entirely speculative and kinase-CESA interaction has yet to be observed. Furthermore, the serines in question have not been observed to be phosphorylated and no non-CESA resistance alleles have been observed. Nevertheless, obtaining phosphorylation profiles for the *ixr* and *fxr* mutants would be informative. It would be interesting to see if the phosphorylation states of the CESAs are different amongst the mutants and in the presence of CBI and absence of herbicide. Additionally ^{32}P-radiolabelling experiments involving *pid*/*the*; ixr/*fxr* double mutants would shed light on this issue.

Despite their central importance, relatively little is known about CESAs, cellulose biosynthesis and degradation. Increasing awareness of the negative environmental impacts of fossil fuel usage has resulted in an increased interest in renewable energy technologies such as cellulosic biofuels. Such technologies rely on the cost effective and energy efficient access and degradation of the encapsulated cellulose. This technology is attractive because of the ubiquitous nature of cellulose making it an available and low-cost biofuel feedstock. The advent of this technology is currently hindered by the lack of understanding in the processes and factors involved in cellulose biosynthesis and subsequent degradation. Cellulose biosynthesis is a dynamic and complex process which remains poorly understood. Despite formidable limitations, incremental progress is slowly being made and novel details of the pathway are consistently being illuminated. A deeper understanding of the underlying processes of wall biosynthesis can translate into direct and indirect commercial applications in current and emerging industries.

Appendix

Chapter 2 Supplemental Tables and Figures

Table 2.2.2S1: List of the CBI resistant mutants and RFLP markers. DNA amplified using primers listed in Table 2.3.2 were digested with restriction enzymes sensitive to the mutant SNP. In the RFLP column, + denotes markers where the restriction cuts the site in the wild-type allele but not in the mutant. - represents RFLP markers where the enzyme cuts the mutant allele but not wild-type.

Eco-type	Allele	Codon Change	Substitution	Gene	Restriction Enzyme	RFLP type
Col	*ixr1-1*	GGT → GAT	G(988)D	*cesa3*	PflMI	+
Ler	*ixr1-1B*	GGT → GAT	G(988)D	*cesa3*	PflMI	+
Col	*ixr1-2*	ACC → ATC	T(942)I	*cesa3*	MnlI	+
Ler	*ixr1-3*	GGT → AGT	G(998)S	*cesa3*	PflMI	+
Ler	*ixr1-4*	AGG → AAG	R(806)K	*cesa3*	AcuI	-
Ler	*ixr1-5*	CTT → TTT	L(797)F	*cesa3*	Tsp509I (MluCI)	-
Ler	*ixr1-6*	TCT → TTT	S(377)F	*cesa3*	Hpy188I	+
Ler	*ixr1-7*	CGT → CAT	R(279)H	*cesa3*		
Col	*ixr2-1*	CGG → TGG	R(1064)W	*cesa6*	BssKI	+
Ler	*ixr2-2*	TCT → TTT	S(1002)F	*cesa6*	BsmAI (BcoDI)	+
Col	*fxr1-1*	TCG → TTG	S(1040)L	*cesa3*		
Ler	*fxr1-2*	TCT → TTT	S(1037)F	*cesa3*		
Ler	*fxr1-3*	TCT → TTT	S(983)F	*cesa3*	BsmAI (BcoDI)	+
Ler	*fxr2-1*	GGG → AGG	G(1013)R	*cesa1*		
Ler	*fxr2-2*	CCG → CTG	P(1010)L	*cesa1*	AciI	+
Ler	*fxr2-3*	GGT → GAT	G1009D	*cesa1*	BamHI	-
Ler	*fxr2-4*	TCG → TTG	S307L	*cesa1*	MnlI	+

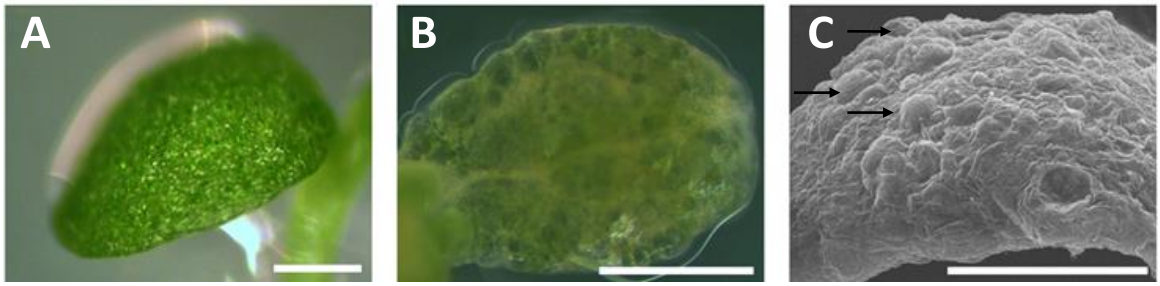

Figure 2.2.5S1: Effects of flupoxam on wild-type cotyledons.

A) *Ler* seedling 5 DAG grown in the absence of flupoxam (bar= 1 mm).

B) A close up light-microscope image of a 5 DAG *Ler* seedling cotyledon displaying CBI sensitivity after being grown on 5 nM of flupoxam (bar= 1 mm).

C) An SEM image of a *Ler* seedling cotyledon grown in 5 nM flupoxam. Cellulose deficiencies are evident in the loss of anisotropy in the blistering cells (arrows) (bar = 1mm)

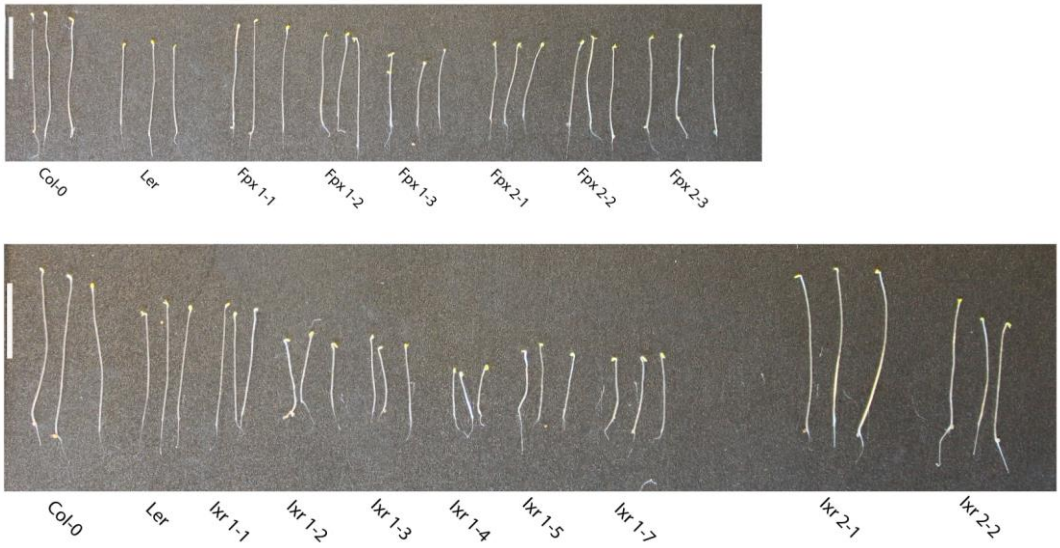

Figure 2.2.6S1: Hypocotyls of dark grown *ixr* and *fxr* mutant seedlings. Three representative etiolated seedlings of *ixr* and *fxr* lines are shown with the wild-types on the far left (bar = 1 cm).

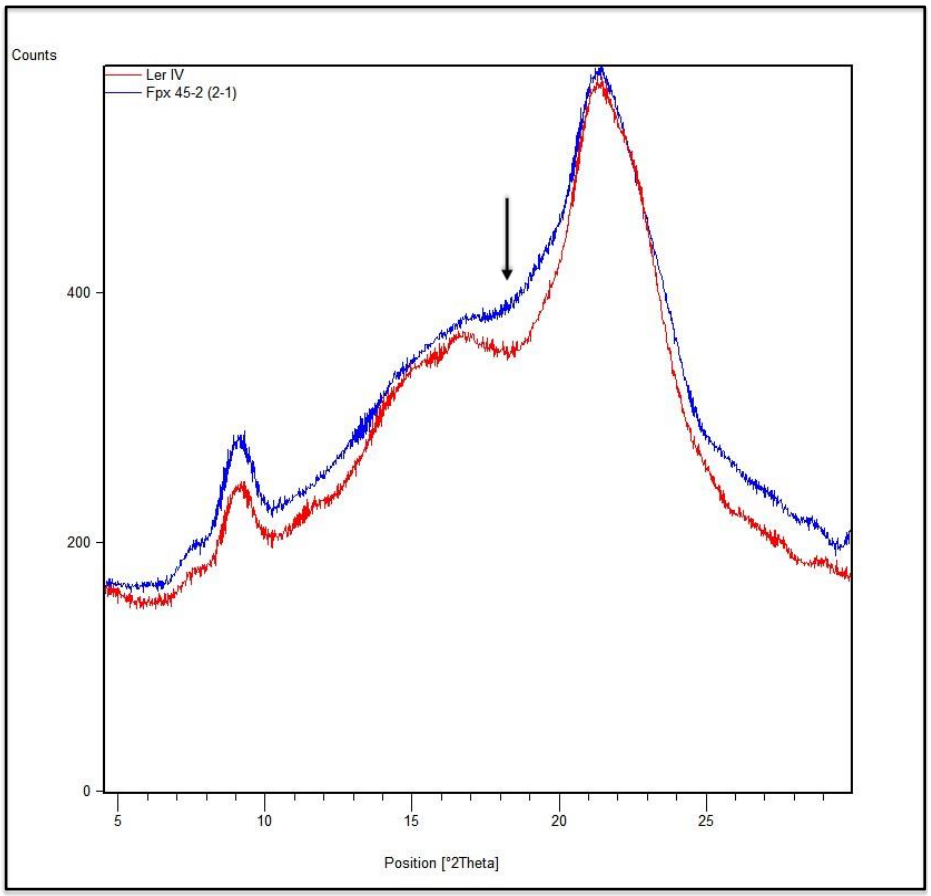

Figure 2.2.8S1: XRD spectrum comparing wild-type and mutant crystallinity. The spectra of *Ler* (red) and *fxr2-1*(blue) are compared illustrating the increase in the amount of amorphous cellulose in the mutant (arrow). The lower RCIs of CBI resistant mutants were the result of larger values for amorphous regions rather than lower crystalline peaks.

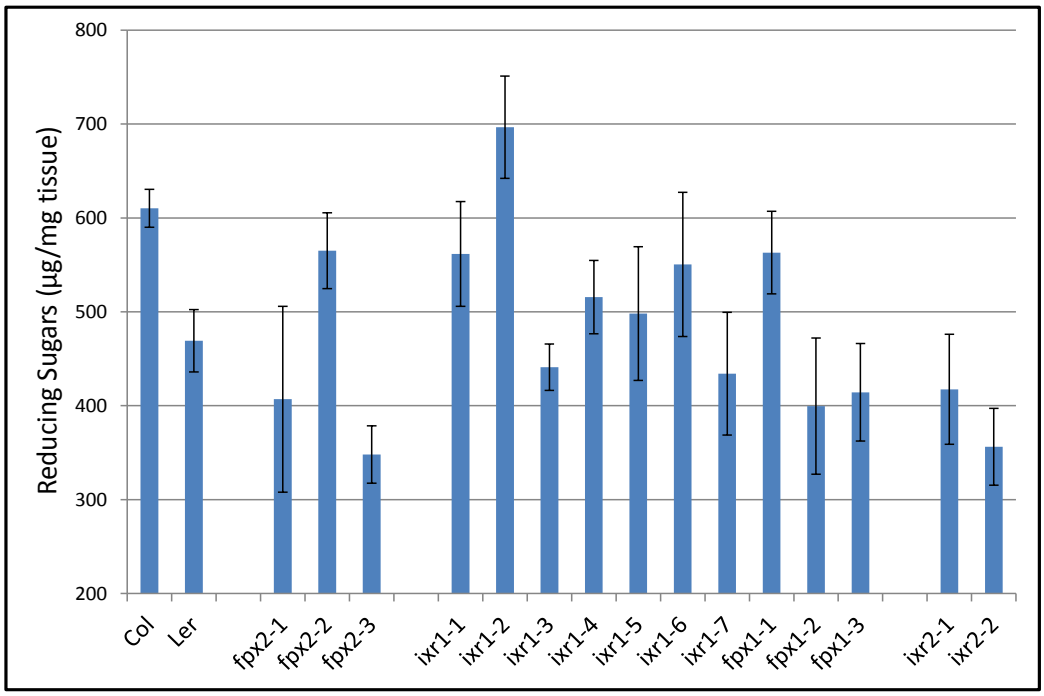

Figure 2.2.9S1: Total sugars released by *ixr* and *fxr* in the sequential acid and enzymatic hydrolytic analysis. Values are averages expressed in micrograms of reducing sugar equivalents per milligram of dry senesced tissue +/- standard deviation (n = 3). The sugar equivalents were determined using 0.2% anthrone.

Chapter 3 Supplemental Tables and Figures

Table 3.2.2S1: Hydrolytic screening data for *rah* mutants. Sugar readings higher than two standard deviations greater than wild-type are highlighted (n. d = not determined). Under the ectopic lignin column, R, H, C and (-) specifies the location of staining as in the root, hypocotyl, cotyledon and none observed respectively.

	1M H_2SO_4 fresh leaf disc				0.2M H_2SO_4 senesced tissue				Cellulase		Cellulase + Xylanase		Cellulase + Xylanase + Peroxidase		Starch	Ectopic Lignin
Name	Abs	SD	Estimated total sugars (ug/leaf disc)	SD	Abs	SD	Estimated total sugars (ug/mg DW)	SD	Glucose (ug/mg DW)	SD	Glucose (ug/mg DW)	SD	Glucose (ug/mg DW)	SD		
Col-0	0.12	0.00	4.12	0.10	0.54	0.01	34.83	0.64	66.36	1.21	150.01	3.75	157.16	15.33	-	-
mur11-1	0.22	0.04	10.37	2.43	1.10	0.08	72.00	5.25	73.39	5.84	176.03	10.38	205.35	5.02	strong	-
rah1	0.39	0.11	20.68	6.59	0.83	0.13	54.23	8.51	92.63	13.40	163.43	24.18	169.28	6.98	strong	-
rah2	0.38	0.05	20.30	3.12	0.60	0.01	39.33	0.95	77.82	4.98	149.95	24.14	220.23	29.10	strong	R
rah3	0.37	0.10	19.24	6.41	0.59	0.17	38.39	11.34	64.16	1.20	125.83	10.68	173.74	7.12	strong	
rah4	0.31	0.05	15.88	3.14	n.d.	n.d.	n.d.	n.d.	73.03	13.92	127.07	20.29	195.68	9.29	-	R
rah5	0.30	0.14	15.41	8.35	0.54	0.05	35.10	3.08	62.83	4.33	105.08	2.96	104.93	7.27	strong	-
rah6	0.30	0.06	15.34	3.88	n.d.	n.d.	n.d.	n.d.	99.82	7.94	140.91	11.08	211.68	26.08	weak	-
rah7	0.30	0.11	15.22	6.91	0.68	0.05	44.08	3.19	89.44	6.87	158.47	18.41	175.97	8.81	-	-
rah8	0.29	0.08	14.85	4.74	0.66	0.14	43.26	9.12	92.99	1.56	106.85	6.14	186.01	22.38	-	-
rah9	0.29	0.08	14.68	4.83	0.65	0.14	42.69	9.58	181.65	17.36	347.20	20.21	510.33	10.64	strong	-
rah10	0.29	0.07	14.50	4.57	0.46	0.01	30.02	0.51	68.51	3.46	145.16	15.37	178.20	9.64	-	R,H
rah11	0.29	0.12	14.33	7.41	0.83	0.09	54.28	5.71	105.14	8.52	227.11	14.61	272.30	7.27	-	-
rah12	0.27	0.03	13.30	2.10	0.82	0.03	53.86	2.29	78.88	21.93	122.99	20.93	199.77	8.93	weak	-
rah13	0.27	0.07	13.18	4.00	0.64	0.02	41.45	1.04	83.05	10.53	128.67	11.49	230.64	12.80	-	-
rah14	0.26	0.13	13.00	7.89	0.58	0.06	37.46	3.73	81.10	7.85	179.93	19.73	185.64	15.15	strong	-
rah15	0.26	0.05	12.90	2.82	0.79	0.12	51.56	7.95	100.61	1.87	214.52	21.70	232.50	16.90	-	-
rah16	0.26	0.01	12.58	0.85	0.43	0.02	27.88	1.07	82.79	2.40	111.46	22.51	225.06	25.72	weak	-
rah17	0.26	0.03	12.50	2.04	0.57	0.03	36.82	1.86	85.09	14.49	137.89	5.33	174.86	8.25	-	-
rah18	0.26	0.06	12.49	3.86	0.50	0.10	32.18	6.95	81.37	3.07	125.83	3.24	185.64	19.24	-	-
rah19	0.26	0.07	12.41	4.11	0.57	0.02	37.02	1.23	77.20	12.26	135.76	14.54	219.11	13.98	-	-
rah20	0.25	0.05	12.36	3.16	1.48	0.06	97.63	3.67	83.85	8.66	144.63	13.73	188.24	21.23	-	-
rah21	0.25	0.07	12.30	4.21	0.69	0.02	45.36	1.30	71.08	10.86	146.58	14.93	168.16	35.40	strong	-
rah22	0.24	0.07	11.57	4.29	0.74	0.03	48.49	1.84	118.09	6.14	278.20	13.82	342.96	10.84	strong	-
rah23	0.24	0.03	11.34	1.94	0.49	0.00	31.63	0.23	63.81	10.56	158.47	13.25	132.46	5.84	-	R,H
rah24	0.23	0.02	11.17	0.92	0.56	0.05	36.40	3.57	77.02	18.33	107.74	8.51	206.47	40.60	-	-
rah25	0.23	0.02	10.72	1.41	0.56	0.08	36.31	5.60	76.58	14.11	120.15	11.38	158.12	4.11	-	R
rah26	0.23	0.03	10.67	1.89	0.59	0.03	38.65	1.97	89.70	8.68	159.71	11.61	218.74	15.14	-	-
rah27	0.23	0.06	10.63	3.83	n.d.	n.d.	n.d.	n.d.	69.93	11.39	110.40	11.21	160.72	36.46	weak	-
rah28	0.22	0.05	10.52	3.25	0.60	0.03	39.25	2.00	83.41	6.41	167.51	2.68	233.99	4.50	-	-
rah29	0.22	0.06	10.13	3.49	0.62	0.04	40.15	2.90	61.50	4.07	119.44	3.24	172.25	20.64	-	-
rah30	0.22	0.04	10.01	2.49	0.51	0.06	33.13	3.87	62.03	5.43	123.88	12.02	145.47	15.01	weak	-
rah31	0.21	0.02	9.70	1.20	0.51	0.02	33.09	1.32	76.40	5.65	153.86	4.06	197.17	22.29	weak	-
rah32	0.21	0.05	9.60	3.10	0.47	0.08	30.42	5.13	64.25	4.13	112.53	7.84	144.36	9.49	-	-
rah33	0.20	0.05	9.11	3.00	0.58	0.04	37.55	2.76	76.22	10.28	140.55	16.32	158.86	6.73	weak	-
rah34	0.20	0.02	9.05	1.33	0.83	0.07	54.48	4.70	75.60	7.17	169.11	13.19	265.98	14.63	-	-
rah35	0.20	0.01	8.79	0.54	0.69	0.10	45.25	6.74	72.94	7.53	202.81	34.41	187.13	6.06	-	R,H
rah36	0.19	0.02	8.56	1.14	1.17	0.17	76.97	10.98	70.55	4.33	143.57	24.39	175.60	49.25	-	-
rah37	0.19	0.03	8.30	1.93	0.52	0.08	33.60	5.49	81.72	13.88	189.15	31.38	282.71	41.29	-	-
rah38	0.19	0.03	8.26	1.74	0.58	0.10	37.83	6.92	58.09	6.59	132.93	16.44	126.51	4.46	-	-
rah39	0.19	0.02	8.19	0.98	0.67	0.06	43.75	3.70	66.82	4.95	144.63	12.62	162.58	4.28	-	-
rah40	0.18	0.02	8.05	1.22	0.57	0.07	37.44	4.34	82.79	24.17	160.95	10.76	186.38	10.10	-	-
rah41	0.18	0.02	7.98	1.34	0.94	0.03	61.65	2.26	57.24	4.69	126.72	22.35	180.06	5.11	-	-
rah42	0.18	0.00	7.98	0.01	0.54	0.07	35.45	4.82	58.66	18.04	130.09	12.27	141.75	5.08	-	-
rah43	0.18	0.03	7.92	1.79	0.55	0.09	35.74	6.09	59.90	4.04	145.34	6.14	153.28	10.99	strong	-
rah44	0.18	0.03	7.76	1.94	0.68	0.02	44.57	0.99	81.63	4.13	114.30	3.25	150.68	18.42	-	-
rah45	0.18	0.01	7.74	0.38	0.64	0.01	41.76	0.58	65.93	1.86	151.02	10.51	185.64	11.72	-	R,H,C
rah46	0.18	0.06	7.66	3.44	0.80	0.05	52.51	3.22	73.47	20.18	165.74	25.09	150.31	10.60	weak	-
rah47	0.18	0.02	7.65	1.30	0.77	0.07	50.44	4.87	84.47	2.97	138.60	10.19	163.33	8.52	-	-
rah48	0.18	0.03	7.62	1.98	1.36	0.31	89.46	20.78	89.79	1.11	193.77	18.30	191.96	14.93	-	R
rah49	0.18	0.04	7.58	2.52	0.93	0.15	61.25	10.19	79.86	9.37	171.59	14.08	267.84	47.58	-	-
rah50	0.17	0.02	7.49	1.27	0.88	0.11	57.63	7.32	77.55	11.05	171.95	9.37	136.55	14.56	-	-
rah51	0.17	0.02	7.47	1.42	0.82	0.12	53.99	8.14	81.55	4.56	143.21	18.01	180.43	20.91	weak	-
rah52	0.17	0.06	7.40	3.72	0.46	0.09	29.87	5.74	78.09	5.81	127.43	3.49	212.05	4.44	-	-
rah53	0.17	0.01	7.31	0.74	0.47	0.04	30.33	2.91	43.58	21.79	125.83	9.94	123.16	3.59	strong	-
rah54	0.17	0.02	7.30	1.22	0.68	0.09	44.50	6.08	81.63	12.37	121.40	4.53	157.00	3.46	-	-
rah55	0.17	0.02	7.30	1.21	0.54	0.03	34.92	2.16	73.30	15.05	177.45	19.34	177.46	27.59	-	-
rah56	0.16	0.05	6.56	2.81	0.54	0.18	35.10	11.68	87.58	10.61	116.96	17.94	164.81	4.15	-	-
rah57	0.16	0.04	6.46	2.17	0.54	0.04	35.03	2.70	46.87	3.78	123.35	12.89	138.04	15.30	-	-
rah58	0.15	0.02	6.16	1.21	0.74	0.07	34.92	2.16	68.77	4.23	143.75	11.24	118.70	9.02	-	-
rah59	0.15	0.01	5.80	0.82	0.81	0.05	52.80	3.48	71.35	22.63	148.71	21.89	209.44	8.00	-	-
rah60	0.14	0.02	5.59	1.38	1.04	0.06	68.47	4.06	92.81	9.01	144.99	17.64	238.08	12.93	strong	-
rah61	0.14	0.01	5.20	0.50	0.57	0.09	37.26	5.92	105.94	20.43	145.52	23.18	184.15	1.68	-	-
rah62	0.13	0.04	4.92	2.68	0.69	0.08	44.96	5.39	77.47	1.71	147.29	21.18	157.00	7.45	weak	-
rah63	0.13	0.03	4.90	1.66	0.65	0.02	42.34	1.07	79.42	7.09	194.12	6.17	259.28	6.73	-	R

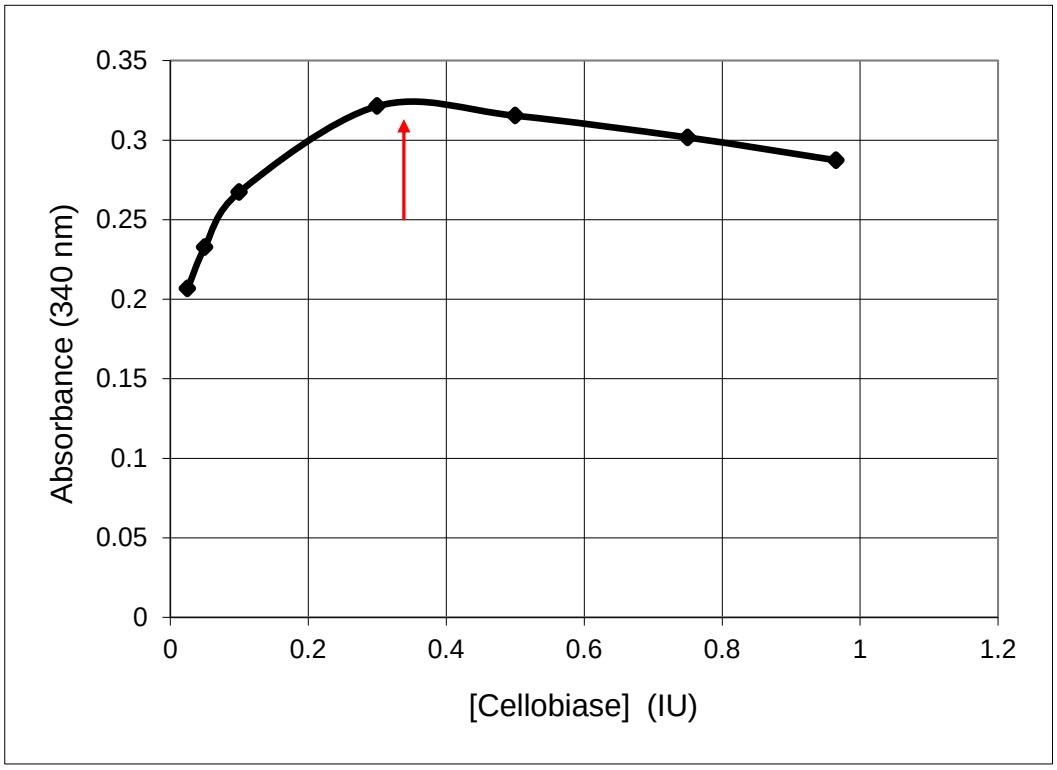

Figure 3.2.2S1: Cellobiase optimization curve. The optimal amount of cellobiase was determined using 5 mg of senesced stem *Col-0* tissue and 0.075 FPU of cellulase in a 200 µL reaction volume. By this method 60-80 IU of cellobiase was found to be optimal with 15 FPU per gram of tissue (red arrow). Absorbance at 340 nm correlates with glucose concentrations using the HK method (see Figure 3.2.2S2).

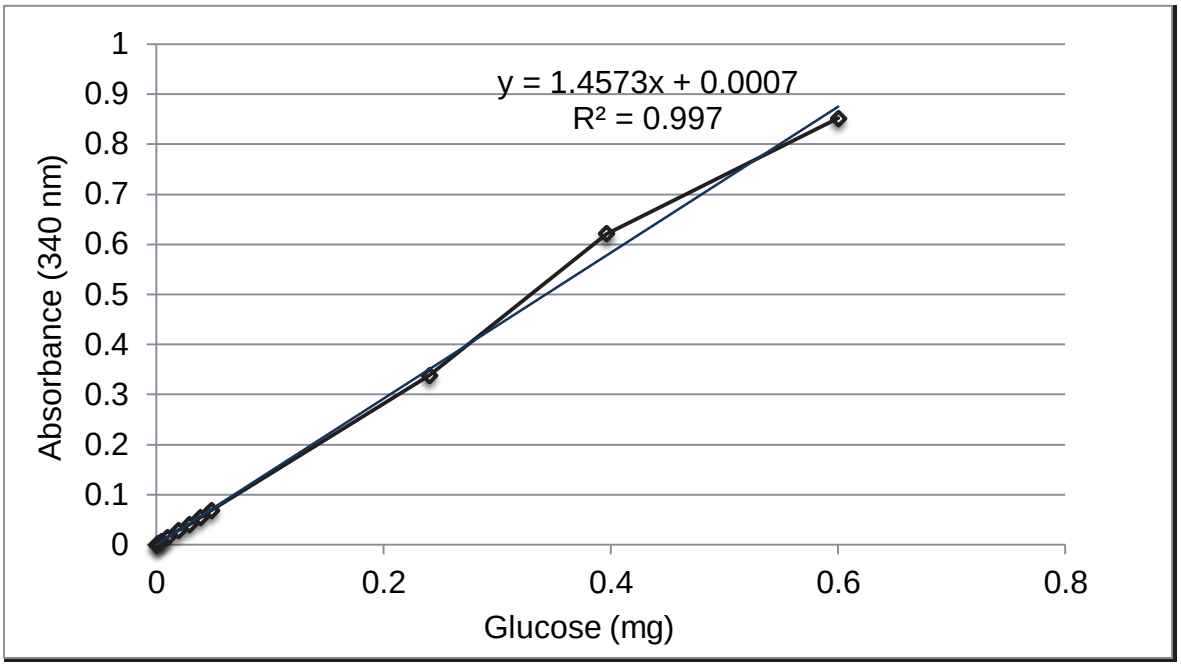

Figure 3.2.2S2: Standard for glucose detection using the HK method. Absorbance was taken at 340 nm of well volumes of 120 µL. The effective detectable concentration range was determined to be 0.01 mg/mL to 10 mg/mL.

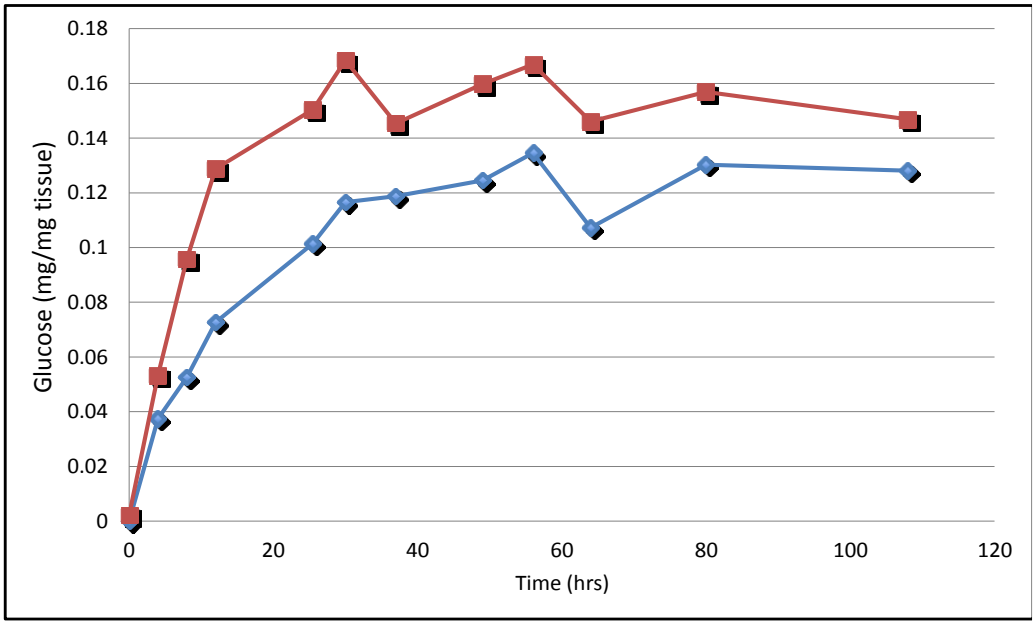

Figure 3.2.3S1: Time course cellulase digestion of *rah9* compared to wild-type. Five milligrams of senesced stem tissue from *rah9* (red) and *Col-0* (blue) were treated with 0.1 FPU of cellulase and 1.2 IU of cellobiase in a final volume of 0.5 mL. Values are expressed as milligrams of glucose released per milligram of tissue. Glucose concentrations were determined by the HK method.

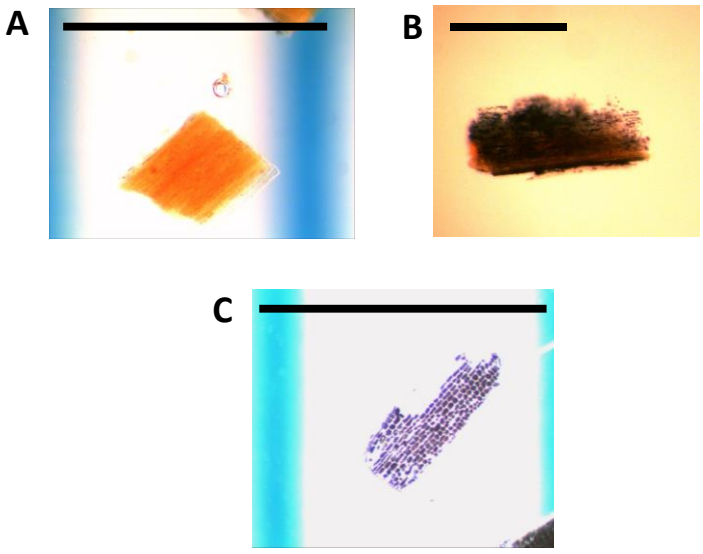

Figure 3.2.3S2: Lugol staining of washed senesced stem tissue of *rah9*.

A) Senesced stem tissue of *Col-0* displays no staining and tests negative for starch (bar = 1 mm).

B) RAH9 stem tissue drastically accumulates starch and stains heavily with Lugol (bar = 1 mm).

C) The epidermal layerof the stem tissue is the source of the staining in RAH9 (bar = 1 mm).

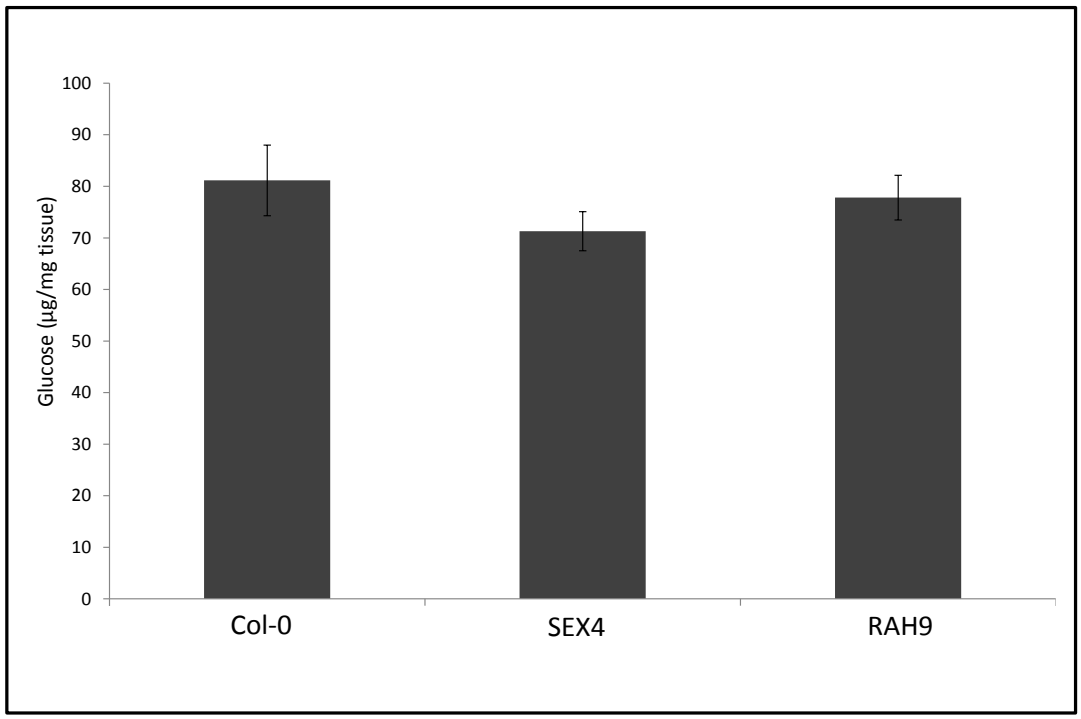

Figure 3.2.3S3: Cellulase digestion of post-amylase treated senesced stem tissue. Sugars released after cellulase digestion following amylase pre-treatment from *rah9*, *sex4* and wild-type. Values are averages of glucose expressed in micrograms per milligram of tissue +/- standard deviation (n = 3). Sugars were quantified using the HK method.

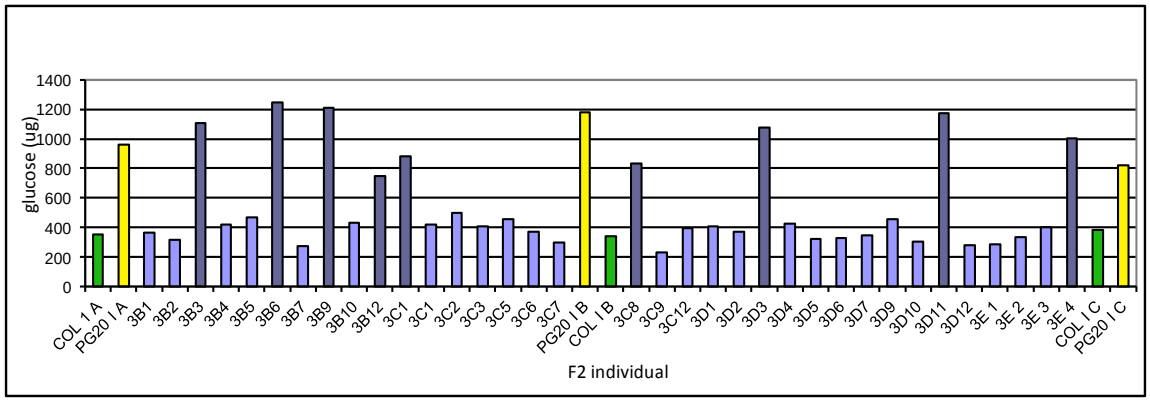

Figure 3.2.3S4: Phenotyping the *rah9* mapping population. The mapping population of *rah9*;*Ler* F2s are screened for enhanced saccharification under the enzymatic digestion schemes. Negative and positive controls of wild-type and *rah9* (denoted as PG20) are the green and yellow bars respectively. The dark purple bars are hits and their DNA was be pooled for bulk segregant analysis (Figure 3.2.3A-B). Amongst the mapping population 49/224 displayed the rah9 saccharification phenotype. The observed frequency is not a significant deviation from the expected Mendelian segregation ratio for recessive alleles in the F2 generation of a monohybrid cross (p = 0.28 using *chi*-squared test). Values are expressed as micrograms of glucose released per 5 milligrams of tissue determined by the HK method.

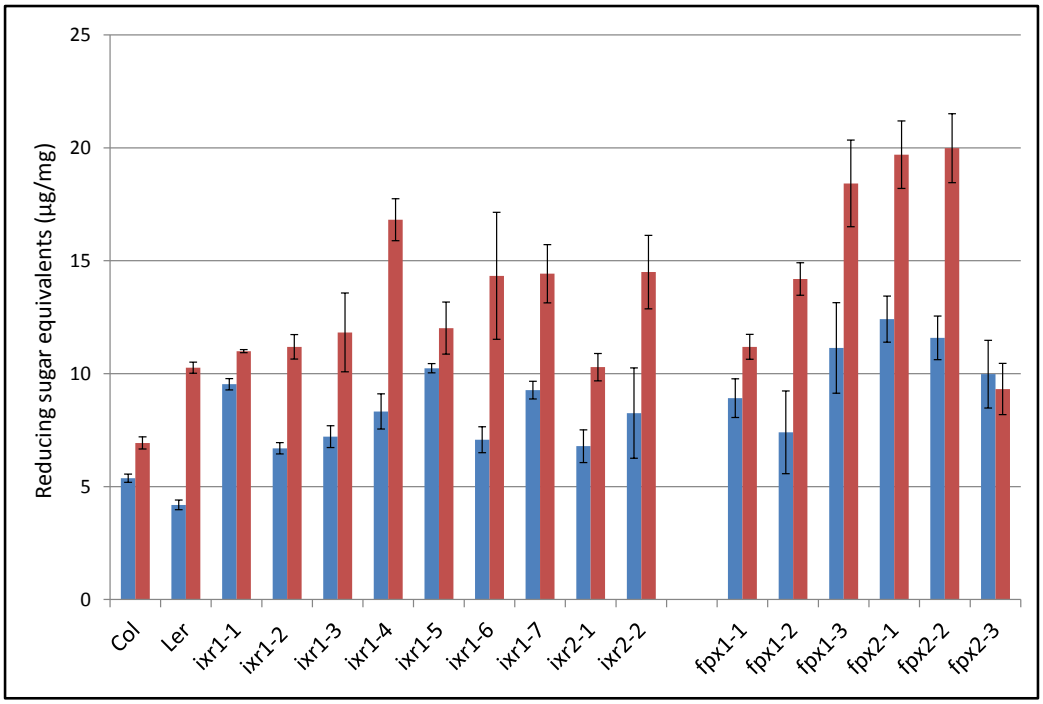

Figure 3.2.8S1: Sugar relased by water maceration from *ixr* and *fxr* tissue. Chloroform-methanol washed 28 DAG *Arabidopsis* tissue treated with 5 µM NPA (red bars) and without (blue bars). Values are averages +/- standard deviation (n = 3). Sugar content was determined with 0.2% anthrone and is expressed as micrograms of reducing sugar equivalents per milligram of tissue.

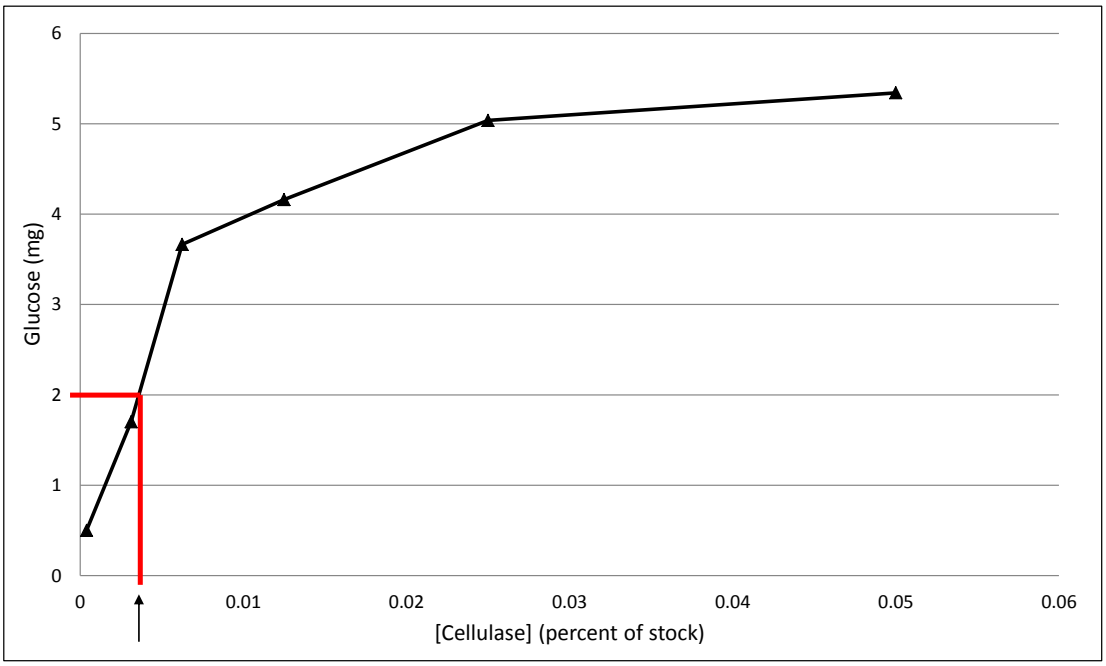

Figure 3.3.4S1: Determination of cellulase titre using the Filter Paper Assay. Fifty milligrams of Whatman #1 filter paper cut into 1. 0 x 6. 0 cm strips were digested by a series of enzyme dilutions for 60 minutes in 0.5 mL final. One FPU is defined as the dilution which releases 2 mg of glucose under these conditions (red line) (Ghose 1987). A dilution factor of 3.33×10^{-3} released the desired 2 mg of glucose in one hour (arrow). This corresponds to an activity of 110.9 FPU/mL for the undiluted enzyme stock.

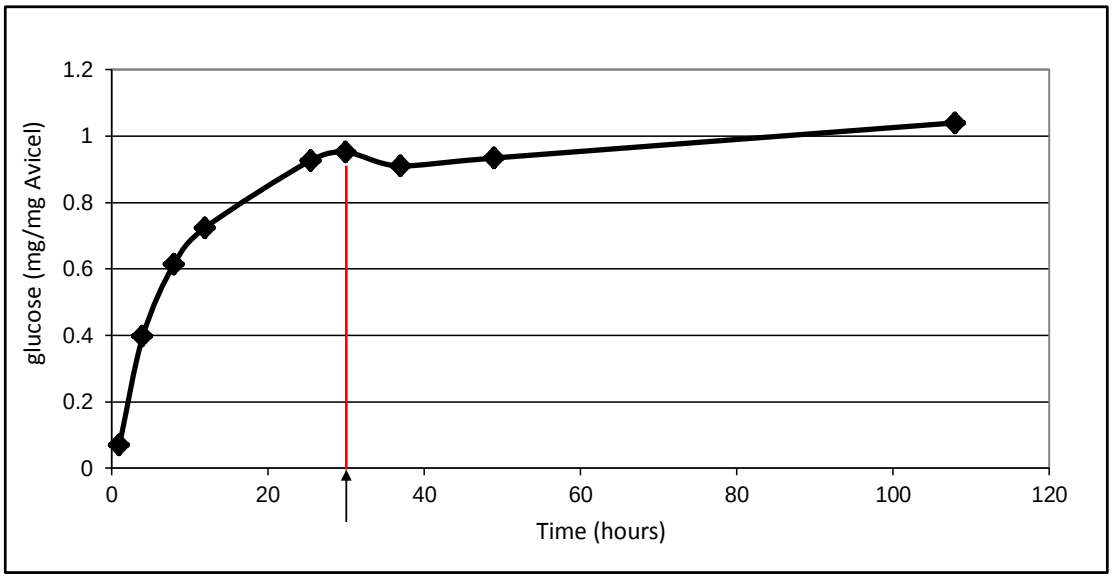

Figure 3.3.4S2 Cellulase incubation time optimization. Ten milligrams of Avicel cellulose was incubated with 0.1 FPU of cellulase and 1.2 IU of cellobiase. More than 95% of the cellulose was converted into glucose within 25 hours (arrow). Values are expressed in milligrams of glucose released per milligram of Avicel determined by the HK method.

References

1) Aloni, Y., Delmer, D. P., Benziman, M. (1982) "Achievement of high rates of in vitro synthesis of 1,4-β-glucan: activation by cooperative interaction of the *Acetobacter xylinum* enzyme system with GTP, polyethylene glycol, and a protein factor". *Proceedings of the National Academy of Sciences USA* 79:6448-6452

2) Arioli, T., Peng, L., Betzner, A. S., Burn, J., Wittke, W., Herth, W., Camilleri, C., Hofte, H., Plzinski, J., Birch, R., Cork, A., Glover, J., Redmond, J., Williamson, R. E. (1998) "Molecular Analysis of Cellulose Biosythesis in *Arabadopsis"*. *Science* 279(5351): 717-720

3) Austin, R. S., Vidaurre, D., Stamatiou, G., Breit, R., Provart, N., Bonetta, D., Zhang, J., Fung, P., Gong, Y. (2011) "Next-generation mapping of *Arabidopsis* genes". *The Plant Journal* 67(4) 715-725

4) Barratt, D. H. P., Derbyshire, P., Findlay, K., Pike, M., Wellner, M., Lunn, J., Feil, R., Simpson, C., Maule, A., Smith, A. M. (2009)"Normal growth of Arabidopsis plants requires cytosolic invertase but not sucrose synthase". *Proceedings of the National Academy of Sciences USA* 106: 13124-13129

5) Bernasconi, P., Patel, B. C., Reagan, J. D., Subramanian, M. V. (1996) "The N-1-Naphthylphthalamic Acid-Binding Protein Is an Integral Membrane Protein". *Plant Physiology* 111(2): 427-432

6) Bischoff, V., Cookson, S. J., Wu, S., Scheible, W. (2009)" Thaxtomin A affects CESA-complex density, expression of cell wall genes, cell wall composition, and causes ectopic lignification in *Arabidopsis thaliana* seedlings". *Journal of Experimental Botany* 60(3): 955-965

7) Cannon, M. C., Terneus, K., Hall, Q., Tan, L., Wang, Y., Wegenhart, B. L., Chen, L., Lamport, D. T. A., Chen, Y., Kieliszewski, M. J. (2008) "Self-assembly of the plant cell wall requires an extensin scaffold". *Proceedings of the National Academy of Science USA* 105: 2226–2231

8) Carpita, N., McCann, M., Buchanan, B. ed., Gruissem, W., Jones, R. ed. (2000) "Biochemistry and Molecular Biology of Plants". Chapter 2: The Cell Wall, pp. 52-108. *American Society of Plant Physiologists*. New Jersey, USA

9) Carroll, A., Mansoori, N., Li, S., Lei, L., Vernhettes, S., Visser, R. G. F., Somerville, C., Gu, Y., Trindade, L. M. (2012) "Complexes with Mixed Primary and Secondary Cellulose Synthases Are Functional in Arabidopsis Plants". *Plant Physiology* 160:726-737

10) Carroll, A and Somerville, C. (2009) "Cellulosic Biofuels". *Annual Review of Plant Biology* 60: 165-182

11) Charnock, S. J. and Davies, G. (1999) "Structure of the Nucleotide-Diphospho-Sugar Transferase, SpsA from *Bacillus subtilis*, in Native and Nucleotide-Complexed Forms". *Biochemistry* 38(20): 6380-6385

12) Charnock, S. J., Henrissat, B., Davies, G. (2001) "Three-Dimensional Structures of UDP-Sugar Glycosyltransferase Illuminate the Biosynthesis of Plant Polysaccharides". *Plant Physiology* 125:527-531

13) Chen, S., Ehrhardt, D. W., Somerville, C. R. (2010) "Mutations of cellulose synthase (CESA1) "Phosphorylation sites modulate anisotropic cell expansion and bidirectional mobility of cellulose synthase". *Proceedings of the National Academy of Sciences USA* 107(40): 17188-17193

14) Christensen, S. K., Dagenais, N., Chory, J., Weigel, D. (2000) "Regulation of auxin response by the protein kinase PINOID". *Cell* 100: 469–478

15) Cosgrove, D. J. (2000) "Loosening of plant cell walls by expansins". *Nature* 407: 321-326

16) Delmer, D. P. (1999) "Cellulose Biosynthesis: Exciting Times for a Difficult Field of Study". *Annual Reviews of Plant Physiology Plant Molecular Biology* 50: 245-276

17) Desnos, T., Orbovic, V., Bellini, C., Kronenberger, J., Caboche, M., Traas, J., Hofte, H. (1996) "*Procuste1* mutants identify two distinct genetic pathways controlling hypocotyl cell elongation, respectively in dark- and light-grown *Arabidopsis* seedlings". *Development* 122: 683-693

18) Desprez, T., Juraniec, M., Crowell, E. F., Jouy, H., Pochylova, Z., Parcy, F., Hofte, H., Gonneau, M., Vernhettes, S. (2007) "Organization of cellulose synthase complexes involved in primary cell wall synthesis in *Arabidopsis thaliana*". *Proceedings of the National Academy of Sciences USA* 104(39): 15572-15577

19) Desprez, T., Vernhettes, S., Fagard, M., Refregier, G., Desnos, T. Aletti, E., Py, N., Pelletier, S., Hofte, H. (2002) "Resistance against Herbicide Isoxaben and Cellulose Deficiency Caused by Distinct Mutations in Cellulose Synthase Isoform CESA6". *Plant Physiology* 128: 482-490

20) Dische, Z., Whistler, R. L. ed., Wolfrom, M. L. ed. (1962) "Color reaction of carbohydrates". pp 477-512 *Academic Press.* New York, USA

21) Doblin, M. S., Kurek, I., Jacob-Wilk, D., Delmer, D. (2002)" Cellulose Biosynthesis in Plants: from Genes to Rosettes". *Plant Cell Physiology* 43(12): 1407-1420

22) Eicher, T., Hauptmann, S. (2003) "The Chemistry of Heterocycles: Structures, Reactions, Synthesis, and Applications" Section 5. 26 Isoxazole, pp. 138. *Wiley*. Weinheim, Germany

23) European Food Safety Committee (2010) "Conclusion on the peer review of the pesticide risk assessment of the active substance isoxaben". *EFSA Journal 2010* 8(9):1714

24) Favery, B., Rtan, E., Fireman, J., Linstead, P., Boudonck, K., Steer, M. m Shaw, P., Dolan, L. (2001) "KOJAK encodes a cellulose synthase-like protein required for root hair cell morphogenesis in *Arabidopsis*". *Genes and Development* 15: 79-89

25) Fagard, M., Desnos, T., Desprez, T., Goubet, F., Refregier, G., Mouille, G., McCann, M., Rayon, C., Vernhettes, S., and Hofte, H. (2000) "PROCUSTE1 encodes a cellulose synthase required for normal cell elongation specifically in roots and dark-grown hypocotyls of Arabidopsis". *Plant Cell* 12: 2409–2424

26) Feraru, E., Feraru, M. I., Kleine-Vehn, J., Martinière, A., Mouille, G., Vanneste, S., Vernhettes, S., Runions, J., Frimi, J. (2011) "PIN polarity Maintenance by the Cell Wall in *Arabidopsis*" *Current Biology* 21: 338-343

27) Festucci-Buselli, R. M., R. A., Otoni, W. C., Joshi, C. P. (2007) "Structure, organization, and functions of cellulose synthase complexes in higher plants". *Brazilian Journal of Plant Physiology* 19(1): 1-13

28) Friml, J., Yang, X., Michniewicz, M., Weijers, D., Quint, A., Tietz, O., Benjamins, R., Ouwerkerk, P. B., Ljung, K., Sandberg, G., Hooykaas, P. J., Palme, K., Offringa, R. (2004) "A PINOID-dependent binary switch in apical-basal PIN polar targeting directs auxin efflux". *Science* 306: 862-865

29) Fujii, S., Hayashi, T., Mizuno, K. (2010) "Sucrose Synthase is an Integral Component of the Cellulose Synthesis Machinery". *Plant and Cell Physiology* 51(2): 294-301

30) Gälweiler, L., Guan, C., Müller, A., Wisman, E., Mendgen, K., Yephremov, A., Palme, K. (1998) "Regulation of polar auxin transport by AtPIN1 in Arabidopsis vascular tissue". *Science* 282: 2226-2230

31) Ghose, T. K. (1987) "Measurement of cellulase activities". *Pure and Applied Chemistry* 59: 257–268

32) Harris, D. M., Corbin, K., Wang, T., Gutierrez, R., Bertolo, A. L., Tetti, C., Smilgies, D., Estevez, J. M., Bonetta, D., Urbanowicz, B. R., Ehrhardt, D. W., Somerville, C., Rose, J. K. C., Hong, M., Debolt, S. (2012) "Cellulose microfibril crystallinity is reduced by mutating C-terminal transmembrane region residues CESA1^{A903V} and CESA3^{T942I} of cellulose synthase". *Proceedings of the National Academy of Sciences USA* 109(11): 4098-4103

33) Harris, D., Stork, J., Debolt, S. (2009) "Genetic modification in cellulose-synthase reduces crystallinity and improves biochemical conversion to fermentable sugar". *Global Change Biology Bioenergy* 1(1): 51-61

34) Hartwell, L. H., Hood, L., Goldberg, M. L., Reynolds, A. E., Silver, L. M., Veres, R. C. (2008) "Genetics: From Genes to Genomes 3rd edition". Chapter 11: The Direct Detection of Genotype Distinguishes Individual Genomes, pg 396-397. *McGraw Hill*. New York, USA

35) Hauser, M., Morikami, A., Benfy, P. (1995) "Conditional root expansion mutants of *Arabidopsis*". *Development* 121: 1237-1252

36) Heim, D. R., Skomp, J. R., Tschabold, E. E., Larrinua, I. M. (1989) "Isoxaben Inhibits the Synthesis of Acid Insoluble Cell Wall Materials in *Arabidopsis thaliana*". *Plant Physiology* 96: 695-700

37) Heisler, M. G., Hamant, O., Krupinski, P., Uyttewaal, M., Ohno, C., Jonsson, H., Traas, J., Meyerowitz, E. M. (2010) "Alignment between PIN1 Polarity and Microtubule Orientation in the Shoot Apical Meristem Reveals a Tight Coupling between Morphogenesis and Auxin Transport". *PLoS Biol* 8(10): e1000516

38) Hejazi, M., Fettke, J., Kotting, O., Zeeman, S. C., Steup, M. (2010) "The Laforin-Like Dual-Specificity Phosphatase SEX4 from Arabidopsis Hydrolyzes Both C6- and C3-Phosphate Esters Introduced by Starch-Related Dikinases and Thereby Affects Phase Tracsition of α-Glucans". *Plant Physiology* 152: 711-722

39) Hematy, K., Sado, P., Tuinen, A. V., Rochange, S., Desnos, T., Balzergue, S., Pelletier, S., Renou, J., Hofte, H. (2007) "A Receptor-like Kinase Mediates the Response of Arabidopsis Cells to the Inhibition of Cellulose Synthesis". *Current Biology* 17: 922-931

40) Holland, N., Holland, D., Helentjaris, T., Dhugga, K. S., Xoconostle-Cazares, B., Delmer, D. P. (2000) "A Comparative Analysis of the Plant Cellulose Synthase (*cesA*) Gene Family". *Plant Physiology* 123: 1313-1323

41) Huang, F., Zago, M. K., Abas, L., Marion, A., Galvan-Ampudia, C. S., Offringa, R. (2010) "Phosphorylation of Conserved PIN Motifs Directs *Arabidopsis* PIN1 Polarity and Auxin Transport". *The Plant Cell* 22: 1129-1142

42) Jing, W. and DeAngelis, P. L. (2000) "Dissection of the two transferase activities of the Pasteurella multocida hyaluronan synthase: two active sites exist in one polypeptide". *Glycobiology* 10(9): 883-889

43) Kaida, R., Satoh, Y., Bulone, V., Yamada, Y., Kaku, T., Hayashi, T., Kaneko, T. S. (2009) "Activation of β-Glucan Synthases by Wall-Bound Purple Acid Phosphatase in Tobacco Cells". *Plant Physiology* 150: 1822-1830

44) Katekar, G. F. and Geissler, A. E. (1980) "Auxin Transport Inhibitors IV. EVIDENCE OF A COMMON MODE OF ACTION FOR A PROPOSED CLASS OF AUXIN TRANSPORT INHIBITORS: THE PHYTOTROPINS". *Plant Physiology* 66:1190-1195

45) Kim, Y., Schumaker, K. S., Zhu, J. (2005) "EMS Mutagenesis of *Arabidopsis*". *Methods in Molecular Biology* 323: 101-103

46) Kötting, O., Santelia, D., Edner, C., Eicke, S., Marthaler, T., Gentry, M. S., Comparot-Moss, S., Chem, J., Smith, A. M., Steup, M., Ritte, G., Zeeman, S. C. (2009) "STARCH-EXCESS4 Is a Laforin-Like Phosphoglucan Phosphatase Required for Starch Degradation in *Arabidopsis thaliana*". *The Plant Cell* 21: 334-346

47) Krecek, P., Skupa, P., Libus, J., Naromoto, S., Tejos, R., Friml, J., Zazimalova, E. (2009) "The PIN-FORMED (PIN) protein family of auxn transporters". *Genome Biology* 10: 249. 1-249. 11

48) Kurek, I., Kawagoe, Y., Jacob-Wilk, D., Doblin, M., Delmer, D. (2002) "Dimerization of cotton fiber cellulose synthase catalytic sub-units occurs via oxidation of the zinc-binding domains". *Proceedings of the National Academy of Sciences USA* 99: 11109-11114

49) Koyama, M., Helbert, W., Imai, R., Sugiyama, J., Henrissat, B. (1997) "Parallel-up structure evidences the molecular directionality during biosynthesis of bacterial cellulose". *Proceedings of the National Academy of Science USA* 94: 9091-9095

50) Laibach, F. (1965) "60 Jahre Arabidopsis-Forschung, 1905-1965". AIS Vol. 1 Supplement. Available at www.arabidopsis.org /ais/1965/laiba-1965-aagle. html

51) Lamport, D. T. A., Miller, D. H. (1971) "Hydroxyproline Arabinosides in the Plant Kingdom". *Plant Physiology* 48: 454-456

52) Lamport, D. T. A. (1973) "The glycopeptide linkages of extensin, O-D-galactosyl serine and O-L-arabinosyl hydroxyproline". Biogenesis of plant cell wall polysaccharides. Pp 149-164. *Academic Press Inc*., New York, USA

53) Leloir, L. F. (1971) "Two Decades of Research on the Biosynthesis of Saccharides". *Science* 172(3990): 1299-12303

54) Li, X., Weng, J., Chapple, C. (2008) "Improvement of biomass through lignin modification". *The Plant Journal* 54: 569-581

55) Lin, F. C., Brown, R. M. Jr., Scheurch, C. ed. (1989) "Cellulose and Wood-Chemistry and Technology". Purification of cellulose synthase from *Acetobacter xylinum*. pp. 473-492 *Wiley*. New York, USA

56) Lin, F. C., Brown, R. M. Jr., Drake, R. R. Jr., Haley, B. E. (1990) "Identification of the uridine-5`-diphosphoglucose (UDP-glc) binding subunit of cellulose synthase in *Acetobacter xylinum* using the photoaffinity probe 5-azido-UDP-glc". *Journal of Biological Chemistry* 265: 4782-4784

57) Lodish, H., Berk, A., Zipursky, SL. et al. (2000) "Molecular Cell Biology. 4th edition" Section: 22.5 The Dynamic Plant Cell Wall. *W. H. Freeman*. New York, USA. Available from: http://www. ncbi.nlm.nih. gov/books/NBK21709

58) Lukowitz, W., Gillmor, C. S., Scheible, W. (2000) "Positional Cloning in *Arabidopsis*. Why It Feels Good to Have a Genome Initiative Working for you". *Plant Physiology* 123 795-805

59) Mandenius, C. F., Nilsson, B., Persson, I., Tjerneld, F. (1987) "Kinetic models for enzymatic cellulose degradation in aqueous two-phase systems". *Biotechnology and Bioengineering* 31(3): 203-207

60) McMurry, J. (2000) "Organic Chemistry 5th Edition". Chapter 25: Biomolecules: Carbohydrates, pp 1030-1072. *Brooks/Cole*. TOR, CAN

61) McQueen-Mason, S., Durachko, D. M., Cosgrove, D. J. (1992) "Two endogenous proteins that induce cell wall expansion in plants". *Plant Cell* 4: 1425–1433

62) McSteen, P., Malcomber, S., Skirpan, A., Lunde, C., Wu, X., Kellogg, E., Hake, S. (2007) "Barren inflorescence2 Encodes a Co-Ortholog of the PINOID Serine/Threonine Kinase and Is Required for Organogenesis during Inflorescence and Vegetative Development in Maize". *Plant physiology* 144(2): 1000-1011

63) Michniewicz, M., Zago, M. K., Abas, L., Weijers, D., Schweighofer, A., Meskiene, I., Heisler, M. G., Ohno, C., Zhang, J., Huang F., Schwab, R., Weigel, D., Meyerowitz, E. M., Luschnig, C., Offringa, R., Friml, J. (2007) "Antagonistic regulation of PIN phosphorylation by PP2A and PINOID directs auxin flux". *Cell* 130:1044-1056

64) Mohnen, D., Bar-Peled, M., Somerville, C. editor Himmel, M. E. (2008) "Biomass Recalcitrance: Deconstructing the Plant Cell Wall for Bioenergy", Chapter 5: Cell Wall Polysaccharide Synthesis, pp. 94-159. *Blackwell publishing*. London, UK

65) Morgan, J. L. W., Strumillo, J., Zimmer, J. (2012) "Crystallographic snapshot of cellulose synthesis and membrane translocation". *Nature* 493:181-187

66) Mravec, J., Skůpa, P., Bailly, A., Hoyerová, K., Křeček, P., Bielach, A., Petrášek, J., Zhang, J., Gaykova, V., Stierhof, Y., Dobrev, P. I., Schwarzerová, K., Rolčík, J., Seifertová, D., Luschnig, C., Benková,. E., Zažímalová, E., Geisler, M., Friml, J. (2009) "Subcellular homeostasis of phytohormone auxin is mediated by the ER-localized PIN5 transporter". *Nature* 459:1136-1140

67) Mueller, S. C., Brown, R. M. Jr. (1980) "Evidence for an intramembrane component associated with a cellulose microfibril synthesizing complex in higher plants". *Journal of Cell Biology* 84: 315-326

68) Murray, M. G., Thompson, W. F. (1980) "Rapid isolation of high-molecular-weight plant DNA". *Nucleic Acids Research* 8: 4321-4325.

69) Nagahashi, S., Sudoh, M., Ono, N., Sawada, R., Yamaquchi, E., Uchida, Y., Mio, T., Takagi, M. m Arisawa, M., Yamada-Okabe, H. (1995) "Characterization of chitin synthase 2 of *Saccharomyces cerevisiae*. Implication of two highly conserved domains as possible catalytic sites". *Journal of Biological Chemistry* 270(23): 13961-13967

70) Nicol, F., His, I., Jaunear, A., Vernhettes, S., Canut, H., Hofte, H. (1998) "A plasma membrane-bound putative endo-1-4-β-D-glucanase is required for normal wall assembly and cell elongation in *Arabidopsis*". *The EMBO Journal* 17: 5563-5576

71) Nuhse, T. S., Stensballe, A., Jensen, O. N., Perk, S. C. (2004) "Phosphoproteomics of *Arabidopsis* plasma membrane and a new phosphorylation site database". *The Plant Cell* 16(9): 2394-2405

72) Okada, K., Ueda, J., Komaki, M. K., Bell, C. J., Shimura, Y. (1991) "Requirement of the Auxin Polar Transport System in Early Stages of Arabidopsis Floral Bud Formation". *Plant Cell* 3: 677–684

73) Park, S., Szumlanski, A. L., Gu, F., Guo, F., Nielsen, E. (2011) "A role for CSLD3 during cell-wall synthesis in apical plasma membranes of tip-growing root-hair cells". *Nature cell biology* 13: 973-980

74) Persson, S., Paredez, A., Carroll, A., Palsdottir, H., Doblin, M., Poindexter, P., Khitrov, N., Auer, M., Somerville, C. (2007) "Genetic evidence for three unique components in primary cell-wall cellulose synthase complexes in *Arabidopsis*". *Proceedings of the National Academy of Sciences USA* 104(39): 15566-15571

75) Przemeck, G. K., Mattsson, J., Hardtke, C. S., Sung, Z. R., Berleth, T. (1996) "Studies on the role of the *Arabidopsis* gene MONOPTEROS in vascular development and plant cell axialization". *Planta* 200: 229–237

76) Rath, V. L., Ammirati, M., Danley, D. E., Ekstrom, J. L., Gibbs, E. M., Hynes, T. R., Mathiowetz, A. M., Mcpherson, R. K., Olson, T. V., Treadway, J. L., Hoover, D. J. (2000) "Human liver glycogen phosphorylase inhibitors bind at a new allosteric site". *Chemical Biology* 7(9): 677-82

77) Rayle, D. L., Cleland, R. E. (1992) "The Acid Growth Theory of Auxin-Induced Cell Elongation Is Alive and Well". *Plant Physiology* 99: 1271-1274

78) Rédei, G. P. (1992) "A heuristic glance at the past of Arabidopsis genetics". Koncz, C., N. H. Chua and J. Schell (ed.) pp 1-15. *Methods in Arabidopsis Research*. World Scientific, New Jersey, USA

79) Reiter, W. D., Chapple, C, Somerville, C. R. (1997) "Mutants of Arabidopsis thaliana with altered cell wall polysaccharide composition". *Plant Journal* 12: 335–345

80) Richmond, T. A. and Somerville, C. R. (2000) "The Cellulose Synthase Superfamily". *Plant Physiology* 124: 495-498

81) Roudier, F., Fernandez, A. G., Fujita, M., Himmelspach, R., Bomer, G. H. H., Schindelman, G., Song, S., Baskin, T. I., Dupree, P., Wasteneys, G. O., Benfey, P. N. (2005) "COBRA, an *Arabidopsis* Extracellular Glycosylphosphatidylinsitol-Anchored Protein, Specifically Controls Highly Anisotropic Expansion through Its Involvement in Cellulose Microfibril Orientation". *The Plant Cell* 17: 1749-1763

82) Rundle, R. E., French, D. (1943) "The Configuration of Starch and the Starch-Iodine Complex. II. Optical Properties of Crysatlline Starch Fractions". *Journal of the American Chemical Society* 65(4):558-561

83) Sánchez-Rodríguez, C., Bauer, S., Hematy, K., Saxe, F., Ibanez, A. B., Vodermaier, V., Konlechner, C., Sampathkumar, A., Ruggeberg, M., Aichinger, E., Neumetzler, L., Burgert, I., Somerville, C., Hauser, M., Persson, S. (2012) "CHITINASE-LIKE1/POM-POM1 and Its Homolog CTL2 Are Glucan-Interacting Proteins Important for Cellulose Biosynthesis in *Arabidopsis*". *The Plant Cell* 24(2): 589-607

84) Saxena I. M., Brown R. M. Jr., Fevre M., Geremia R. A., Henrissat B. (1995) "Multidomain architecture of b-glycosyl transferases: implications for mechanism of action". *Journal of Bacteriology* 177: 1419–1424

85) Saxena, I. M. and Brown, R. M. Jr. (1997) "Identification of cellulose synthase(s) in higher plants: Sequence analysis of processive β-glycosyltransferases with the common motif "D,D,D35Q(R,Q)XRW"". *Cellulose* 4: 33-49

86) Saxena, I. M., Brown, R. M. Jr., Dandekar, T. (2001) "Structure-function characterization of cellulose synthase: relationship to other glycosyltransferases". *Phytochemistry* 57: 1135-1148

87) Saxena, I. M., Brown, M. Jr. (2005) "Cellulose Biosynthesis: Current views and Evolving Concepts". *Annals of Botany* 96: 9-21

88) Scheible, W., Eshed, R., Richmond, T., Delmer, D., Somerville, C. (2001) "Modifications of cellulose synthase cofer resistance to isoxaben and thiaxolidinone herbicides in *Arabidopsis* Ixr1 mutants". *Proceedings of the National Academy of Sciences USA* 98(18): 10079-10084.

89) Scheller, H. V. and Ulvskov, P. (2010) "Hemicellulose". *Annual Reviews of Plant Biology* 61:263-289

90) Schoemaker, H. E., Piontek, K. (1996) "On the interaction of lignin peroxidase with lignin". *International Union of Pure and Applied Chemistry* 68(11): 2089-2096

91) Segal, L., Creely, J. J., Martin, A. E. Jr., Conrad, C. M. (1959) "An Empirical Method for Estimating the Degree of Crystallinity of Native Cellulose Using the X-Ray Diffractometer". *Textile Research Journal* 29: 786-794

92) Sethaphong, L., Haigler, C. H., Kubicki, J. D., Zimmer, J., Bonetta, D., Debolt, S., Yingling, Y. G. (2013) "Tertiary model of a plant cellulose synthase". *Proceedings of the National Academy of Sciences USA* 110 (18): 7512-7517

93) Skirpan, A., Wu, X., McSteen, P. (2008) "Genetic and physical interaction suggest that BARREN STALK 1 is a target of BARREN INFLORESCENCE2 in maize inflorescence development". *Plant Journal* 55: 787–797

94) Somerville, C. (2006) "Cellulose Synthesis in Higher Plants". *Annual Review of Cell and Developmental Biology* 22:53-78

95) Somerville, C. and Koornneef, M. (2002) "A fortunate choice: the history of *Arabidopsis* as a model plant". *Nature Reviews Genetics* 3(NOV):883-889

96) Stamatiou, G., Vidaurre, D., Shim, I., Tang, X., Moeder, W., Bonetta, D., McCourt, P. (2013) "Forward GeneticScreening for the Improved Producton of Fermentable Sugars from Plant Biomass". *PLOS ONE* 8(1) e55616

97) Strap, J., Latos, A., Shim, I., Bonetta, D. T. (2011) "Characterization of Pellicle Inhibition in *Gluconacetobacter xylinus* 53582 by a Small Molecule, Pellicin, Identified by a Chemical Genetics Screen". *PLOS ONE* 6(12): e28015

97) Taylor, N. G. (2007) "Identification of cellulose synthase CESA7 (IRX3) in vivo phosphorylation sites-apotential role in regulating protein degradation". *Plant Molecular Biology* 64:161-171

98) Taylor, N. G., Howells, R. M., Huttly, A. K., Vickers, K., Turner, S. R. (2003) "Interactions among three distinct CESA proteins essential for cellulose synthesis". *Proceedings of the National Academy of Sciences USA* 100(3): 1450-1455

99) Tegg, R. S., Shabala, S. N., Cuin, T. A., Davis, N. W., Wilson, C. R. (2013) "Enhanced resistance to the cellulose biosynthetic inhibitors, thaxtomin A and isoxaben in *Arabidopsis thaliana* mutants, also provides specific co-resistance, 1-NPA". *BioMed Central Plant Biology* 2013, 13:76

100) Timmers, J., Vernhettes, S., Desprez, T., Vincken, P., Visser, R. G. F., Trindade, L. M. (2009) "Interactions between membrane-bound cellulose synthases involved in the synthesis of the secondary cell wall". *Federation of European Biochemical Societies* 583: 978-982

101) The *Arabidopsis* Geonome Iniative (2000) "Analysis of the genome sequence of the flowering plant *Arabidopsis thaliana*". *Nature* 408: 796-815

102) Torii, K. U., Mitsukawa, N., Oosumi, T., Matsuura, Y., Yokoyama, R., Whittier, R. F., Komeda, Y. (1996) "The *Arabidopsis ERECTA* gene encodes a putative receptor protein kinase with extracellular leucine-rich repeats". *Plant Cell* 8: 735–746

103) Updegraff, D. M. (1969) "Semimicro determination of cellulose in biological materials". *Analytical Biochemistry* 32: 420-424

104) Vaughn, K., and Turley, R., (2001) "Ultra structural effects of cellulose biosynthesis inhibitor herbicides on developing cotton fibers". *Protoplasma* 216: 80-93

105) Wang, J., Elliott, J. E., Williamson, R. E. (2008) "Features of the primary wall CESA complex in wild type and cellulose-deficient mutants of Arabidopsis thaliana". *Journal of Experimental Botany* 59 (10): 2627-2637

106) Wang, J., Howles, P. A., Cork, A. H., Birch, R. J. Wukkuansib, R. E. (2006) "Chimeric Proteins Suggest that the Catalytic and/or C-Terminal Domains Give CESA1 and CESA3 Access to Their Specific Sites in the Cellulose Synthase of Primary Walls". *Plant Physiology* 142: 685-695

107) Wiesner, J. (1878) "Note über das Verhalten des Phloroglucins und einiger verwandter Körper zur verholzten Zellmembran". *Sitzungsberichte der Kaiserlichen Akademie der Wissenschaften Klas* 77: 60–66

108) Wightman, R. and Turner, S. (2010) "Trafficking of the Plant Cellulose Synthase Complex". *Plant Physiology* 153: 427-432

109) Wong, H. C., Fear, A. L., Calhoon, R. D., Eichinger, G. H., Mayer, R., Amikam, D., Benziman, M., Gelfand, D. H., Meade, J. H., Emerick, A. W., Bruner, R., Ben-Bassat, A., Tal, R. (1990) "Genetic organization of the cellulose synthase operon in *Acetobacter xylinum*". *Proceedings of the National Academy of Sciences USA* 87: 8130-8134

110) Wu, X., McSteen, P. (2007) "The role of auxin transport during inflorescence development in maize (*Zea mays*, Poaceae)". *American Journal of Botany* 94: 1745–1755

111) Yemm, E. W., Willis, A. J. (1954) "The estimation of carbohydrates in plant extracts by anthrone". *Biochemical Journal* 57: 508–514

112) Yennawar, N. H., Li, L., Dudzinski, D. M., Tabuchi, A., Cosgrove, D. J. (2006) "Crystal structure and activities of EXPB1 (Zea m 1), β-expansin and group-1 pollen allergen from maize" *Proceedings of the National Academy of Sciences USA* 103(40): 14664-14671

113) Yokoyama, R. and Nishitani, K. (2004) "Genomic Basis for Cell-Wall Diversity in Plants. A Comparative Approach to Gene Families in Rice and *Arabidopsis*. " *Plant Cell Physiology* 45(9): 1111-1121

114) Zhang, X., Henriques, R., Lin, S., Nie, Q., Chua, N. (2006) "*Agrobacterium*-mediated transformation of *Arabidopsis thaliana* using the floral dip method". *Nature Protocols* 1: 641-646

115) Zeeman, S. C., Tiessen, A., Pilling, E., Kato, L. K., Donald, A. M., Smith, A. M. (2002) "Starch Synthesis in Arabidopsis. Granule Synthesis, Composition, and Structure". *Plant Physiology* 129: 516-529

116) Zhong, R., Kays, S. J., Schroeder, B. P., Ye, Z. (2002) "Mutation of a Chitinase-Like Gene Causes Ectopic Deposition of Lignin, Aberrant Cell Shapes, and Overproduction of Ethylene". *The Plant Cell* 14(1): 165-179